A COMPARATIVE STUDY OF THIN-FILM COATED SILICON WAFER SURFACES FOR LASER-INDUCED BREAKDOWN SPECTROSCOPIC ANALYSIS OF LIQUIDS

A Thesis Submitted to
the Graduate School of Engineering and Sciences of
İzmir Institute of Technology
in Partial Fulfillment of the Requirements for the Degree of

DOCTOR OF PHILOSOPHY

in Chemistry

by
Nadir ARAS

July 2021
İZMİR

ACKNOWLEDGEMENTS

There are many people to thank firstly, I am heartily thankful to my supervisor Prof. Dr. Şerife H. YALÇIN for her patient guidance, encouragement, and excellent advice not only throughout this study but also in my life. This thesis could not have been written without his astute guidance. It was an honor to study with her.

I would like to thank the members of my Ph.D. thesis progressing committee Prof. Dr. Lütfi ÖZYÜZER and Prof. Dr. Talat YALÇIN for their encouraging words, thoughtful criticism, time, and attention despite their tight schedules. I would like to thank Prof. Dr. Nusret ERTAŞ, Assoc. Prof. Dr. Belgin GENÇ ÖZTOPRAK and Assoc. Prof. Dr. Ü. Hakan YILDIZ who agreed to be the members of my thesis committee

Also, I would like to thank all old and new members of lab mates, especially Semira ÜNAL.

I ought to thank to my family: my parents Sena and Ercan ARAS, my sister Neval BAĞCI, for their deepest love, invaluable patience, understanding, support, and encouragement throughout my life.

Finally, I would like to express my special thanks to my wife Ferah ARAS for making a difference in my life. With my deepest love, I dedicate this study to my twin; Elif and Güneş.

ABSTRACT

A COMPARATIVE STUDY OF THIN-FILM COATED SILICON WAFER SURFACES FOR LASER-INDUCED BREAKDOWN SPECTROSCOPIC ANALYSIS OF LIQUIDS

Laser-Induced Breakdown Spectroscopy, LIBS, is a relatively new atomic emission spectroscopic technique that shows rapid growth due to its many special peculiarities, like its ability to provide spectral signatures of all chemical species at the same time, in all environments of solid, liquid, or gas.

Liquid sample analysis by LIBS is more troublesome compared to analysis of solids. Therefore, liquid analysis by LIBS requires some pretreatment steps to be applied before direct analysis of the samples. In the literature, a variety of approaches has been successfully applied and there is still plenty of room to improve methodologies used in the liquid-LIBS analysis.

The main purpose of this thesis study was to perform studies for the development of a LIBS-TARGET for sampling liquids on it, after drying, by repetitive laser pulses. With this purpose, silicon wafer-based substrates with differing surface compositions; uncoated (crystalline silicon, c-Si), oxide-coated silicon, SiO_2, and nitride coated silicon, Si_3N_4, were tested for several experimental parameters.

Within the content of this study, a fast and accurate methodology for direct analysis of aqueous samples by LIBS is proposed. This methodology has two important attributes: one is the use of the non-metal substrate, silicon wafer, for the first time for direct analysis of aqueous samples dried on, and two is the use of high energy laser pulses focused outside the minimum focal point of a plano-convex lens at which relatively large laser beam spot covers the entire droplet area for plasma formation.

Si-wafer-based substrates were used for both qualitative and quantitative analysis of Cd, Cr, Cu, Mn, and Pb elements, and analytical figures of merit were determined. The analytical performance of each substrate was evaluated from the experiments performed with aqueous standards and real water samples. Silicon nitride-coated substrate has shown superior properties in terms of enhancing the LIBS signal and as low as 11 pg detection limits for Pb were obtained.

ÖZET

LAZER OLUŞTURMALI PLAZMA SPEKTROSKOPİSİ İLE SIVI ANALİZLERİ İÇİN İNCE FİLM KAPLI SİLİKON GOFRET YÜZEYLERİN KARŞILAŞTIRMALI BİR ÇALIŞMASI

Lazer Oluşturmalı Plazma Spektroskopisi, LIBS, tüm kimyasal türlerin spektral analizini aynı anda ve katı, sıvı, ya da gaz gibi tüm fiziksel formlarında gerçekleştirebilme kapasitesi gibi birçok özel özelliği nedeniyle büyük bir ilgi gören, diğer tekniklere göre nispeten yeni bir atomik emisyon spektroskopisi tekniğidir.

LIBS tekniği ile sıvı örneklerin analizi, katı örneklerin analizine göre daha zordur. Bu nedenle, LIBS ile sıvı örneklerin analizlerinin öncesinde bazı ön işlemlerin gerçekleştirlmesi gerekmektedir. Bu amaç doğrultusunda literatürde çeşitli uygulamalar başarı ile uygulanmakta ve, sıvı örneklerin LIBS ile analizleri için kullanılan metotların yeterliliklerini geliştirebilmek için daha çok çalışmaya ihtiyaç duyulmaktadır.

Bu tez çalışmasının temel amacı, üzerindeki sıvı damlaların kurutulduktan sonra lazer pulsları ile analizleri için bir LIBS-platform geliştirilmesine yönelik çalışmaların yapılmasına dayanmaktadır. Bu amaç doğrultusunda, farklı yüzey kompozisyonlarına sahip silikon gofret bazlı substratlar; kaplamasız (kristal silikon, c-Si), oksit kaplı silikon (SiO_2), ve nitrür kaplı silikon (Si_3N_4), çeşitli deneysel parametreler altında test edilmiştir.

Bu çalışmalar kapsamında, sıvı örneklerin LIBS ile doğrudan analizi için hızlı ve doğru bir yöntem sunulmaktadır. Bu metot iki önemli özelliğe sahiptir; birincisi sıvı örneklerin LIBS ile direkt analizi için ilk kez silikon gofretin kullanımı ve ikincisi ise plazma oluşumu için odaklayıcı lensin minimum odak noktası dışına yerleştirilmesi ile tüm damla alanını nispeten daha büyük çaptaki, yüksek enerjili lazer ışınlarının kullanılmasıdır.

Cd, Cr, Cu, Mn, ve Pb elementlerinin hem kalitatif hem de kantitatif analizleri için silikon gofret bazlı substratlar kullanıldı ve bu tekniğin analitik başarım ölçüsü belirlendi. Her bir substratın performansı, sulu standart çözeltiler ve gerçek su örnekleri kullanılarak gerçekleştirilen deneylerin sonuçlarına göre değerlendirildi. Silikon nitrür kaplı substrat, LIBS sinyallerinin iyileştirilmesi açısından daha iyi sonuçlar göstemiştir ve Pb için 11 pg kadar düşük tayin sınırı elde edilmiştir.

TABLE OF CONTENTS

LIST OF FIGURES

Figure **Page**

Figure **Page**

LIST OF TABLES

LIST OF ABBREVIATIONS AND SYMBOLS

LIBS	Laser-Induced Breakdown Spectroscopy
ICCD	Intensified Charge-Coupled Device
Nd:YAG	Neodymium-Yttrium Aluminum Garnet
LIPS	Laser-Induced Plasma Spectroscopy
LAS	Laser Ablation Spectroscopy
LTE	Local Thermodynamic Equilibrium
t_d	Detector Delay Time
t_g	Detector Gate Width
TE	Thermodynamic Equilibrium
PMT	Photomultiplier Tube
APD	Avalanche Photodiode
PDA	Photodiode Array
MCP	Micro Channel Plate
SENLIBS	Surface-Enhanced Laser-Induced Breakdown Spectroscopy
DLLME	Dispersive Liquid-Liquid Microextraction
NELIBS	Nanoparticle-enhanced laser-induced breakdown spectroscopy
c-Si	crystalline silicon
SiO_2	Silicon dioxide
Si_3N_4	Silicon nitride
LTSD	Lens to Sample Distance
SEM	Scanning Electron Microscopy
S/N	Signal to Noise Ratio
RSD	Relative Standard Deviation
EDX	Energy Dispersive X-Ray Analysis
LOD	Limit of Detection
ppb	parts per billion
ppm	parts per million
λ	Wavelength
μs	microsecond
mJ	milli-Joule
nm	nanometer

ns	nanosecond
pg	Picogram
µs	microgram
µL	microliter
GW	Giga Watt

CHAPTER 1

INTRODUCTION

1.1. Laser-Induced Breakdown Spectroscopy (LIBS)

1.1.1. What is a Laser-Induced Breakdown Spectroscopy?

Laser-Induced Breakdown Spectroscopy, LIBS also known as Laser-Induced Plasma Spectroscopy, (LIPS) and Laser Ablation Spectroscopy, (LAS) is a relatively new atomic emission spectroscopic technique that has started to emerge after the 1980s with Radziemski and Cremers's pioneering work (Cremers and Radziemski 1985).

In this technique, a highly energetic pulsed laser source is focused on a target (solid, liquid, or gas) to form a luminous plasma. The light emitted from the plasma is collected by suitable optics and directed onto the entrance slit of the spectrograph. Spectrochemical analysis of the light emitted from the plasma provides information about the chemical composition of the sample under investigation (Singh and Thakur 2020).

In laser-induced plasma, typical temperatures are around 20.000 K and electron densities may vary between 10^{16}-10^{18} cm^{-3} provided that local thermodynamic equilibrium (LTE) is valid (Sneddon, Thiem et al. 1996).

LIBS has many advantages over other types of atomic emission spectroscopic techniques. First of all, it is a multi-elemental analysis technique in which simultaneous detection of all elements present in the sample is possible. The technique provides spectral signatures of all chemical species, in all environments of solid, liquid, or gas. LIBS technique can be used to analyze extremely hard materials such as ceramics and semiconductors. It requires little or no sample preparation steps that eliminate undesired contamination of the sample during its transport.

The amount of sample consumed during LIBS analysis is so small, therefore LIBS can be considered as a nearly non-destructive process. Analysis of surfaces with craters as small as a few micrometers in diameter and micrometers range of spatial and depth resolution is possible.

Using fiber optic cables, laser pulse and emitted light from the plasma are transported to long distances of hundreds of meters, and remote sensing is obtained. Besides, in-situ analysis by LIBS can also be performed. This technique can also be used for direct analysis, compact probe, and stand-off analyses (Miziolek, Palleschi et al. 2006).

Besides many advantages of the LIBS technique, there are some deficiencies. Plasmas formed on homogeneous samples such as liquids and gases may represent the actual concentrations of the species present in the sample, however, this may not always apply to solid samples. The surface composition can be different from the bulk composition and it causes an error in the result of the analyzed sample. Also, due to the shot-to-shot fluctuations in laser pulse energy, reproducibility may degrade, and hence precision decreases.

There has been a growing interest in LIBS research and applications that cover, but not limited to, a variety of areas like; biomedical (Anzano and Lasheras 2009), industrial (Gallou, Sirven et al. 2011), pharmaceutical (de Carvalho, Nunes et al. 2010), cultural heritage (Gaudiuso, Dell'Aglio et al. 2010), civilian and military (Miziolek, DeLucia et al. 2008) environmental (Chen, Liu et al. 2010), geochemical (Harmon, Remus et al. 2009), aerosol analysis (Hahn, Diwakar et al. 2008), and many more. In addition, LIBS has been used in the analysis of biological samples including characterization of malignant tissues (Kumar, Yueh et al. 2004), detection and identification of bacteria (Baudelet, Guyon et al. 2006), identification of urinary calculus (Anzano and Lasheras 2009) and analysis of teeth and dental materials (Samek, Liška et al. 2000).

1.1.2. Laser-Induced Plasma

As soon as focusing of the energetic laser light on solid target, a plasma is produced due to rapid melting and vaporization of the sample. Also, plasma contains atoms, ions, and free electrons and is in electrically neutral form. In terms of the degree of ionization, LIBS plasma is considered as weakly ionized plasma in which the ratio of electrons is about 10% less than other species present in the plasma.

The temporal history of the LIBS plasma shown in Figure 1.1 includes various processes from the formation to the decay of the plasma. Plasma formation usually occurs at the focal point of the laser beam on the target. Due to the strong electric field of the laser light, continuum emission dominates at the early stages, as soon as the laser pulse is on. When the laser pulse goes off after 10 ns, the plasma begins to decay. Ionic species are also dominant at earlier stages then neutral atoms and molecules are formed due to electron-ion recombination. LIBS plasma contains numerous time-dependent processes therefore time resolution is so crucial to select the interested spectral region. Detector delay time and detector gate width, represented with t_d and t_g symbols, respectively, are the two important experimental parameters. Delay time is the time interval between the initiation of the laser pulse and operating the spectrometer for monitoring the plasma. Detector gate width is the time interval for data acquisition performed by the detector.

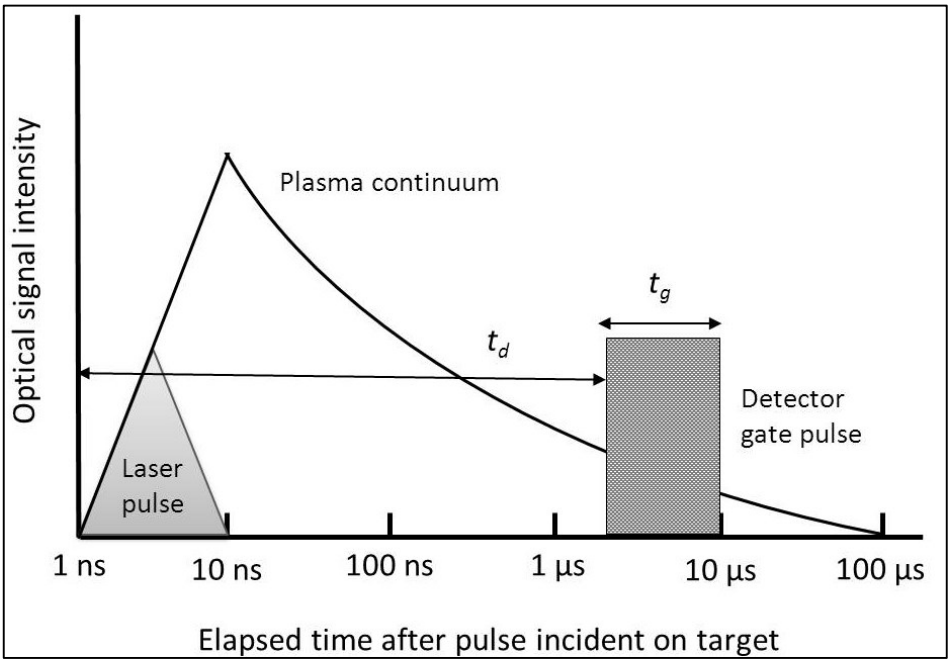

Figure 1.1.Temporal history of LIBS plasma.
(Source: Cremers and Radziemski; 2006)

The LIBS technique aims to create an optically thin plasma that is in thermodynamic equilibrium (LTE) and has the same elemental composition as the sample. In thermodynamic equilibrium conditions, all particles reach the same temperature. It is difficult to reach thermodynamic equilibrium (TE) within the laser-produced plasma in which electrons, ionic and neutral species have all the same energy. Since it is a rarely achieved condition, the use of local thermodynamic equilibrium (LTE)

instead, makes a useful approximation. The difference between TE and LTE is explained that thermodynamic equilibrium may be achieved in a small region of the plasma and differed from region to region in local thermodynamic equilibrium. When this condition is achieved satisfactorily, the relationship between the line intensities and relative concentration of elements show a good agreement among each other. But these conditions are generally theoretical.

Plasma opacity is described as the emitted radiation from the plasma that traverses and escapes without significant absorption or scattering. At this condition, plasma is called optically thin.

Experimental conditions and thermal and mechanical properties of the target may affect the shape and size of the laser-induced plasma. Different types of lasers are used to produce plasma in the LIBS technique and ablation characteristics could be varied with laser type. Plasma formation and decay are time-dependent processes so the time interval between the laser pulses and gate pulse to the detector is important for time-resolved detection. These factors have been investigated below in detail.

1.1.2.1.Laser Characteristics

Laser-induced plasma is formed at high laser irradiance values, $\geq 10^8$ W / cm^2 when laser pulse energy exceeds the threshold value. Also, threshold intensity is related to the physical properties of the target material such as melting temperature, boiling temperature. The peak power density and beam shape of the laser have important effects on the plasma and shape of the craters formed. High laser power density increases the sensitivity of spectral emission intensity which is related to the plasma temperature. A flat-top distribution of laser energy on the target surface provides a homogeneous energy distribution in which laser energy is absorbed on the target surface equally. Another important factor that affects the LIBS measurements is the pulse to pulse variation in laser energy. These fluctuations in laser energy increase the standard deviation of the LIBS signal and analytical figures of merit of the technique may deteriorate.

The physical, chemical and mechanical properties of the target have an important effect on the formation of laser-induced plasma. The fraction of the coupling of the laser energy with the target material is also related to the reflectivity of the target surface.

Ablated mass of material (M) amount by a laser pulse of energy (E) is correlated with same terms as indicated below equation:

$$M = E\,(1-R) / [C_p\,(T_b - T_0) + L_v] \qquad (1.1)$$

in which R is the surface reflectivity, C_P is the specific heat of the matter, T_b is the boiling point (K) of the matter, T_0 is the room temperature and L_v is the latent heat of vaporization. The lower values of reflectivity are associated with higher values of ablated mass due to the more intense laser-matter interaction.

1.1.2.2. Time Resolution

The temporal evaluation of laser-induced plasma is critical in the case of time-resolved detection for spectrochemical identification of the analyte. At first laser-induced plasma has a high electron temperature, then temperature begins to decrease while the plasma expands and moves away from the sample surface. Continuum emission is dominant at early stages while line emissions appear by the decrease in plasma temperature. During the plasma decay, continuum emissions disappear very fast than line emissions. Line emission is also important for the spectrochemical identification of the sample. Therefore, LIBS measurements require a careful timing consideration between the laser pulse and gate pulse to the detector. It is essential that selecting a proper delay time and gate width to maximize the ratio of line emission to background emission. Generally, the lifetime of laser-induced plasma varies between 300 ns and 40 μs. The timing diagram used in LIBS measurements is shown in Figure 1.2.

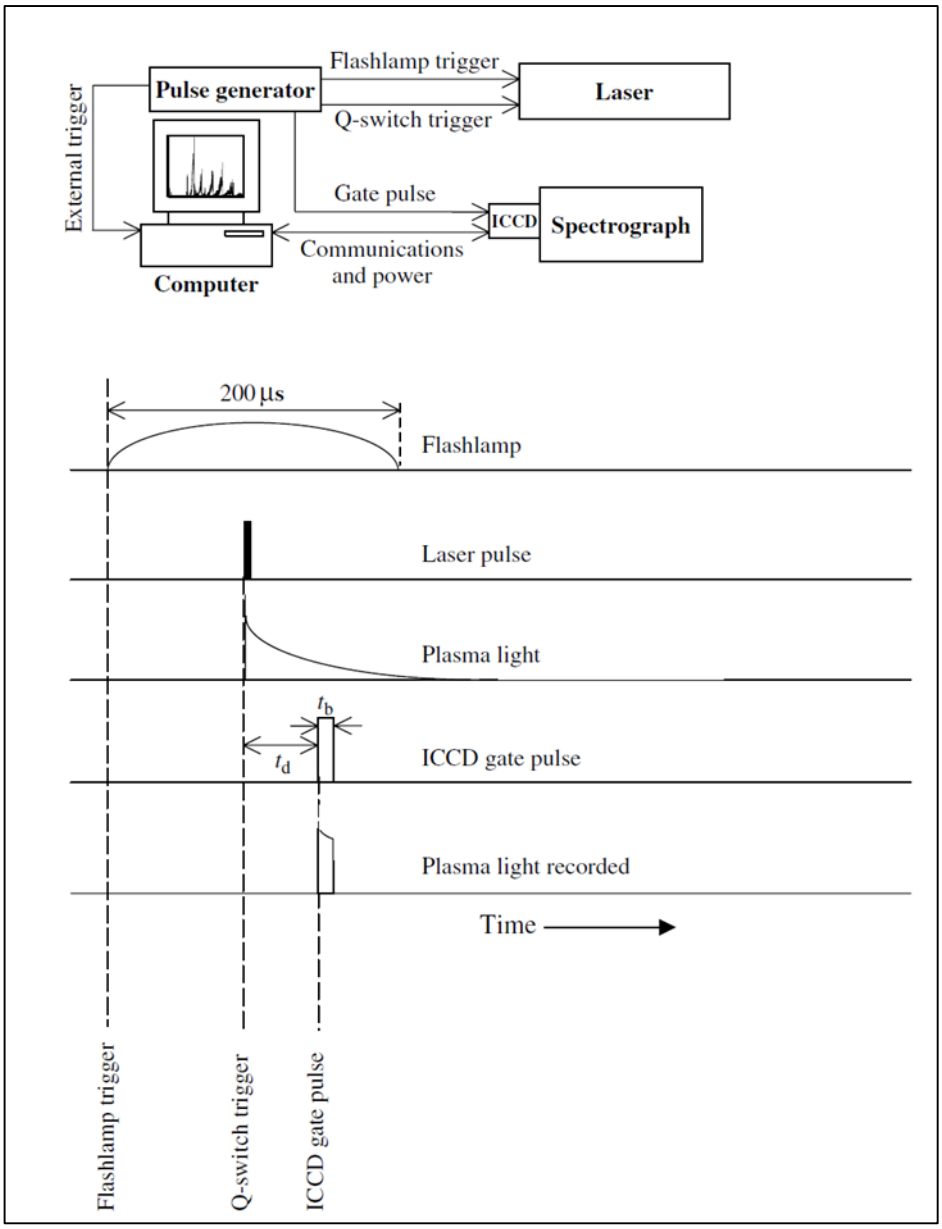

Figure 1.2. The timing diagram of the LIBS experiment.
(Source: Cremers and Radziemski; 2006)

1.1.2.3. Geometrical Set-up

Emission intensity may be differed by the change in optical alignment for focusing laser through the target and collecting light emitted from the luminous plasma. Normally laser beam is focused on the target perpendicularly. At a higher fluence level, it may result in the breakdown of the air and this problem could be resolved with a little change in focusing lens position that sets the focusing lens a little shorter than the focal length.

Emitted light from the plasma is normally collected perpendicularly to the target surface, in parallel with the laser, due to the simplicity and reproducibility. This configuration is less influenced by changes in the sample-to-lens distance in which crater is formed due to the firing of laser shots at the same position on the sample surface. Also, the spatial location of the sampled plasma should be positioned carefully since the emission intensity of the analyte could vary from region to region of the plasma plume.

Collection of emitted light from the plasma with an angle with respect to the laser beam is another widely used approach in which changes in the focal point position results in the movement of the plasma image out of the entrance slit of the spectrograph.

1.1.2.4. Ambient Atmosphere

Plasma expansion occurs away from the surface of the target and emission characteristics are also strongly affected by the presence of gas around the laser-induced plasma. The evaluation of emission intensity is also depended on the types of gas and pressure around the plasma. Under a low-pressure environment, the number of collisions decreases and it results in a decrease in the lifetime of the plasma due to the less trapping recycling of the absorbed laser energy. Reduced plasma shielding under a low-pressure environment enhances the ablation since more of the laser light reaches the sample in this situation. Zhang and coworkers (Zhang, Kashiwakura et al. 2013) have investigated the excitation mechanism of iron under Argon and Neon low-pressure environments. They have analyzed ionic iron signals between 230 nm and 300 nm spectral regions while they have set the ambient pressure at 400 Pascal or 650 Pascal. Excitation mechanisms were different under Ar and Ne plasma gas environments. Charge transfer collisions with Ar have caused the excitation of Fe while Penning type collisions with metastable state of Ne atom have resulted with the excited level of Fe ions under Ne environment.

1.1.3. LIBS Instrumentation

In general, an experimental LIBS set-up consists of three main parts,

- A high energy pulsed laser source for plasma formation,

- focusing and collection optics to direct the laser beam and plasma emission,

- a spectrograph equipped with a time-resolved detector for spectrochemical analysis and material identification.

Figure 1.3 shows a typical LIBS setup. This system consists of a laser, focusing-collimating lenses and mirror (optic system), a spectrometer, detector gating and control electronics, and a computer for the control and data acquisition.

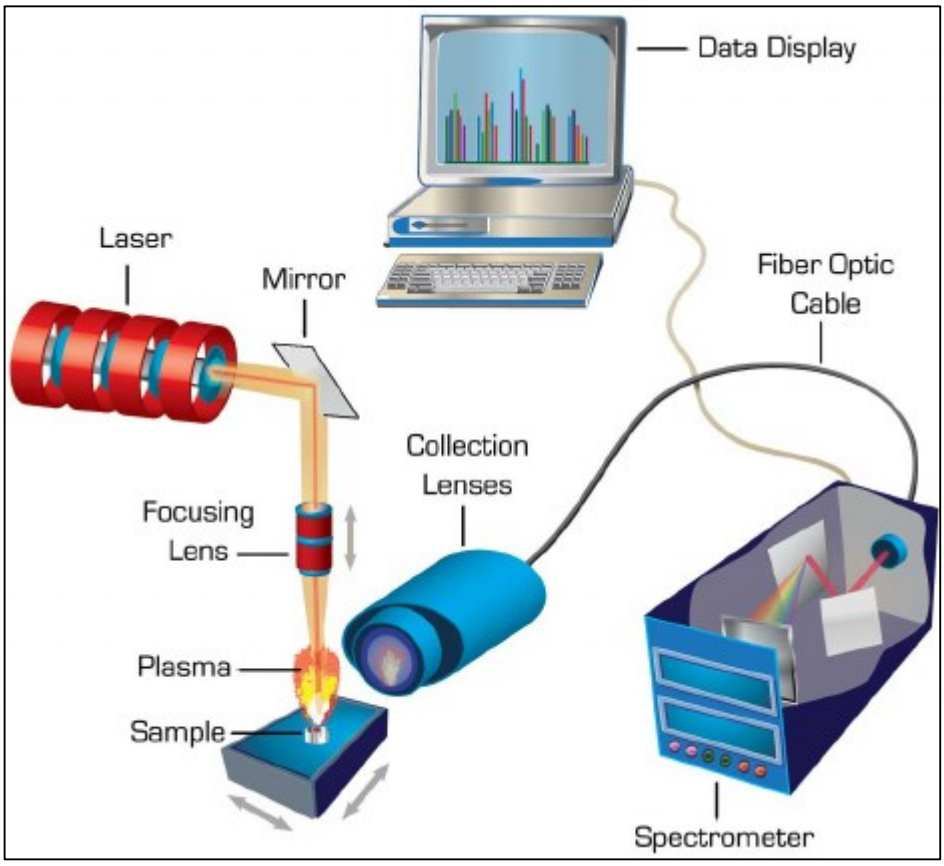

Figure 1.3. A schematical representation of a typical LIBS set-up with basic components.
(Source: Bol'shakov et al. 2010)

1.1.3.1. Lasers

A laser as a light source has superiorities in terms of intensity, directionality, monochromaticity, and coherency over the other types of conventional light sources. Lasers could be classified into two types as their operation mode namely continuous and

pulsed laser. In LIBS measurements pulsed lasers are mostly used to produce the plasma with suitable optics.

Irradiance is one of the important parameters for the laser that is defined as the power per unit area of the laser beam. Directionality is one key property of laser radiation due to the narrow divergence angle of laser radiation. It is important that the narrow beam angle provides a small spot with a higher irradiance level after focusing the laser beam on the target. Lasers generate monochromatic light with a narrow spectral range due to the exactly defined lasing medium.

There are various types of lasers according to their pump source and gain medium and can be listed as dye lasers, gas lasers, semiconductor lasers, and solid-state lasers. In LIBS systems, Nd:YAG solid-state laser is the most widely used one due to its high power density, high repetition rate, ease of operation, and maintenance.

A Nd:YAG laser with basic components is shown in Figure 1.4 schematically. Briefly, broadband light is produced when flashlamps are triggered. Nd ions in the yttrium aluminum garnet (YAG) crystal absorb this broadband light. At sufficient flashlamp pumping, population inversion takes place in which a higher energy state has a greater population than the lower energy state. Then, the transition of the ions from the upper level to a lower state (stimulated emission) results in the amplification of light. Finally, significant light amplification is occurred at the wavelength of lasing transition by direction of the amplified light between two mirrors of the resonant cavity.

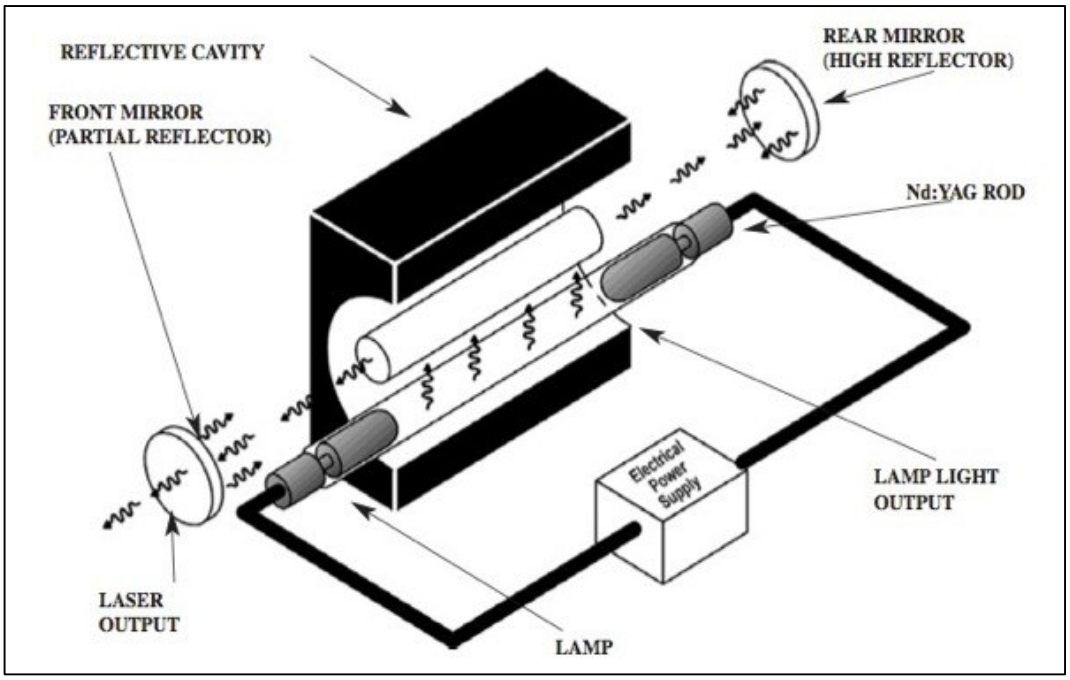

Figure 1.4. A schematical representation of Nd:YAG laser with components. (Source: directedlight.com/laser-components/catalog/nd-yag-rods/)

1.1.3.2. Optical Systems

In LIBS systems to focus the laser beam onto the sample to be analyzed lenses are utilized. There are some points to be considered when focusing the laser beam by a lens. These are the focal length, the diameter, and the construction material of the lens. The lenses used should match with the laser wavelength with maximum transmission and be appropriate in type (plano-convex, double convex, etc.).

Lenses are also used to collect emitted light from the plasma and direct it through the detector. Therefore, collimating lenses need to be optically transparent to the light emitted from the plasma. In brief, type of the material lens produced is important to transmit laser wavelength with maximum efficiency and to collect plasma light efficiently. It should be coated with the anti-reflected layer to minimize back reflection for decreasing energy losses. In some cases, lens type is important that it could provide the minimum aberration.

In LIBS systems, highly reflective mirrors that are used to direct and steer the laser beam onto the optical components should be coated and suitable with the laser wavelength.

Fiber optic cables (FOC) are also widely used optical components in LIBS systems, where plasma emission is easily carried onto the entrance slit of the spectrograph. Fiber optic cables can also be used to transmit the laser beam at longer distances (Cremers and Radziemski 2006). It is important for portable LIBS systems that fiber optic cables make it possible to deliver laser beam and plasma light for spectrochemical analysis.

1.1.3.3. Spectral Resolution and Detection Systems

The final part of the LIBS system for spectrochemical analysis and material identification consists of a spectrograph equipped with a time-resolved detector and computer for the data process. Although single-channel LIBS systems that contain a monochromator and a photomultiplier tube (PMT) can be used in the detection of plasma emission at a specific wavelength, the trend in recent years has been towards multichannel spectrometers in which a monochromator/polychromator is coupled to a series of PMT's or a time-gated, array type detectors.

To analyze emitted lights from the luminous plasma emission lines must be tabulated by dispersing elements. There are several types of devices for the spectral resolution that could prefer depending on the requirements and applications. Devices that could be used for spectral resolution are spectral filters, acousto-optic tunable filter (AOTF), grating monochromator, and echelle spectrograph.

Among different types of spectrographs, the most common design is the Czerny-Turner design, however, the use of echelle type of spectrograph in LIBS measurements is ever increasing. Czerny-Turner spectrometers provide higher resolution compared to Echelle type spectrographs, however, it works for a small wavelength range for one set of measurements. One needs to make several sequential measurements to cover the whole spectral range between 200-800 nm. On the other hand, Echelle spectrographs provide an orthogonal dual dispersion that prism for an order sorter and echelle grating for wavelength resolution. The most common echelle spectrograph characteristics are 25 cm focal length with a high number of numerical aperture, providing a maximum resolution of between 200-800 nm and carrying out a large dynamic range of measurement. As shown in Figure 1.5 the echelle grating is used at a high angle and it provides a high

dispersion in spectra. To prevent overlapping of different orders in the grating, a low dispersion grating or prism is assembled perpendicular to the echelle grating.

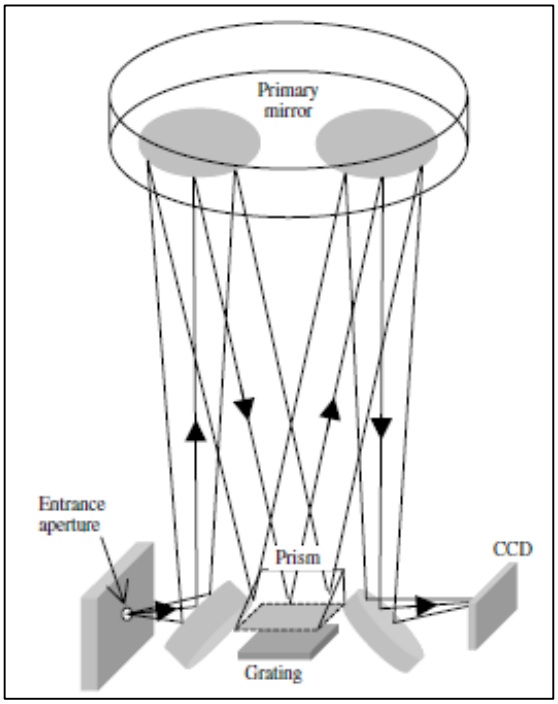

Figure 1.5. Schematical viewing of Echelle Spectrograph.
(Source: Cremers and Radziemski; 2006)

There are various types of detectors used in LIBS systems including photomultiplier tube (PMT), avalanche photodiode (APD), photodiode array (PDA), intensified photodiode array (IPDA), charge-coupled device (CCD), and intensified charge-coupled device (ICCD).

PMT is a compact, sensitive, and relatively inexpensive detector that could equip with a line filter or monochromator for single wavelength detection. PDA may integrate to a spectrograph for simultaneous detection over a certain spectral range and it is possible that can be achieved one-dimensional spatial information about the plasma lights. CCD detectors are often used in LIBS systems with their two-dimensional analysis capability. Integrated spectrograph with CCD detector enables simultaneous detection over a certain spectral range with high sensitivity and resolution.

The multielement capability is one of the major attributes of LIBS and an ideal experimental LIBS system should be able to make simultaneous multielement measurements. An ICCD array detector coupled to an Echelle spectrograph or compact

Czerny Turner spectrometer serves this purpose for numerous applications. A schematical representation of an ICCD detector is given in Figure 1.6.

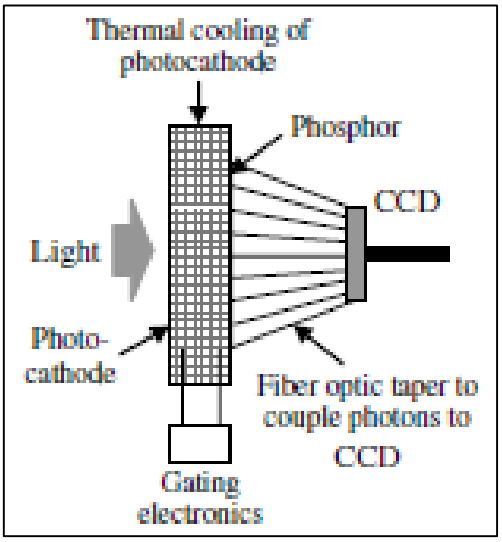

Figure 1.6. Schematical viewing of ICCD.
(Source: https://andor.oxinst.com/learning/view/article/intensified-ccd-cameras)

ICCD is a detector that consists of an optical connection with CCD and an image intensifier. It is composed of three parts; a photocathode, a microchannel plate (MCP), and a phosphor screen.

The photons from the light source are converted to electrons when photons fall onto the photocathode. By applying electrical potential, electrons are accelerated through the MCP. Incoming electrons are multiplied in this part (MCP). Multiplied electrons are accelerated towards the phosphor screen. This time these electrons energies are converted into the photons in the phosphor screen and then the image intensified after it is sent through the CCD camera by a fiber optic or a lens.

Intensified CCD detectors are the preferred choice in LIBS systems due to providing two-dimensional spatial information, the ability to make simultaneous multi-element analyses, and time-resolved detection capability.

CHAPTER 2

LIQUID ANALYSIS BY LIBS

Laser-Induced Breakdown Spectroscopy could be used for both qualitative and quantitative analysis of solid, liquid, and gas samples. The main advantages of LIBS among the other techniques are the capability of high speed, portability, microlocal analysis, and multi-element analysis. LIBS technique is generally used for the analysis of solid samples with great accuracy and precision, however, analysis of liquids by LIBS technique has some drawbacks including; splashing, bubble formation, and shockwave formation (Singh and Thakur 2020). Splashed materials from the sample require cleaning of optics frequently. Shockwave formation above the liquid can results in aerosol formation due to the vaporization of liquid samples thus interaction between laser and matter and collimation of emitted lights through the spectrometer could not be performed properly as routine LIBS measurements. Also, the laser beam could not be absorbed exactly due to the formation of bubbles inside the sample by the incident laser beam. These bubbles affect the plasma formation and characteristics that reduce the reproducibility of the LIBS measurements. For this reason, direct analysis of liquids by LIBS possesses inferior figures of merit among the other analytical techniques. To overcome these drawbacks there are some special methods or sample preparation techniques applied before analysis of liquid samples directly by LIBS.

Plasma formation; on flowing jet liquids, inside bubbles, on droplets are some of the methodologies for the liquid analysis by LIBS. (Nakamura, Ito et al. 1996, Aras and Yalçın 2019, Xue, Tian et al. 2019).

Using sequential laser pulses is another approach to enhance the analytical performance of the LIBS for liquid analysis (Scaffidi, Pender et al. 2003, Lawrence-Snyder, Scaffidi et al. 2007). In this technique, the first laser pulse creates a gaseous cavity inside the liquid sample, and then plasma formation occurs with the sequential laser pulse. This results in a longer plasma lifetime and lower background emission that obtained enhancement on LIBS signals relative to its single pulse LIBS measurements. (Colao, Lazic et al. 2002, Babushok, DeLucia Jr et al. 2006).

Electrospray ionization or aerosol formation is one of the sample introduction techniques in liquids. In this method, aerosol particles could be obtained by pneumatic, ultrasonic, and electrospray nebulization techniques before LIBS measurements (Aras, Yeşiller et al. 2012)

The absorption of liquid samples on the solid substrate is the alternative method in which liquid solution is converted into the solid phase for LIBS analysis. The details of this methodology are given below, in detail.

2.1. Liquid to Solid Matrix Conversion on Solid Substrates

This technique is the most promising strategy because of the outstanding properties like minimum sample treatment, requiring a small amount of sample, and reusability of the substrate (Jantzi, Motto-Ros et al. 2016). These matrix conversion methods provide convenience during the LIBS measurements in which a small volume of sample is transferred to the surface of the substrate or solid support material. After the evaporation of the sample solvent, LIBS measurements are performed on the solid substrate directly. The method enhances the analytical capability of the LIBS technique due to the better laser solid matter interaction with respect to the liquids, nearly no matrix effect, and improvement of the detection limits for LIBS. However, one key parameter is the choice of substrate type because it should be free from any contaminant and free from any interference signal from analyte signals. There are various types of substrates used as solid support material (such as filter paper, graphite, metallic substrates) and studies based on the interactions of laser with physically/chemically modified surfaces for the enhancement of analyte emission signal are classified under the category of Surface Enhanced Laser-Induced Breakdown Spectroscopy (SENLIBS).

2.1.1. Literature Works on Surface Enhanced LIBS

Surface-enhanced Laer-Induced Breakdown Spectroscopy (SENLIBS) is one promising method that liquid samples could be analyzed directly on the substrate after the liquid to solid phase transition. SENLIBS technique shows rapid growth due to the

better detection limits, simple sample preparation steps, and low cost of equipment. For about a decade, SENLIBS measurements have shown that enhances signal intensity up to several orders of magnitude, RSD decreases, S/N increases, and hence analytical figures get better.

One of the first studies about the liquid to solid matrix conversion was performed by Pace et al. in 2006 (Pace, D'Angelo et al. 2006). In this study, liquid solutions were converted into solid pellets of calcium hydroxide for LIBS measurements. Samples were prepared by mixing 6 mg of calcium oxide with 6 mL aqueous solutions with various concentrations of Cr, Pb, Cd, and Zn. After the homogenizing and drying process, pellets were prepared from powder with 3 cm diameter and 1 cm thick. The LODs were at the level of ppm concentrations as 1.2, 20, 21, and 129 μg mL^{-1} for Cr, Pb, Zn, and Cd, respectively.

An interesting study (Chen, Li et al. 2008) was trace metal analysis in aqueous solutions by LIBS using wood slice substrates. Toxic heavy metal element analysis in water solutions have been performed on wood slice substrate to investigate the capability of the LIBS technique for direct liquid analysis. Detection limits of Cr, Mn, Cu, Cd, and Pb were in the range of 0.029-0.59 μg mL^{-1}.

Sarkar et al. have demonstrated that using a pure graphite planchet as solid support material for the determination of boron in groundwater by LIBS (Sarkar, Aggarwal et al. 2010). This study indicated that LIBS could be used for the analysis of groundwater samples directly without any sample preparation step. They have achieved the detection of sub-ppm amounts of boron in the groundwater sample. Pure graphite planchets for LIBS analysis offered some convenience like inexpensiveness, ease to handle, and simple chemical composition.

Another different analysis technique (Sobral, Sanginés et al. 2012) was carried out by Sobral et al. In this study, detection of trace elements of Cu, Mg, Pb, Hg, Cd, Cr, and Fe in water and ice were carried out by LIBS. The purpose of this study was investigation of the LODs for each metal in ice samples and a comparison of these results with obtained from the analysis performed on the surface of liquid water by LIBS. The limit of detection values obtained from ice was an average of 1.0 μg mL^{-1} and the results of the comparative LIBS analysis on ice and water indicated improvements of 6-fold in LODs for obtained by LIBS analysis in ice.

Zhu et al. have utilized the LIBS technique for the determination of trace metals in an aqueous solution by using bamboo charcoal as a solid-phase extraction adsorbent

(Zhu, Chen et al. 2012). Bamboo charcoal is a renewable material that is used for removing heavy metals from liquid solutions with microporous and biological properties. In this study, detection of trace metal elements (Pb) in an aqueous solution has been carried out by using bamboo charcoal as an adsorbent material during the LIBS measurements. As a result of the quantitative measurements, the limit of detection was 26.7 μg mL^{-1} calculated for the lead which showed a good agreement with ICP-AES analysis.

The work done (Aguirre, Legnaioli et al. 2013) in 2013 is one of the pioneering study performed by Surface-Enhanced Laser-Induced Breakdown Spectroscopy (SENLIBS). In this study, they have combined the LIBS system with liquid-liquid microextraction techniques for trace element analysis. Analysis microdroplets on the aluminum substrate have been carried out in this study. They have achieved a 50-fold enhancement by SENLIBS with respect to the direct analysis of microdroplets. The limit of detection (LOD) was 6 μg g^{-1} of Mn in a 10 % Triton matrix by SENLIBS. They have observed improvement in the sensitivity, precision, and linearity of the calibration curve with respect to the direct analysis of microdroplets.

One interesting study performed by Shi et al. (Shi, Niu et al. 2014) was the combination of the nano-channel material with laser-induced breakdown spectroscopy for sensitive and quick determination of metal ions in liquid samples. They have chosen a 3D anodic aluminum oxide porous membrane (AAOPM) as a solid support material for LIBS measurements. They have observed 19-fold enhancements with 3D AAOPM substrate compared with that on the tablet sample made of aluminum oxide powder. They explained this enhancement with strong coordination metal-oxygen bond between hydroxyl groups and metal ions, the larger contact area between matrix and analytes, and coupling of the laser beam with the nano-channel material. Because of these positive contribution, LODs were 0.18, 0,12, 0.081, and 0.11 μg mL^{-1} for Cu^{2+}, Ag^{+}, Pb^{2+}, and Cr^{3+}, respectively.

Bae et al. have demonstrated a different methodology of LIBS for the analysis of water droplets with the laser-patterned silicon wafer (Bae, Nam et al. 2015). To eliminate the uncontrollable distribution of analytes on the substrate during the drying process, a laser-patterned silicon wafer (LPSW) substrate has been tested. The detection limit for potassium has been indicated as a $0.23x10^{-9}$ mole with nearly 4% precision. Also, they have concluded that surface properties of the substrate have an important role in the analytical performance of surface-enhanced LIBS.

Surface-enhanced laser-induced breakdown spectroscopy (SENLIBS) is mostly preferred recently for liquid analysis. One study performed by Yang et al. was the sensitive determination of Cu, Pb, Cd, and Cr elements in aqueous solutions using chemical replacement combined with SENLIBS (Yang, Hao et al. 2016). Metal ions were enriched on magnesium alloy surfaces as a solid support material. The clean magnesium alloy was immersed in 8 mL standard solutions for 1 minute and then dried with a hot air blower. Detection limits obtained for Cu, Pb, Cd, and Cr were 0.250, 0,118, 0.420, and 0.025 $\mu g\ mL^{-1}$, respectively was indicated that the method could be used for waste-water quality monitoring.

Another study was given by Zheng et al. (Zheng, Niu et al. 2016) in 2016 is about the matrix effect in chlorine analysis by LIBS in a pellet or in a dried solution layer on a pure aluminum target. They have investigated the matrix effect for the samples prepared with different mineral salts in the forms of pellet and solution. Their results have indicated a negligible matrix effect for the solution samples analyzed by surface-assisted LIBS technique while a strong matrix effect has been observed for the analysis of pellets. In addition, the relative standard deviation of the slopes of growth curves was as small as 0.95% with the surface-assisted LIBS configuration.

Another interesting study was performed (Chen, Shi et al. 2016) for metallic element analysis in particle samples using a LIBS technique in 2016. In this study, the soil samples were transferred from the mixing chamber to the adsorption plate with argon flow. Due to the good stickiness of the adsorption plate, numerous solid particles could be held on the substrate surface. By using this novel method, 124.571 $\mu g\ g^{-1}$ Ti and 0.0126% Mg in soil samples were determined quantitatively.

In another study, they (Yang, Hao et al. 2017) have carried out a simultaneous determination of La, Ce, Pr, and Nd elements in aqueous solution using surface-enhanced LIBS. Analysis of the rare earth elements (REEs) has been performed on a Zn metal substrate surface. The LODs were at the level of 0.85, 4.07, 2.97, and 10.98 $\mu g\ mL^{-1}$ for La, Ce, Pr, and Nd, respectively. Obtained results from the analysis of REEs elements on Zn substrate were enhanced about 2-4 times with respect to the analysis performed with filter paper.

Niu et al. have performed detection of trace-level heavy metal in solutions on a metallic target (Niu, Zheng et al. 2018). In this study, a laser-pretreated aluminum substrate was utilized for the detection of Ni, Cr, and Cd by LIBS. The polished aluminum target was ablated with laser pulses while the substrate was moved in one direction at a

speed of 0.5 mm/s. LODs values were for 1-mL volume deposition on target for Ni, Cr, and Cd 22, 19, and 184 $\mu g.L^{-1}$ while LODs values were for the 20-mL enriched samples on target for Ni, Cr, and Cd 1.18, 0.975 and 2.46 $\mu g.L^{-1}$, respectively.

A recent study carried out by Yang et al. was about the improvement of the detection limits by the number of repeating sample preparations in a fixed area (Yang, Li et al. 2020). In this work, element concentration was increased per unit area by increasing the sample loading in a fixed point on Zn-metal substrate. As a result of the quantitative measurements, the limit of detection values of Cu, Pb, Cr, and Cd was decreased from 0.072 ~ 0.36 to 0.027 ~ 0.057 5 $\mu g\ mL^{-1}$. The main advantage of this method was the higher sensitivity and including low cost of equipment for the analysis of trace elements in a liquid sample.

One of the most recent study performed by Maji et al. was about the enhancement of the LIBS signal intensities in colloids (Maji, Kumar et al. 2021). Sodium hydroxide was added to the sample solution to form hydroxides of metals that was resulted in colloid formation. As the result of the analysis of the pre-concentrated colloids in filter paper, the LODs of Cu and Cr were calculated as 0.020 and 0.025 $\mu g\ mL^{-1}$. The signal intensities were enhanced two orders of magnitude with colloid analysis. Also, this enhancement was explained by the decrease in plasma threshold value in colloids.

Zhang et al. were investigated the influence of the substrate temperature on detection sensitivity for the analysis of heavy metals in water (Zhang, Chen et al. 2021). Different types of substrates were used in Surface-enhanced LIBS, however, the effect of the temperature on this analysis was not clear. The pure aluminum substrate was placed on the heating table by thermal grease. The substrate temperature was increased from 25 ºC to 200 ºC. The emission intensities of Pb and Cr were increased with the substrate temperature. The calculated LODs of Pb and Cr was decreased from 31.7 and 4.6 $ng\ mL^{-1}$ at 25 ºC to 8.0 and 1.2 $ng\ mL^{-1}$at 200 ºC.

Another interesting study was about the determination of V and Mo by dispersive liquid-liquid microextraction (DLLME) combined with LIBS (de Jesus, Aguirre et al. 2014). The DLLME procedure was performed to eliminate some difficulties observed in the direct liquid analysis by LIBS. After the extraction of the liquid sample, 10 µL of the sample solution was loaded on an aluminum foil then it was placed on a hot plate to dry the organic phase from the microdroplet. The limit of detection and quantification for Mo 30 and 70 $\mu g\ mL^{-1}$ and for V 5 and 20 $\mu g\ mL^{-1}$, respectively. The advantages of the proposed method were fast, easy to use, inexpensive, and generation of little waste.

Wang et al. (Wang, Shi et al. 2014) combined the LIBS technique with dispersive solid-phase micro-extraction for the simultaneous and sensitive analysis of Ag, Mn, and Cr. Nano-graphite was utilized as a solid support material due to its superior absorption ability, low cost, and solubility in water. Sodium diethyldithiocarbamate was used as the complexing reagent to provide effective interaction between nano-graphite and metal ions. As a result of the LIBS measurements, calibration curves were obtained in the range of 0.1-1.2 mg L^{-1} concentration range with good linearity. In addition, they obtained a good accuracy level between 92.66 % and 105.8 % for all elements.

Aguirre et al. evaluated the dispersive liquid-liquid microextraction (DLLME) for metal enrichment for the simultaneous determination of Cr, Cu, Mn, Ni, and Zn in water samples (Aguirre, Selva et al. 2015). Metals in aqueous solutions were extracted with tetrachloromethane as pyrrolidinedithiocarbonate complexes (APDC). Under optimum chemical and instrumental conditions, they have observed about 4.0-5.5 enhancement compared to the direct liquid analysis performed by LIBS.

Aguirre et al. developed a new technique based on the single drop microextraction (SDME) followed by LIBS for trace metal determination in liquid samples (Aguirre, Nikolova et al. 2015). In this technique, analyte species were extracted into toluene as ammonium pyrrolidinedithiocarbonate (APDC) chelates. After enrichment of the analyte in toluene, it was transferred to the substrate for LIBS measurements. They obtained about 2.5-fold enhancement in sensitivity and LODs compared to the direct analysis of the liquids by LIBS. Detection limits obtained from the SDME-LIBS method were 21, 301, 54, 189, and 50 µg kg^{-1} for Zn, Mn, Cu, Ni, and Cr, respectively.

Another one of successful work was carried out by Wang et al. (Wang, Wei et al. 2015). It was based on the metal precipitation and membrane separation for simultaneous elemental analysis in liquid samples by LIBS. After the reaction of the metal elements with chelating reagent 2,4,6-trimercapto-1,3,5-triazine (TMT), they were separated by a mixed cellulose ester microfiltration membrane. The LODs were 2.59, 0.957, 0.958, and 1.29 ng mL^{-1} for Cu, Ag, Mn, and Cr, respectively, which indicated a good improvement with these results for the direct liquid analysis by LIBS.

Jiang et al. have carried out electrochemical LIBS measurements for enhanced detection of cadmium without interference in rice on layer-by-layer assembly of graphene oxides (Jiang, Guo et al. 2016). Cadmium is highly toxic at trace levels for human nervous, immune, and gastrointestinal systems. In this work, the Ti plate was cleaned in acetone and deionized water ultrasonically then the cleaned plate was immersed in 1wt%

Poly(diallyldimethylammonium chloride) (PDDA) solution to get the positive charge on the surface, finally, this positively charged surface coated with graphene oxide (negatively charged). After the preparation of the Ti plate, sample solutions were enriched into the surface of the Ti plate by electrochemical deposition. Three orders of magnitude enhancement and ppb level limits of detection of cadmium were achieved by electrochemical deposition and the modification of graphene oxide on the electrode of the cadmium.

Ultra-trace detection in liquid samples by LIBS based on matrix conversion crosslinked polyvinyl alcohol (PVA) was performed by Lin et al. (Lin, Han et al. 2016). In this approach, the aqueous solution was mixed with PVA leading to phase conversion, then analyte species were distributed in thin-film PVA film. Laser energy was used effectively due to the low PVA thermal decomposition temperature. They observed a great enhancement with this method compared with those from direct liquid analysis by LIBS. The LODs were 1, 8, 16 ng mL^{-1} and 1, 1, 2, and 5 µg mL^{-1} for Ag, Cu, Cr, Pb, Ni, Co, and Cd and they observed the better analytical figure of merit like linearity, reproducibility, accuracy with this method.

In a recent study, Ruiz et al. have performed preconcentration and detection of Zn, Cd, Mn, Ni, and Pb in aqueous samples by the combination of dispersive micro solid-phase extraction with LIBS method (Ruiz, Ripoll et al. 2019). Graphene oxide and activated carbon were used as an adsorbent for the solid-phase extraction method. After the microextraction process, the solid residue was placed on circular-shaped prepared silicone sheets for LIBS measurements. Under optimum experimental and instrumental conditions limits of detection values were below 100 µg kg^{-1} and 50 µg kg^{-1} for both conditions used activated carbon and graphene oxide as an adsorbent, respectively.

Nanoparticle-enhanced laser-induced breakdown spectroscopy (NELIBS) (De Giacomo, Gaudiuso et al. 2013) is one way to improve the capability of the LIBS technique for direct liquid analysis. NELIBS technique is required simple experimental and instrumental conditions that a small volume of the sample solution containing nanoparticles is deposited on the sample surface. After the evaporating sample solvent, the laser beam is focused through the solid residue on the surface of the solid support material. The first study about the NELIBS study was carried out by Giacomo et al. in 2013. In this study, the applicability of the technique for the analysis of metallic samples has been tested. 0.5 µL drops of 20 nm Ag nanoparticle solution (0.02 mg mL^{-1} in aqueous buffer) was placed on different types of substrate including; metals, alloys (Ti and Cu,

Pb), certified copper-based alloys (L3, B21, and SN1, SN2, Sn3, TB2, and TB3), certified steel (C8), commercial galvanized steel, Teflon and silicon wafer. They observed an improvement of 1-2 orders of magnitude in LIBS signals with contained Ag nanoparticles on metal samples. They concluded this enhancement by NELIBS with the change in the ablation process due to the decrease in ablation threshold in metal samples. However, they did not observe any difference or enhancement between LIBS and NELIBS measurements with insulator and semiconductor substrates.

De Giacomo et al. have also investigated the effect of nanoparticles deposited on sample surface on laser ablation and plasma emission (De Giacomo, Gaudiuso et al. 2014). Surface roughness and flakes on the surface have an important role in ablation efficiency due to the decreased ablation threshold value. Some features made the NELIBS technique advantageous like the simplicity of the technique, the applicability of the NELIBS technique to commercial LIBS system, 1-2 orders of magnitude enhancement in LIBS signals, and higher reproducibility and sensitivity.

In their last study, De Giacomo et al. performed the elemental chemical analysis of micro drops of solutions with lead and silver concentration at the sub-ppm level (De Giacomo, Koral et al. 2016). A micro drop of 1 μL volume of analyte solution was placed onto the substrate for analysis, while 1 μL of a colloidal nanoparticle solution was dried on the substrate prior to sample loading. As a result of the quantitative measurements, absolute detectable amounts for Pb and Ag were calculated as 2 and 0.2 pg, respectively. In addition, analysis of the lead-contaminated human serum solutions was analyzed both LIBS and NELIBS techniques. 74 ng mL^{-1} Pb could be detected from the 1 μL of the solution by NELIBS while this value was remained at 5 μg mL^{-1} by LIBS.

Another study about the combination of dual-pulse LIBS and NELIBS study performed by Yang et al. was emission enhancement by combining nanoparticle and dual pulse on crystal SiO_2 for femtosecond laser-induced breakdown spectroscopy (Yang, Hao et al. 2017). The crystal SiO_2 sample was coated with gold nano particles by thermal dewetting before NELIBS analysis. Their results indicated that the size and distribution of the nanoparticles affect the enhancement factor for LIBS measurements. The 30-fold enhancement was achieved by using combined dual-pulse LIBS and nanoparticle enhanced LIBS at a lower laser fluence of 4.4 J/cm^2.

Sládková et al. showed the effect of the low-pressure conditions on laser-induced plasma produced on substrate surface covered with Ag nanoparticles (Sládková, Prochazka et al. 2017). They performed their studies under 60, 400, 800, and 975 mBar

vacuum conditions, however, the best values with 4-fold enhancement were observed at 60 mBar with 61 mJ laser pulse energy. Formation of coffee ring-shaped solid residue on the surface due to the irregular drying of droplets, relative standard deviation values were increased.

Table 2.1. Literature studies for the determination of cadmium based on matrix conversion method with different techniques by LIBS.

Emission Line (nm)	**LOD (ng mL^{-1})**	**Reference**	**Methodology**
Cd (I) 228.80	5.6	(Jiang, Guo et al. 2016)	Graphene Oxide/PDDA modified Ti plate by electrochemical deposition
Cd (II) 226.50	5000	(Lin, Han et al. 2016)	Matrix conversion-Polyvinyl alcohol (PVA) supporting material
Cd (I) 508.58	420	(Yang, Hao et al. 2016)	Chemical replacement-magnesium alloy substrate
Cd (I) 508.58	590	(Chen, Li et al. 2008)	Wood slice substrates
Cd (I) 326.10	129000	(Pace, D'Angelo et al. 2006)	Calcium hydroxide pellet
Cd (II) 226.50	5.2	(Gaubeur, Aguirre et al. 2015)	Dispersive liquid-liquid microextraction-Al substrate
Cd (II) 226.50	46000	(Bukhari, Awan et al. 2012)	Absorption paper
Cd (II) 226.50	158	(Aras and Yalçın 2016)	SiO_2 coated Si wafer substrate
Cd(I) 508.58	184	(Niu, Zheng et al. 2018)	Laser-pretreated aluminum substrate
Cd(I) 214.4	24	(Ruiz, Ripoll et al. 2019)	Dispersive liquid-liquid microextraction-graphene oxide as an adsorbent

Table 2.2. Literature studies for the determination of chromium based on matrix conversion method with different techniques by LIBS.

Emission Line (nm)	**LOD (ng mL^{-1})**	**Reference**	**Methodology**
Cr (I) 357.87	50	(Aguirre, Nikolova et al. 2015)	Single drop microextraction-droplet on Al plate substrate
Cr (I) 425.44	1.3	(Wang, Wei et al. 2015)	Metal precipitation-membrane separation
Cr (I) 425.43	9.5	(Wang, Shi et al. 2014)	Dispersive solid-phase micro-extraction-nano-graphite adsorbent
Cr (I) 425.43	16	(Lin, Han et al. 2016)	Matrix conversion-Polyvinyl alcohol (PVA) supporting material
Cr (I) 520.84	25	(Yang, Hao et al. 2016)	Chemical replacement-magnesium alloy substrate
Cr (I) 427.48	110	(Shi, Niu et al. 2014)	3D anodic aluminum oxide porous membrane (AAOPM)
Cr (I) 357.87	41	(Aguirre, Selva et al. 2015)	Dispersive liquid-liquid microextraction-Al plate substrate
Cr (I) 267.72	1400	(Sobral, Sanginés et al. 2012)	In ice
Cr (I) 425.43	34	(Chen, Li et al. 2008)	Wood slice substrates
Cr (I) 357.87	1200	(Pace, D'Angelo et al. 2006)	Calcium hydroxide pellet
Cr (I) 427.48	230000	(Bukhari, Awan et al. 2012)	Absorption paper
Cr(I) 425.43	19	(Niu, Zheng et al. 2018)	Laser-pretreated aluminum substrate
Cr(I) 357.9	8	(Ruiz, Ripoll et al. 2019)	Dispersive liquid-liquid microextraction-graphene oxide as adsorbent

Table 2.3. Literature studies for the determination of copper based on matrix conversion method with different techniques by LIBS.

Emission Line (nm)	**LOD (ng mL^{-1})**	**Reference**	**Methodology**
Cu (I) 324.75	54	(Aguirre, Nikolova et al. 2015)	Single drop microextraction-droplet on Al plate substrate
Cu (I) 324.75	2.6	(Wang, Wei et al. 2015)	Metal precipitation-membrane separation
Cu (I) 324.75	8	(Lin, Han et al. 2016)	Matrix conversion-Polyvinyl alcohol (PVA) supporting material
Cu (I) 324.75	250	(Yang, Hao et al. 2016)	Chemical replacement-magnesium alloy substrate
Cu (I) 324.75	180	(Shi, Niu et al. 2014)	3D anodic aluminum oxide porous membrane (AAOPM)
Cu (I) 324.75	23	(Aguirre, Selva et al. 2015)	Dispersive liquid-liquid microextraction-Al plate substrate
Cu (I) 324.75	2300	(Sobral, Sanginés et al. 2012)	In ice
Cu (I) 324.75	29	(Chen, Li et al. 2008)	Wood slice substrates
Cu (I) 324.75	2.5	(Aras and Yalçın 2016)	SiO_2 coated Si wafer substrate

Table 2.4. Literature studies for the determination of manganese based on matrix conversion method with different techniques by LIBS.

Emission Line (nm)	**LOD ($ng\ mL^{-1}$)**	**Reference**	**Methodology**
Mn (II) 259.37	301	(Aguirre, Nikolova et al. 2015)	Single drop microextraction-droplet on Al plate substrate
Mn (I) 403.08	1.0	(Wang, Wei et al. 2015)	Metal precipitation-membrane separation
Mn (I) 403.08	10.8	(Wang, Shi et al. 2014)	Dispersive solid-phase micro-extraction-nano-graphite adsorbent
Mn (II) 259.37	49	(Aguirre, Selva et al. 2015)	Dispersive liquid-liquid microextraction-Al plate substrate
Mn (I) 403.31	36	(Chen, Li et al. 2008)	Wood slice substrates
Mn (II) 259.37	6000	(Aguirre, Legnaioli et al. 2013)	Liquid-liquid microextraction-Al plate substrate
Mn (I) 403.08	6.7	(Aras and Yalçın 2016)	SiO_2 coated Si wafer substrate
Mn(I) 259.4	36	(Ruiz, Ripoll et al. 2019)	Dispersive liquid-liquid microextraction-graphene oxide as adsorbent

Table 2.5. Literature studies for the determination of lead based on matrix conversion method with different techniques by LIBS.

Emission Line (nm)	**LOD (ng mL^{-1})**	**Reference**	**Methodology**
Pb (I) 405.78	2.0	(De Giacomo, Koral et al. 2016)	Nanoparticle–enhanced LIBS (Au NPs droplets on inert substrate; glass, silicon or Teflon)
Pb (I) 405.78	1000	(Lin, Han et al. 2016)	Matrix conversion-Polyvinyl alcohol (PVA) supporting material
Pb (I) 405.78	118	(Yang, Hao et al. 2016)	Chemical replacement-magnesium alloy substrate
Pb (I) 405.78	81	(Shi, Niu et al. 2014)	3D anodic aluminum oxide porous membrane (AAOPM)
Pb (I) 405.78	74	(Chen, Li et al. 2008)	Wood slice substrates
Pb (I) 405.78	20000	(Pace, D'Angelo et al. 2006)	Calcium hydroxide pellet
Pb (I) 405.78	8500	(Zhu, Chen et al. 2012)	Bamboo charcoal
Pb(I) 405.78	95	(Aras and Yalçın 2016)	SiO_2 coated Si wafer substrate
Pb(I) 368.3	21	(Ruiz, Ripoll et al. 2019)	Dispersive liquid-liquid microextraction-graphene oxide as an adsorbent

2.2. Aim of the Study

Laser-Induced Breakdown Spectroscopy (LIBS) is among the most popular technique due to its unique properties including simplicity, high speed, portability, and multi-element analysis capability. In order to improve the sensitivity of the LIBS technique for liquids analysis, special sample pretreatment methods such as; aerosol formation, chemical derivatization, and matrix conversion are employed by several groups studying LIBS.

Liquid to solid conversion before LIBS measurements is a simple and sensitive methodology in which a small volume of sample is transferred to the surface of the solid support material. Solid residue remained on the support material after the evaporation of the sample solvent is subjected to subsequent laser pulses for LIBS measurements. This method enhances the analytical capability of the LIBS technique due to better laser-matter interaction compared to direct liquid analysis, with almost no matrix effect. Therefore, improvements in detection limits are achieved. However, the type of the selected substrate has a crucial role to improve the capability of the LIBS technique for liquid analysis.

This thesis study is aimed to investigate the surface enhancement effect of the non-metallic, silicon wafer, substrates for the analysis of aqueous solutions of cadmium, chromium, copper, manganese, and lead elements

For this purpose, 3 different types of Si-wafer-based substrates, crystalline silicon (c-Si), oxide-coated silicon (SiO_2-Si), and nitride coated silicon (Si_3N_4-Si), were utilized and analytical performances were compared. LIBS measurements have been performed by using unusually large laser beam spot (appr. 1.3 mm diameter in size) to cover and ablate all parts of the solid residue on the substrate in a single laser pulse. Calibration curves were constructed for quantitative analysis of Cd, Cr, Cu, Mn, and Pb, elements, separately, for all three substrates, c-silicon, SiO_2 coated and Si_3N_4 coated silicon wafer. Among all Si_3N_4 coated silicon wafer substrates exhibited the highest sensitivity, precision, and better detection limits for all Cd, Cr, Cu, Mn, and Pb, elements studied. LODs corresponding to absolute detection of 62 pg Cd, 1.5 pg Cr, 0.5 pg Cu, 2 pg Mn, and 11 pg Pb have been achieved from the analysis of 0.5 µL of droplet volume with Si_3N_4 coated silicon wafer substrate. The proposed methodology provides a fast,

accurate, and sensitive detection for toxic elements in standard aqueous solutions and real water samples.

CHAPTER 3

EXPERIMENTAL

In this thesis study, simple, fast, and accurate analysis for the liquid samples by laser-induced breakdown spectroscopy is proposed that direct analysis of aqueous samples without any sample preparation step was carried out with three different types of silicon wafer-based substrates; crystalline silicon (c-Si), oxide-coated silicon (SiO_2-Si), and nitride coated silicon (Si_3N_4-Si). The experimental issues about the LIBS system, sampling, and substrates were explained in detail below.

3.1. LIBS Set-up

In this study, an experimental LIBS system was designed, constructed, and optimized for direct analysis of aqueous samples on silicon-based substrates. The schematical and pictorial representations of the experimental LIBS set-up constructed from its commercially available parts are shown in Figure 3.1 and Figure 3.2, respectively.

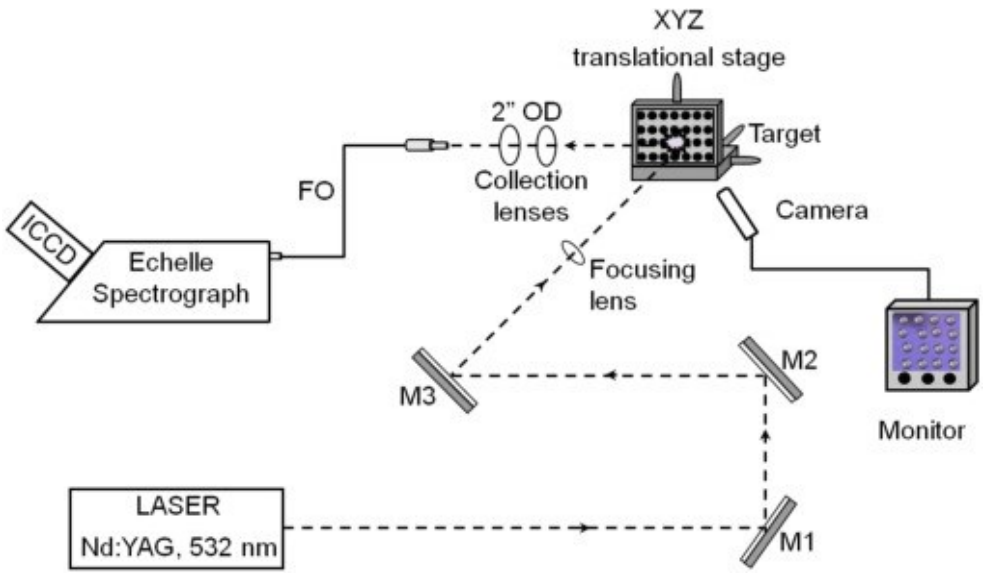

Figure 3.1. Schematic representation of LIBS system. M1, M2, and M3: reflecting mirrors, FO: fiber optic cable, ICCD: Intensified charge-coupled detector.

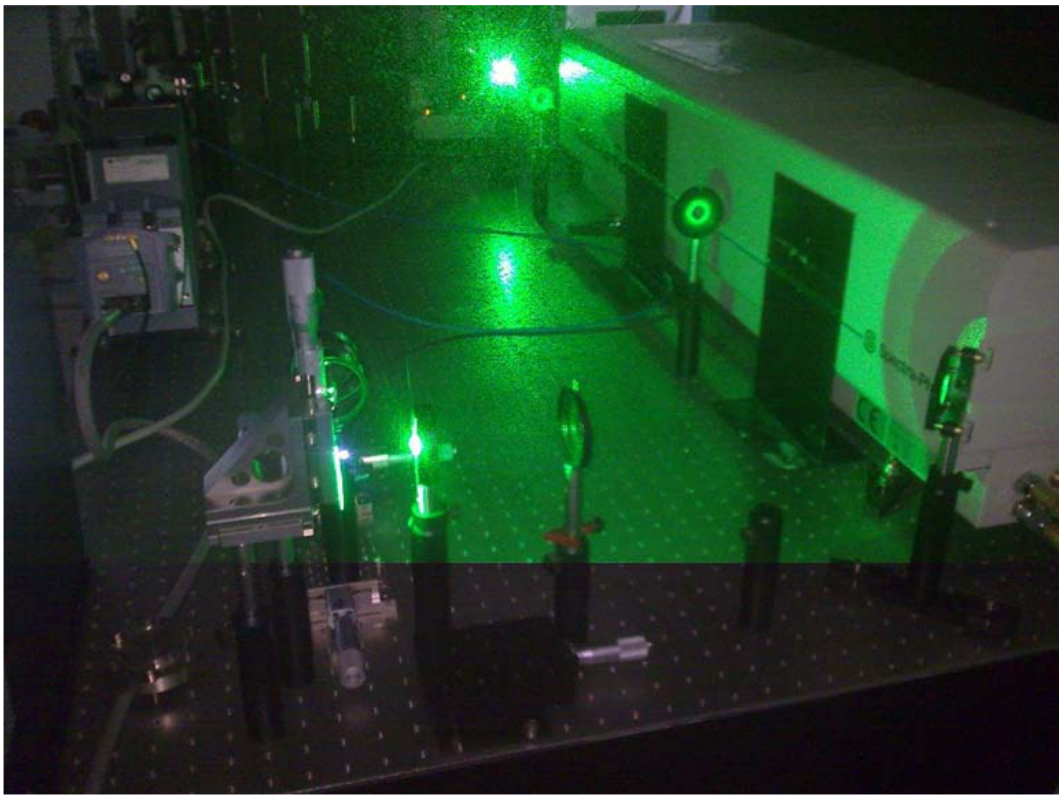

Figure 3.2. Actual view of the LIBS set-up.

In this setup, a Q-switched Nd:YAG laser source (Quanta-Ray Lab-170, Spectra Physics, California-USA) operating at its second harmonic wavelength, 532 nm, with 10 ns duration time is used. The laser beam is directed on the target by using 532 nm reflective mirrors (1" OD, coated, 532 nm reflective, *New Focus*), and is focused onto the sample surface via a plano-convex lens (1" OD, focal length:17.5 cm, *New Focus*). The laser pulse energy was one of the critical parameters that could affect the LIBS measurements. The laser pulse energy is measured by a power meter (PE50BB-DIF-V2, Nova II, Ophir, Israel). A 17.5 cm F.L. focusing lens was placed 15 cm away from the target so that lens to sample distance (LTSD) was 2.5 cm shorter than the normal focusing position. In this configuration, the laser beam was nearly 1.3 mm in diameter and the whole droplet area could be ablated within a single laser shot. Samples were mounted on an XYZ-translation stage (*New Focus*) to provide fresh spots during sampling. The sampling position on the target with respect to the laser beam was controlled with a camera and a monitor system (*Honeywell, HMM9/HMM9X*). The emission from the luminous plasma was collected at an angle of 90^{o} with respect to the incoming laser beam. The emission collection part of the experimental set-up consists of two plano-convex lenses with 10 cm focal length (2" OD, *New Focus*), that the first one makes the emitted

light from the plasma parallel through the second lens and the second lens focuses the emitted light in front of the fiber optic cable. A fiber optic cable with 450 micrometers core diameter was used to carry plasma emission onto the entrance slit of an echelle spectrograph (*Mechelle 5000, Andor Inc.*) equipped with an intensified charged coupled device (ICCD) (*iStar DH734, Andor Inc*.). The spectrograph and detection system spectral range is between 200-850 nm with 0.08 nm resolution at 400 nm. The wavelength calibration of the detector was performed by using a Hg-Ar spectral calibration lamp. All specifications of the experimental LIBS set-up were listed in Table 3.1.

Table 3.1. LIBS system specifications

Q-Switched Nd:YAG laser	Quanta-Ray Lab 170, Spectra Physics
Power meter	PE50BB-DIF-V2, Nova II, Ophir (Israel)
Reflective mirrors	1" OD, coated, 532 nm reflective, New Focus, Darmstad,-Germany
Focusing Lens	17.5 cm, 1" OD, 245-335 nm coated silica, New Focus, Darmstad-Germany
XYZ translational stage	New Focus-9067 (Darmstad-Germany)
Collecting Lenses	10 cm, 2" OD, LA 4545, uncoated UV fused silca, Thorlabs
Fiber Optic Cable	P450-2-UV-VIS, 450 µm diameter
Echelle Spectrograph	Mechelle 5000, Andor, f/7 (European)
ICCD detector	iStar DH734, Andor Inc. (European)
Mercury-Argon Lamp	HG-1, Ocean Optics Inc.
Camera and monitor system	Honeywell, HMM9/HMM9X

3.2. Silicon-wafer Substrates

During the LIBS measurements, three different types of silicon wafer-based substrates were utilized for the analysis of aqueous samples. These commercially available substrates (*Nanografi Inc.)* were p-type silicon wafer (c-Si), thermally oxidized silicon wafer with 300 nm oxide layer coating (SiO_2+Si), and 300 nm silicon nitride layer

coated silicon wafer substrate (Si_3N_4+Si). Technical properties of all wafers used in this thesis study are given in Table 3.2., below.

Table 3.2. Technical Properties of silicon wafers.

	Prime CZ-Si wafer	Prime Si + SiO_2 wafer	Prime Si+Si_3N_4 wafer
Quality	Prime	Prime	Prime
Materials	CZ-Si	Si + SiO_2 (wet)	Si+Si_3N_4
Coating	None	300 nm	300 nm
Thickness	500 µm	500 µm	381 µm
Doping	Boron	Boron	Boron
Polished	Double Side	One side	Double side

Silicon is one of the most common elements on earth. Silicon wafers are also commonly used in electronics and technology. Silicon wafers with their flat and mirror-like surfaces and high purities are used for various purposes. Silicon wafers could be doped with different types of materials like gallium, indium, boron, and nitrogen. The type and amount of the dopant materials affect some electronic and optical properties of the silicon wafers highly (Ravindra, Marthi et al. 2015).

Silicon dioxide wafer (Hiller, Zierold et al. 2010) is produced at high temperatures ranging from 900 ºC – 1200 ºC. This thermal oxide layer provides higher uniformity and dielectric strength to the silicon wafer. Also, silicon dioxide wafers have a good thickness uniformity and high purity. The oxide layer on the silicon wafer is also produced by the wet oxidation method.

Silicon nitride has high-temperature strength, oxidation resistance, and good thermal shock resistance. Due to its excellent mechanical and thermal stability (Wilmart, El Dirani et al. 2019), it is the preferred choice of the material in extremely demanding applications, i.e. automotive parts, bearings, metal cutting tools, etc. Nitride-coating as a dielectric material is used for passivation layers. Due to low reflectivity and high absorptivity, thin layer nitride-coated surfaces are highly used in energy sector applications. Among several techniques, the chemical vapor deposition technique, based on the chemical reaction of gaseous nitrogen and silicon, is the most widely used one for the thin layer coating of nitrides. Some physical and mechanical properties of coated and un-coated Si-wafers are listed in Table 3.3.

Table 3.3. Mechanical and thermal properties of Si wafers.

	Si (min-max)	SiO_2 (min-max)	Si_3N_4 (min-max)
Density (g/cm^3)	2.28-2.38	2.17-2.65	2.37-3.25
Fracture Toughness ($MPa.m^{1/2}$)	0.7-0.9	0.62-0.67	1.8-6.5
Young's Modulus (GPa)	140-180	66.3-74.8	166-297
Melting Point (K)	1700-1723	~ 1600	2661-2769
Specific Heat (J/kg.K)	668-715	680-730	673-1100
Thermal Conductivity (W/m.K)	84-100	1.3-1.5	10-43
Dielectric Constant	11-12	3.6-4.2	9.5-10.5
Thermal Expansion ($10^{-6}/K$)	7-8	0.55-0.75	1.4-3.7

Before the experiments, each silicon substrate was cleaned with nitrogen gas to remove any dust particles. Then aqueous solutions were manually deposited on each silicon wafer substrates with a micropipette dispenser. 0.5 µL sample solutions loaded onto the silicon substrates is given below in figure 3.3. These droplets were dried at room temperature for about 5 minutes for LIBS measurements. After the liquid to the solid conversion process, solid residue on the substrate was placed on the translational stage to provide fresh spots during experiments. The sampling position of the solid residue on the substrate with respect to the focused laser beam was controlled with a camera and monitor system.

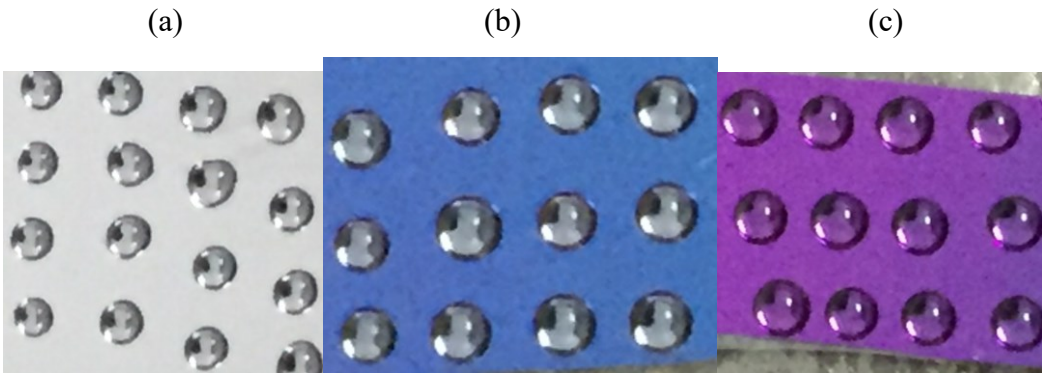

Figure 3.3. Picture view of the loaded 0.5 µL aqueous solutions on a)a p-type silicon wafer (c-Si), b) a thermally oxidized silicon wafer with 300 nm oxide layer (SiO_2+Si), and c) a 300 nm silicon nitride layer coated silicon wafer substrate (Si_3N_4+Si), before drying.

3.3. Focusing Geometry

LIBS measurements are normally performed by tightly focusing laser beam perpendicular to the sample surface with suitable optics. Focusing conditions of the laser beam highly affect the actual energy density at the sample during the measurements. The optical and geometrical focusing conditions have an important effect on plasma size, shape, and the spatial conditions of each element present in the plasma. Maximum irradiance conditions are obtained with the minimum focal area of the laser spot on the sample surface. At this condition, air breakdown is possible in front of the focal point of the lens. It could result in the observation of emissions from the dust particles present in the medium and also scattering of the laser beam occurs. Thus, the analytical performance of LIBS measurements is affected negatively. To eliminate this problem distance between the focusing lens and the sample is kept a little shorter than the focal length of the lens. In this situation, the laser beam is focused on the sample very shallowly, and the interaction area with the sample increases due to the larger spot size. Also, by using a more energetic laser pulse for plasma formation, plasma size gets bigger and enhancement in LIBS signal is observed.

In this thesis study, LIBS measurements were performed at the out-of-focus condition to provide an advantage from this optical geometry. The schematical representation of the focusing geometry used in this study is shown in Figure 3.4.

In the diffraction limit, the diameter of the laser beam at the focal point of the lens can be calculated as;

$$W_f = \frac{2.44 \times \lambda \times \mathrm{f}}{W_{uf}} \tag{1.2}$$

where; λ : wavelength of the laser, W_f:focused beam size, W_{uf}: unfocussed beam size

According to this formula, 22.7 μm focussed beam size is obtained from a Nd:YAG laser with a 10 mm unfocussed beam diameter and at the focal point of a 17.5 cm plano-convex lens. However, when the sample to lens distance is shortened and silicon wafer substrates were placed at 2.5 cm inside the focal point position, the laser beam size becomes around 1.3 mm diameter, which is large enough to cover the entire droplet area. With typically used laser pulse energies of 150mJ/pulse in this study, the power density of the laser pulses on the dried droplet region would be 1.13 GW/cm2, which is well

beyond a typical ablation threshold of $> 10^8$ W/cm^2 for most of the metals. Thus each larger laser pulse had the capability to ablate the entire droplet area within a single laser shot.

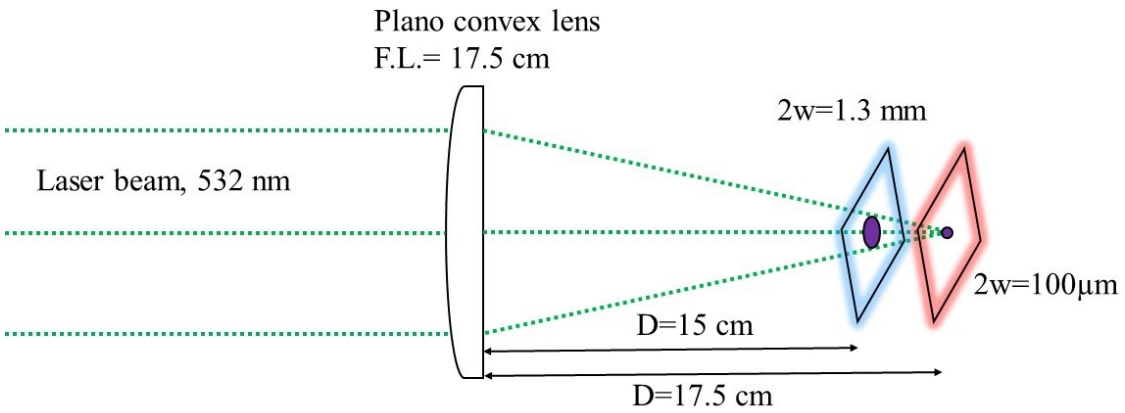

Figure 3.4. Schematic diagram of focusing conditions for LIBS measurements. D: Focusing lens distance to the target, F.L: focal length of a plano-convex lens, 2w: laser beam diameter.

3.4. Chemicals and Reagents

Aqueous standard solutions of Cadmium, Chromium, Copper, Manganese, and Lead were prepared from their stock solutions (1000 mg L^{-1}, High-Purity Standards) contained in 2% HNO_3, by suitable dilution with ultrapure water. All reagents were of analytical grade. Method validation studies were performed by using Certified Reference Material, Trace Metals in Drinking Water, CRM-TMDW-A (High-Purity Standards), and ICP Multielement Standard (AccuStandard) solutions.

Silicon wafer-based substrates; crystalline silicon wafer (c-Si), a thermally oxidized silicon wafer with 300 nm oxide layer on a crystalline silicon wafer (Si + SiO_2) and 300 nm silicon nitride layer on the crystalline silicon wafer substrate (Si + Si_3N_4) (Nanografi Inc.)., were used for manual loading of aqueous solutions on it, as purchased, without any pretreatment, except nitrogen gas purging for the removal of dust and undesired particles on it.

CHAPTER 4

RESULTS AND DISCUSSION

4.1. Optimization Studies

LIBS signal intensities should be maximized for each element at the analytical line of interest in the spectral region to enhance the analytical capability of LIBS analysis. For this purpose, optimization studies were carried out for each element, separately. The effect of the focusing geometry, sample volume, and instrumental LIBS parameters like detector delay time, gate width, and laser pulse energy on LIBS signal strength were investigated for each element. LIBS analysis of dried droplets were performed under these optimum conditions.

4.1.1. Focusing Geometry

Detailed information about optical and geometrical focusing conditions of the LIBS system was given in the experimental part of this thesis.

Optimization studies for focusing geometry were carried out by using an oxide-coated silicon wafer (Si + SiO_2) substrate. Here 0.5 μL copper solutions were placed on a Si +SiO_2 substrate surface by a micropipette. Then droplets on the substrate were left to dry at room temperature for 5 minutes. As shown in the SEM picture given in Fig. 4.1, the droplet dries nicely in a circular shape with about 1.3 mm diameter size, however, the distribution of the copper crystals was irregular on the substrate. It is certain that this uneven distribution will cause large variation in LIBS signal intensity from one pulse to another, if sampling is done with tightly focused laser pulses, laterally. Therefore, it requires a more careful sampling procedure at the focus condition.

In this study, in order to ablate the whole solid residue of the dried droplet on the silicon wafer substrate in a single laser pulse, the position of the focusing lens was kept at a distance to provide a laser spot size as large as 1.3 mm in diameter. The magnitude

of the laser spot at this ***"out-of-focus"*** condition was large enough to cover the whole droplet area for ablation.

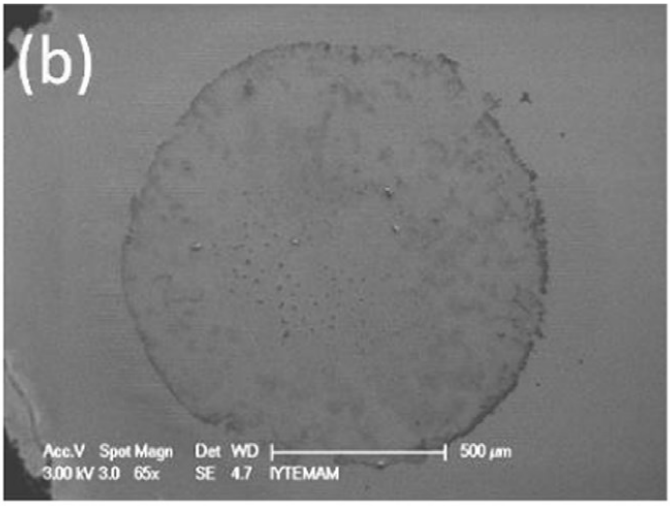

Figure 4.1. SEM images of 0.5 µL dried droplet of 1 mg L^{-1} copper solution on Si Si + SiO_2 surface.

A SEM picture of a crater after ablation with a laser beam size as large as dried droplet area at the out-of-focus condition is shown in Figure 4.2. It is clearly observed that the ablation is uniform all around the droplet area. One can assume that most of the solid residue from the droplet area was ablated within a single laser pulse as there was no remarkable LIBS signal was observed from the second and the subsequent laser pulses on the same sampling spot.

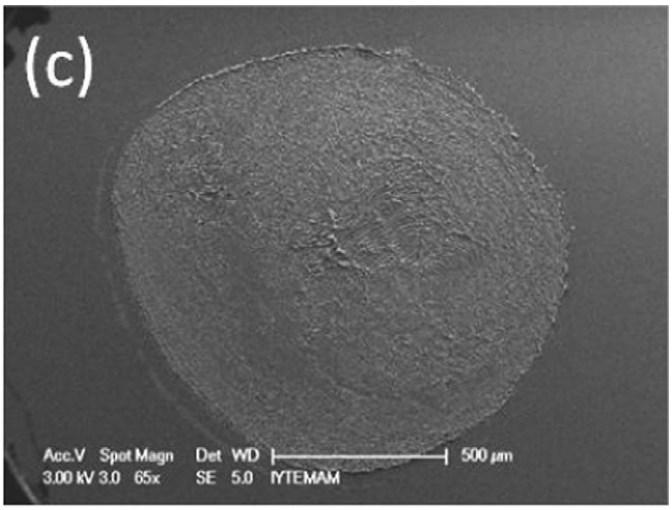

Figure 4.2. SEM images of a crater of a laser-ablated droplet by a 200 mJ single laser pulse on Si + SiO_2 surface at the out-of focus condition.

Craters formed from 16 side-by-side samplings in a single droplet area with tightly focused laser pulses of around 100µm in diameter are shown in Figure 4.3. Debris around the craters due to surface explosion and the contaminated area around the craters from the previous samplings is observed. Instead of making sequential sampling of a single droplet with a tightly focused laser beam, sampling the whole droplet area with a single laser shot could remove the variation on LIBS signals due to inhomogeneous deposition of the solid residue on the substrate. This way, sample losses are prevented and enhancement in LIBS signal is observed.

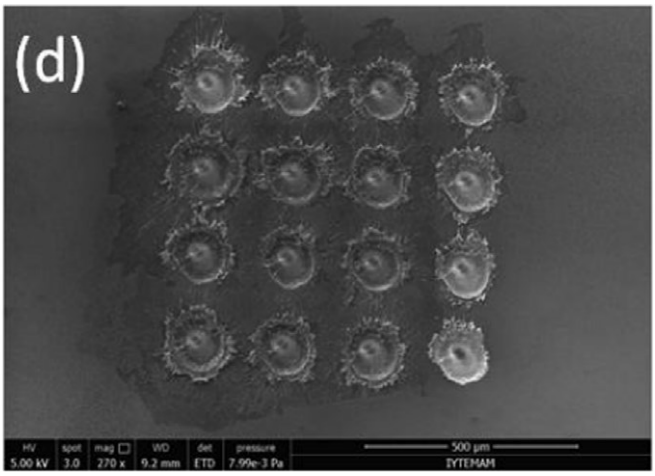

Figure 4.3. SEM images of 16 sequential samplings in a single droplet area with tightly focused laser pulses on Si + SiO_2 surface

In order to investigate the variations in LIBS signal strength with focusing geometry, experiments at the almost-minimum-focus and out-of-focus conditions were carried out with laser beam sizes of around 0.1 mm and 1.3 mm, respectively. For minimum focus experiments, 5 replicate droplets of 0.5 µL copper solutions were loaded on a Si + SiO_2 substrate manually by a micropipette dispenser. After drying at room temperatures, each droplet area was scanned in 16 different sampling positions by tightly focused laser pulses of 0.1-millimeter diameter and 5 mJ laser pulse energy. At each sampling position of the droplet, emissions from 5 repetitive laser pulses were acquired and stored separately for data analysis.

For out-of-focus experiments, sampling from 20 separate droplets of 0.5 µL copper solution on Si + SiO_2 substrate was performed. At this configuration laser pulses of 1.3-millimeter diameter and 200 mJ laser pulse energy were used. Irradiance values corresponding to specified pulse energies at the minimum-focus and out-of-focus conditions were 6.36 GW cm^{-2} and 1.51 GW cm^{-2}, respectively.

For statistical analysis of the acquired data, the most prominent lines of copper at 324.75 nm and 327.40 nm were selected. The relative signal strength of copper neutral emission lines at two different optical geometry conditions; the minimum-focus and out-of-focus, is given in Figure 4.4. Data presented as the solid line in the figure is from the minimum-focus position and acquired from the average of five droplets. In each droplet, summation of 16 different sampling positions and in each samplings positions accumulation of 5 repetitive pulses were used. Data at the out-of-focus condition, presented as a dashed line in the same figure, is from the average of single pulse samplings of 20 separate droplets.

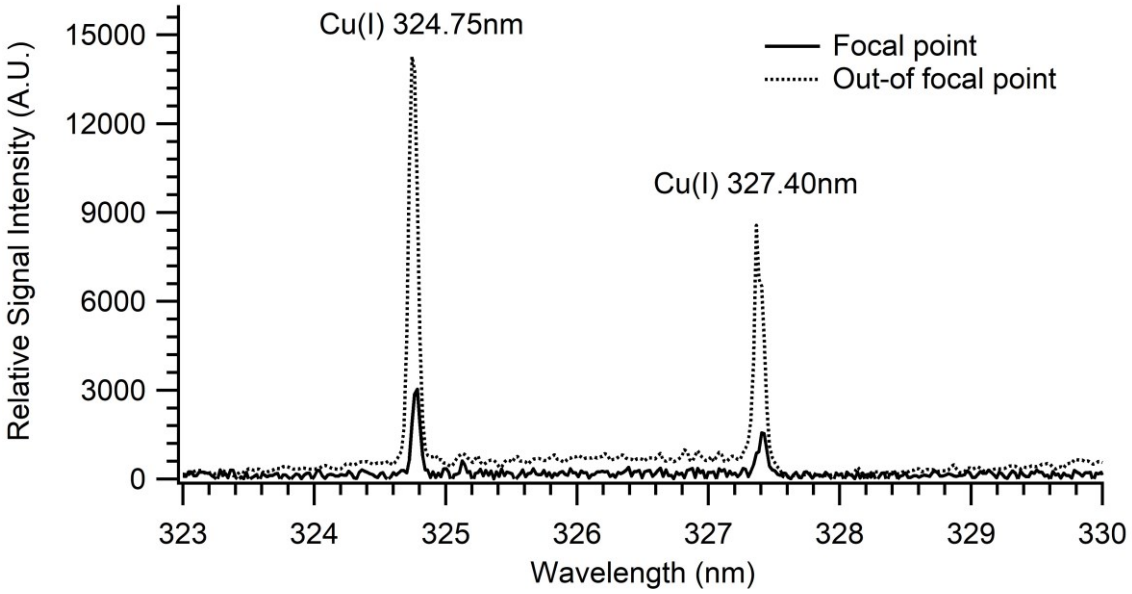

Figure 4.4. LIBS emission signals at the minimum focus and out-of-focus conditions for Cu(I) at 324.75nm and 327.40 nm.

Statistical analysis results of the optical geometry experiments for the copper line at 324.75 nm are given in Table 4.1. Experiments were carried out with 6.36 GW cm^{-2} and 1.51 GW cm^{-2} laser irradiances at the minimum focus and out-of-focus conditions, respectively. Signal to noise ratio (S/N) and relative standard deviation (RSD) of the measurements were calculated from the LIBS emission signal. The signal is defined as the peak area of the background subtracted line and noise is defined as three times the standard deviation of the background. The background is calculated from the vicinity of the analytical line of copper at 324.75 nm. As is shown in the table, more than 7 times enhancement in S/N at the out-of-focus position was obtained compared to the minimum-focus condition, although the laser irradiance value was almost 4 fold higher. In addition, % RSD of the signal to noise ratio values were 28% at minimum focus position and 16% at the out-of-focus position in which 2 times more improvement was observed at the out-of-focus position.

Table 4.1. Statistical analysis results of Cu(I) signal at 324.75 nm from the experiments at the minimum focus and out-of-focus conditions.

	Minimum focal point	Out of focal point
D (cm)	17.5	15
2w (μm)	100	1300
Laser energy (mJ)	5	200
Irradiance GW cm^{-2}	6.36	1.51
S/N	29	205
% RSD	28	16

D: focusing lens distance to the sample, 2w: laser beam diameter

4.1.2. Optimization of the Sample Volume

The effect of sample size loaded on the substrate in terms of complete removal of the sample and signal strength was investigated for Cd, Cu, Mn, and Pb elements. Different volumes of analyte solutions ranging from 100 nL to 700 nL were loaded on three types of substrates and then dried solid residue was analyzed by LIBS. The variation of the signal intensity with respect to the sample volume, for each element and substrate, is shown in Figures 4.5 to 4.8. Data are the average of the emission signals of each element from the first laser shots of five separate droplets. As shown in these figures signal intensities for all elements increases with sample volume. The higher variations in the emission intensity due to inhomogeneous distribution of the sample may decrease the performance of the dry droplet analysis by LIBS. However, each laser pulse was large enough to ablate the entire solid residue in the droplet area. Generally, an almost linear increase was observed up to the volume of 500 nL, for all elements and all substrate types. After this point, an increase in signal intensities slowed down. The reason for that decrease could be due to larger droplet sizes obtained with increasing sample volume and the laser pulse was not large enough to cover the entire droplet area for ablation. Therefore, 500 nL sample volume was selected as the optimum sample size throughout the experiments.

It is also observed that, except for Cd, signal strength was the highest for Si_3N_4 coated substrates compared to the other two substrates, SiO_2, and c-Si, for all elements.

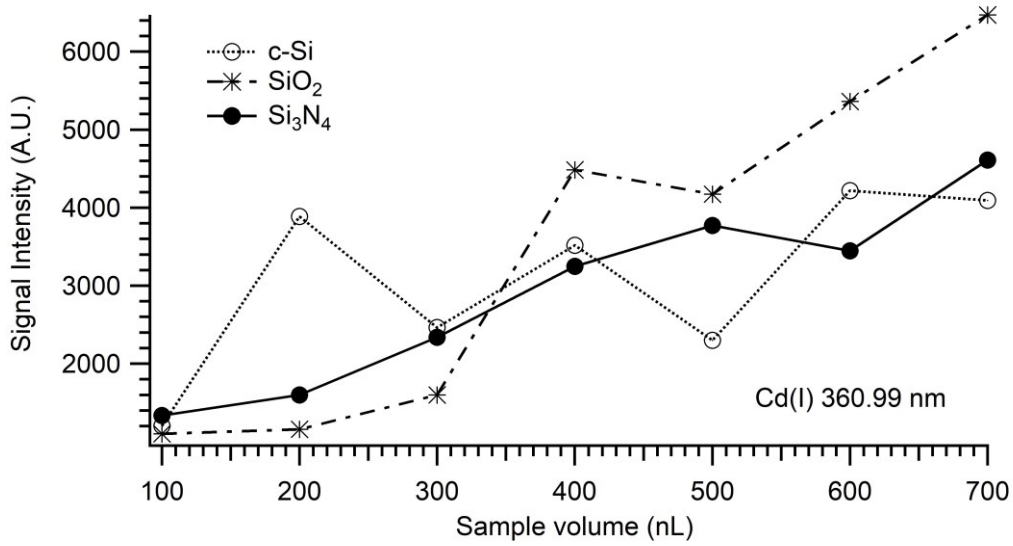

Figure 4.5. The effect of sample volume on Cd(I) signal intensity at 360.99 nm for c-Si, SiO_2, and Si_3N_4 wafers.

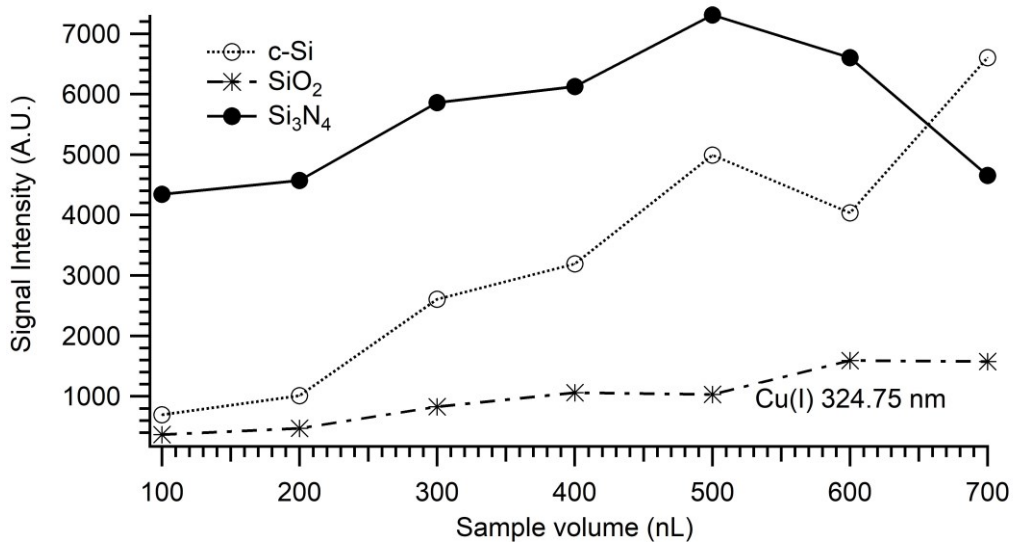

Figure 4.6. The effect of sample volume on Cu(I) signal intensity at 324.75 nm for c-Si, SiO_2, and Si_3N_4 wafers.

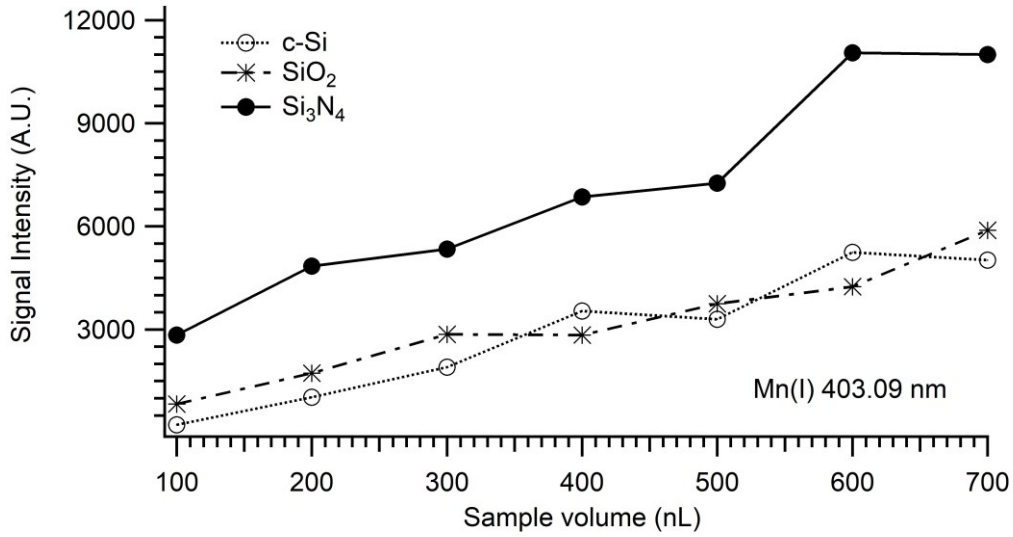

Figure 4.7. The effect of sample volume on Mn(I) signal intensity at 403.09 nm for c-Si, SiO_2, and Si_3N_4 wafers.

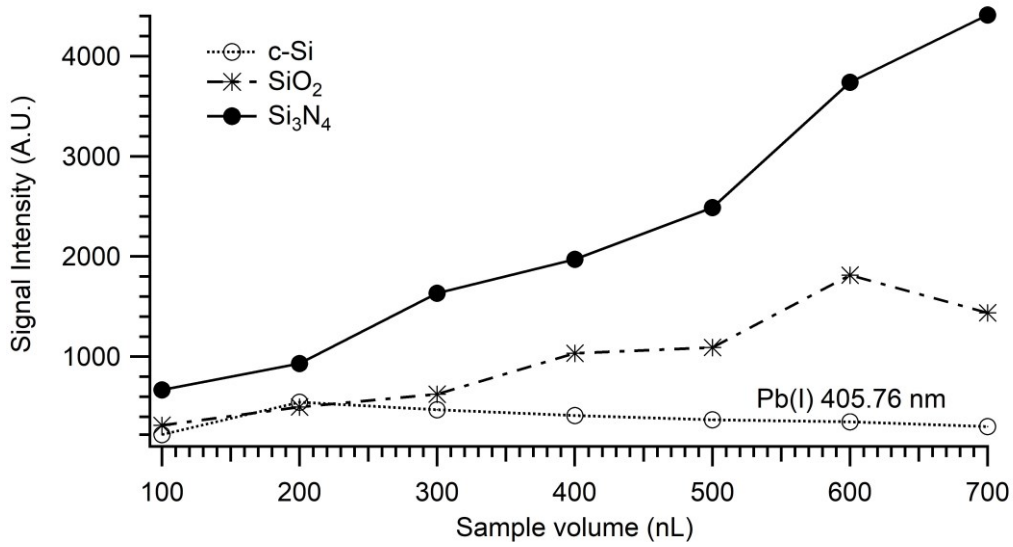

Figure 4.8. The effect of sample volume on Pb(I) signal intensity at 405.78 nm for c-Si, SiO_2, and Si_3N_4 wafers.

4.1.3. Optimization of the Instrumental Parameters

4.1.3.1. Detector Timing Parameters

A plasma is an electrically neutral local assembly of atoms, ions, and free electrons. Plasmas are mostly characterized by their degree of ionization like weakly and highly ionized plasmas. Laser-induced plasmas are mostly classified as weakly ionized plasmas so that the ratio of the number of electrons to other species is less than 10%. Also, spectral evolution of the LIBS plasmas is a time-dependent process. Ionization is higher at the early stages. Neutral atoms and then molecules form as electron-ion recombination occurs. Time resolution studies of the luminous plasma allow for discrimination and enhancement in favor of the region in which emission signals predominate. Time-resolved LIBS spectra exhibit a decrease in signal intensity as delay time increases and signal intensity of ionized lines decay faster than neutral lines.

To investigate the dependence of detector delay time and gate width on LIBS signals, plasma emissions from the analyte species was examined at various detector delay time and gate width with respect to the incoming laser pulse. The detector delay time was changed between 500 ns - 2 microsecond intervals and for gate width 250-750 microsecond ranges were used.

The optimum delay time and gate width values obtained from these studies for each element are listed in Table 4.2.

Table 4.2. Optimum experimental detector timing conditions for the spectral lines of interest. (t_d : delay time, t_g : gate width)

Element	Wavelength (nm)	t_d (µs)	t_g (µs)
Cd(I)	508.58	0.75	500
Cu(I)	324.75	1.75	500
Cr(I)	360.53	1.50	250
Mn(I)	403.08	1.00	750
Pb(I)	405.78	2.00	500

4.1.3.2. Laser Pulse Energy

Laser pulse energy is one of the critical factors that strongly affects the capability of LIBS measurements. Some of the phenomena regarding plasma parameters, like plasma temperature, degree of ionization, ablation, and breakdown thresholds are all depend on the magnitude of the laser pulse energy used. Also, the focusing geometry used in this work was different from that of the generally used minimum focus condition. Here, a relatively larger laser beam size on the orders of 1.3 mm in diameter is used. For this reason, the higher laser pulse energy is required to exceed the breakdown threshold of dried droplet residues.

In order to investigate the effect of the laser pulse energy on LIBS measurements in terms of signal strength of the analyte element, the magnitude of the laser pulse energy was changed from 70 mJ to 170 mJ. Energy dependence of LIBS signal intensities was investigated for Cadmium, Copper, Manganese, and Lead elements on three different substrates; crystalline silicon wafer (c-Si), thermally oxidized silicon wafer with 300 nm oxide layer (SiO_2+Si), and 300 nm silicon nitride layer on the silicon wafer substrate (Si_3N_4+Si). For the experiments, 0.5 µL aqueous solutions with 1 mg L^{-1} cadmium, copper, manganese, and lead concentrations were placed on each substrate. After drying,

solid residue on the substrates was subjected to energetic laser pulses. In the spectral range between 200-900 nm, the most prominent neutral emission lines for cadmium at 508.58 nm, copper at 324.75 nm, manganese at 403.09 nm, and lead at 405.78 nm were used for data analysis. The variation of LIBS signal intensity with respect to the laser pulse energy is given in Figures 4.9 - 4.12, for cadmium, copper, manganese, and lead, respectively.

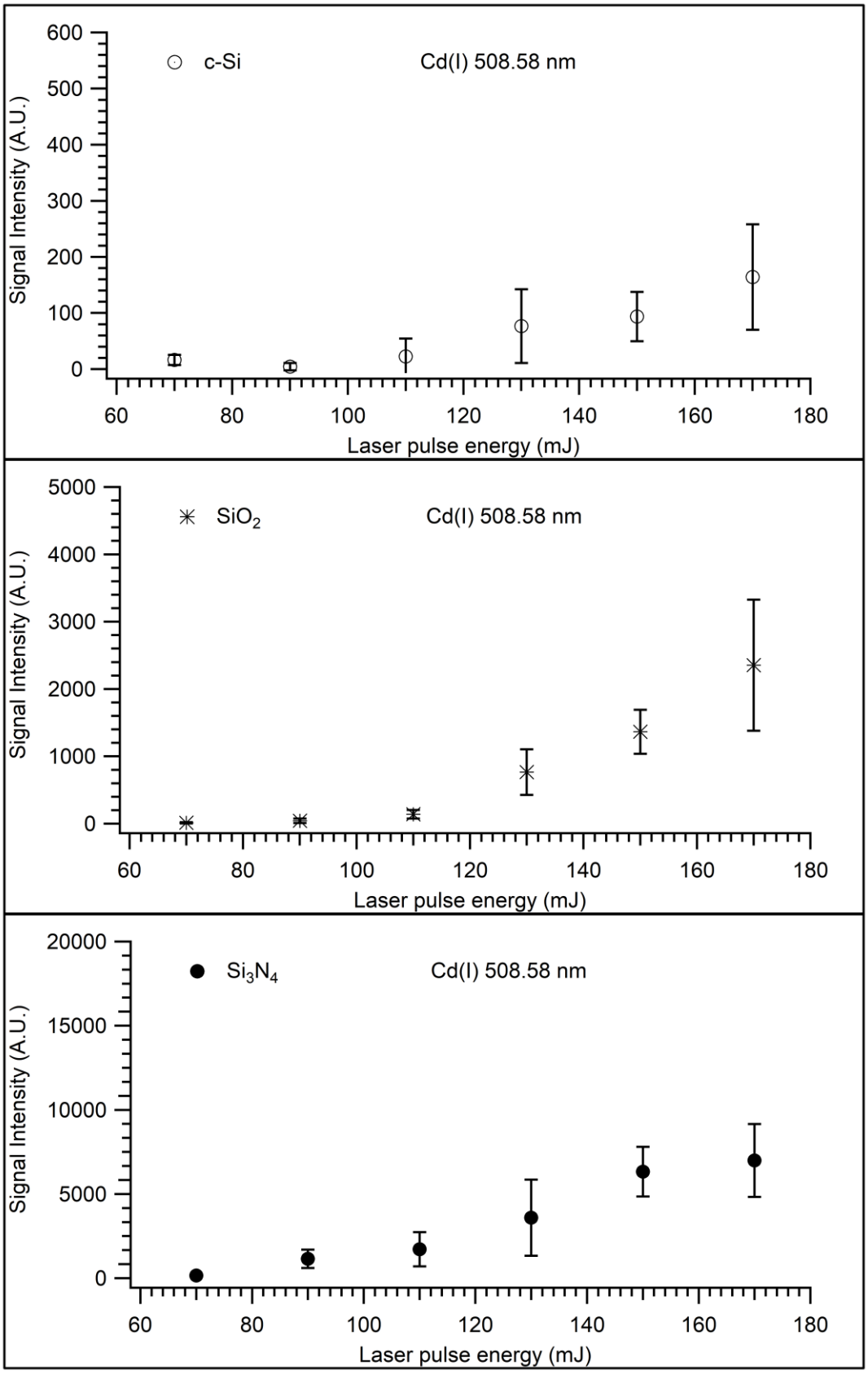

Figure 4.9. Variation of LIBS signal intensities with respect to the laser pulse energy for emission signal of Cd (I) 508.58 for c-Si, SiO_2, Si_3N_4 substrates.

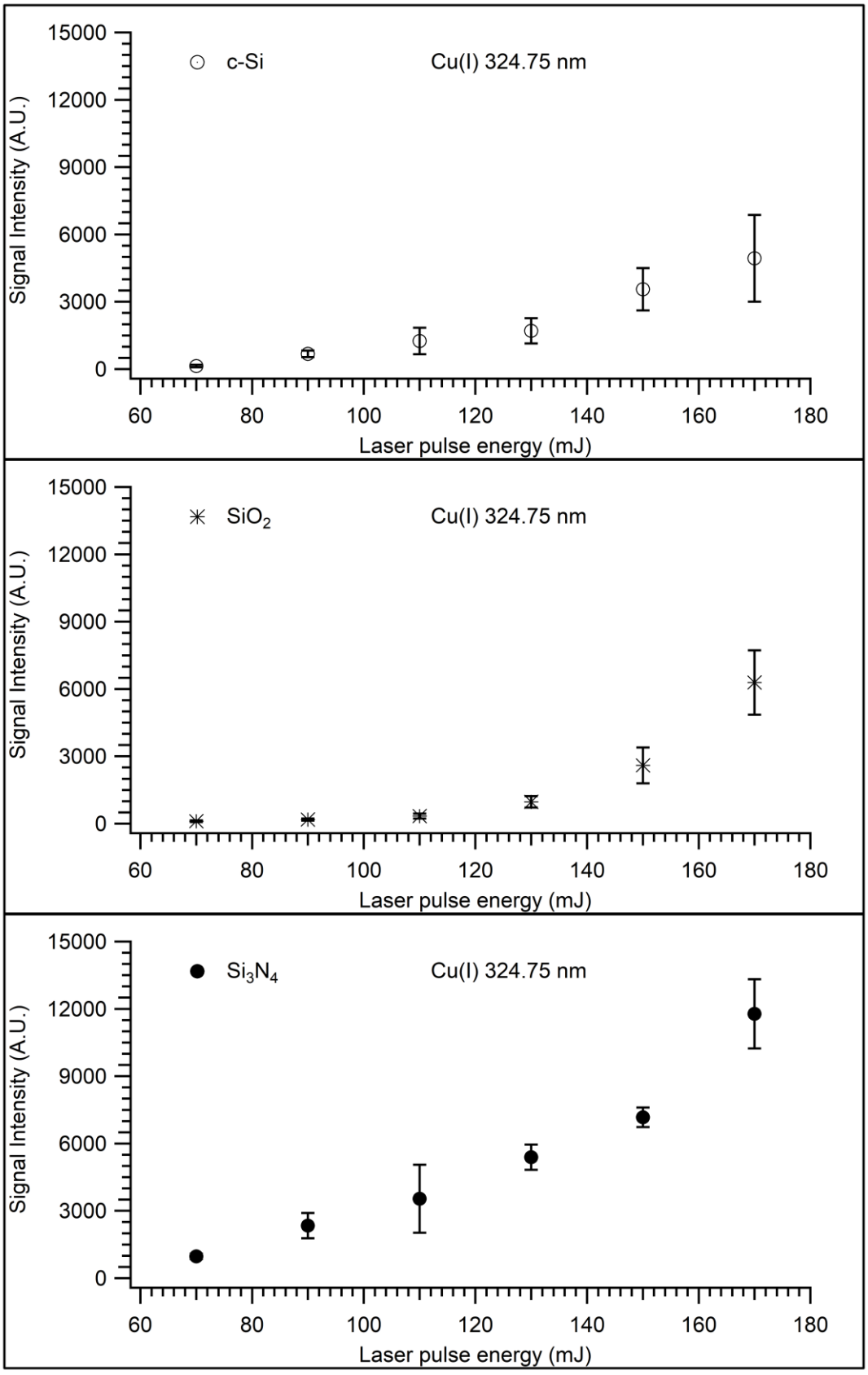

Figure 4.10. Variation of LIBS signal intensities with respect to the laser pulse energy for emission signal of Cu (I) 324.75 for c-Si, SiO_2, Si_3N_4 substrates.

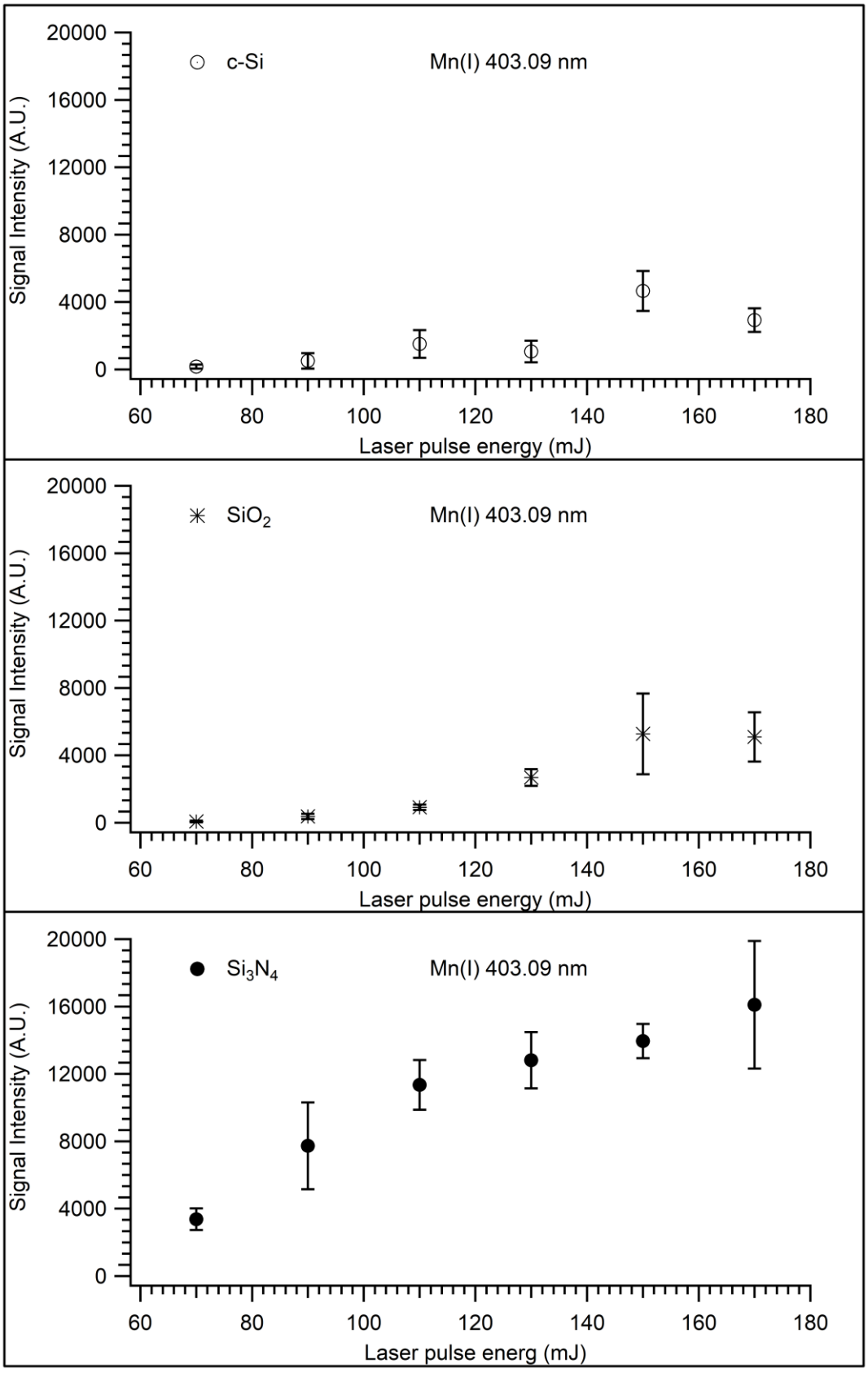

Figure 4.11. Variation of LIBS signal intensities with respect to the laser pulse energy for emission signal of Mn (I) 403.09 for c-Si, SiO_2, Si_3N_4 substrates.

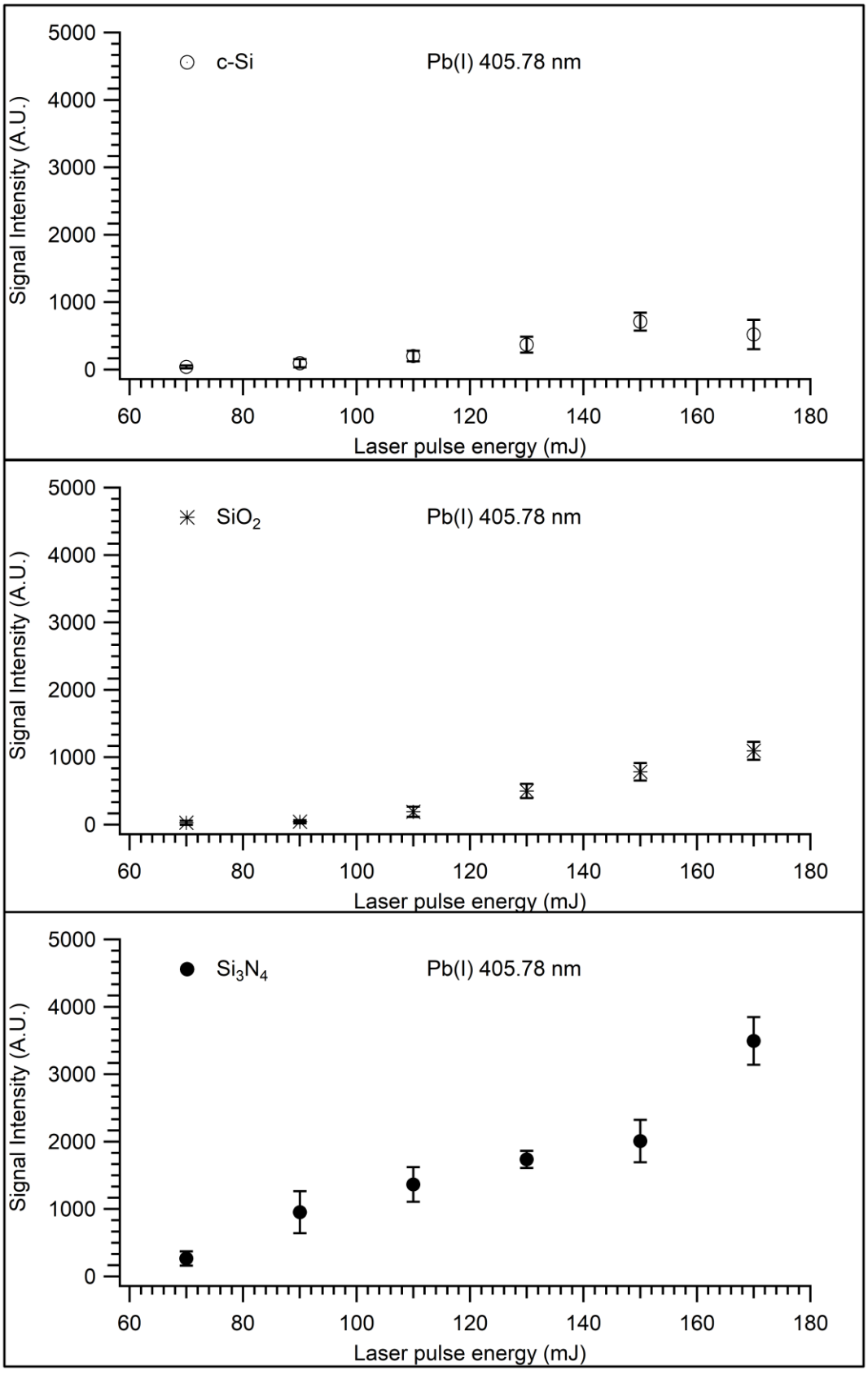

Figure 4.12. Variation of LIBS signal intensities with respect to the laser pulse energy for emission signal of Pb (I) 405.78 for c-Si, SiO_2, Si_3N_4 substrates.

In general, for all elements and substrates investigated, signal intensities with respect to the laser pulse energy were linearly increased. Between 70-170 mJ pulse energy range studied, 150 mJ laser pulse energy was determined as an optimum energy value. At laser pulse energies higher than 150 mJ, signal strength was also higher however, these signals suffered from the high noise signal and higher standard deviation. Also, at higher laser fluence, plasma shielding is more likely to occur which could result in nonstoichiometric ablation. Therefore, 150 mJ laser pulse energy was chosen to be the optimum value for all measurements with sufficiently strong signal and low noise in the spectra.

4.2. Analysis of the Silicon Wafer Based Substrates by LIBS

Before the analysis of the analyte solution by LIBS, the content of the silicon wafers was identified under optimum conditions. Substrates must be free from line emissions that may overlap with that of analyte emission. For this purpose, LIBS measurements were performed in order to determine possible spectral interferences due to substrate emission and also from the blank solution. LIBS analysis of substrates with and without blank solution loaded on the wafer substrates were carried out to identify the chemical composition of each substrate and blank solution. Analyses were performed under the same experimental conditions and representative LIBS spectra for all types of substrates, and blank solutions between 200-900 nm spectral intervals are shown in Figures 4.13, 4.14, and 4.15. It is clearly seen that the emission spectrum of all substrates are similar. The spectral regions in which emissions of matrix elements observed, including silicone, Si(I) at 288.15 nm, magnesium, Mg(I) at 279.55 nm and 280.27 nm, calcium, Ca(I) at 393.37 nm and 396.85 nm, and sodium, Na(I) at 589.0 nm and 589.6 nm are shown at the bottom of each figure. It is seen from enlarged overlay spectra that, the emissions of Ca, Mg, and Na are more intense in blank-containing substrate indicating the presence of impurities in the content of ultrapure water. Here, another difference observed among the substrates was the highest responses exhibited by Si_3N_4 coated substrate.

The presence of magnesium, calcium, sodium along with silicon represents the impurities in c-Si, SiO_2, and Si_3N_4 substrates.

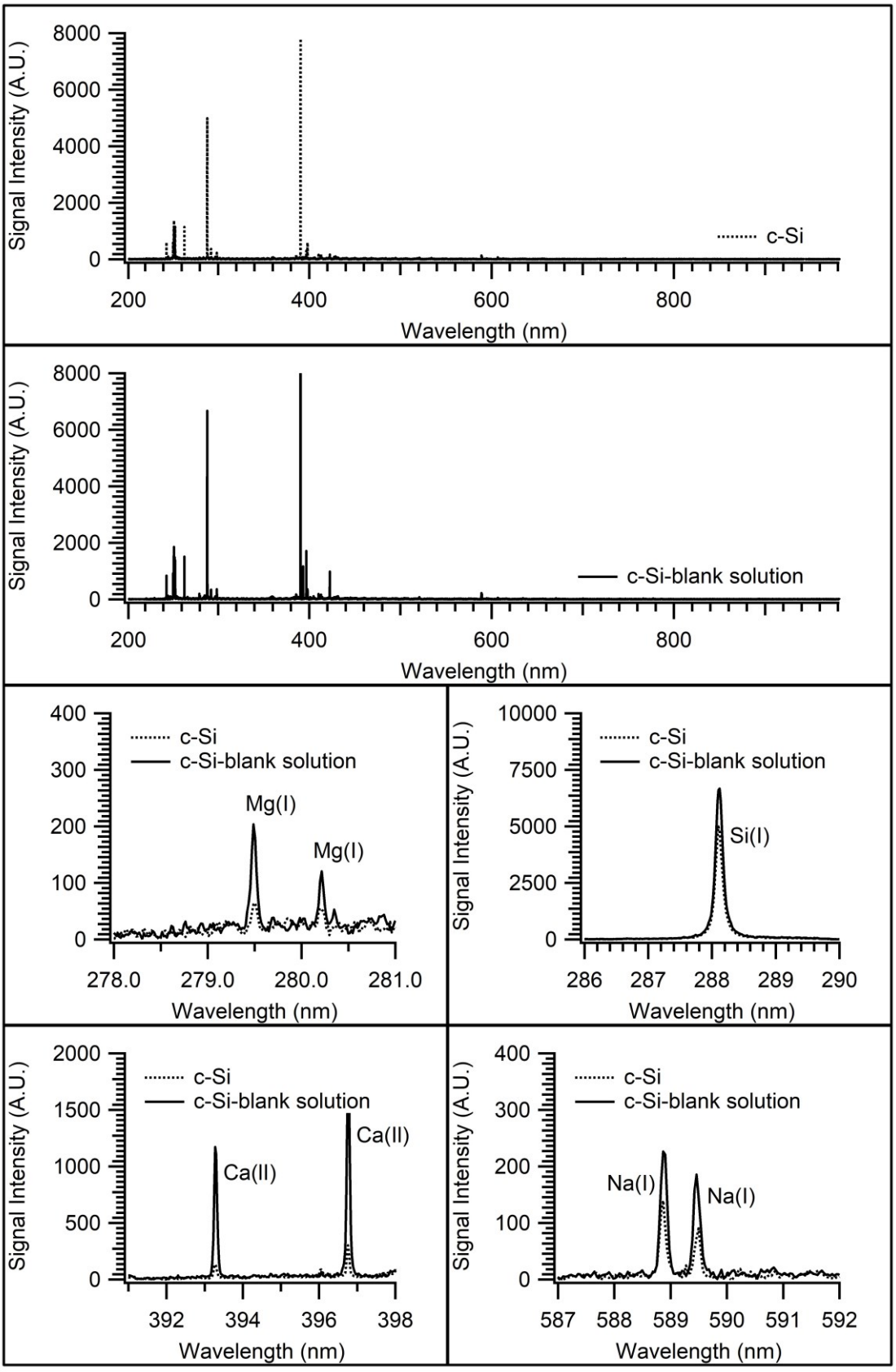

Figure 4.13. Full spectra of the c-Si wafer and c-Si wafer contained a blank solution. Enlarged viewing of the spectral regions in which matrix emissions are observed

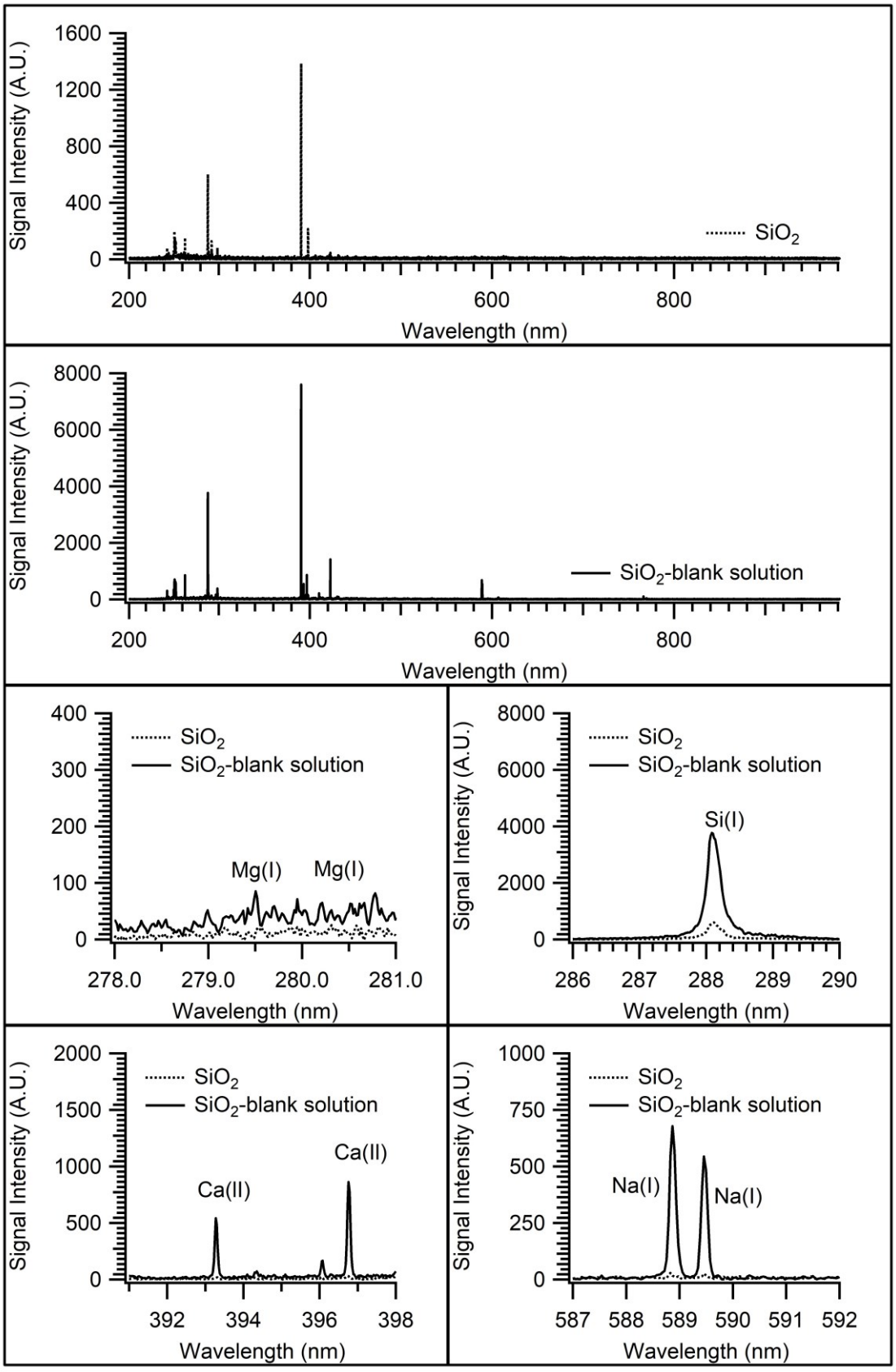

Figure 4.14. Full spectra of the SiO_2 wafer and SiO_2 wafer contained blank solution. Enlarged viewing of the spectral regions in which matrix emissions are observed.

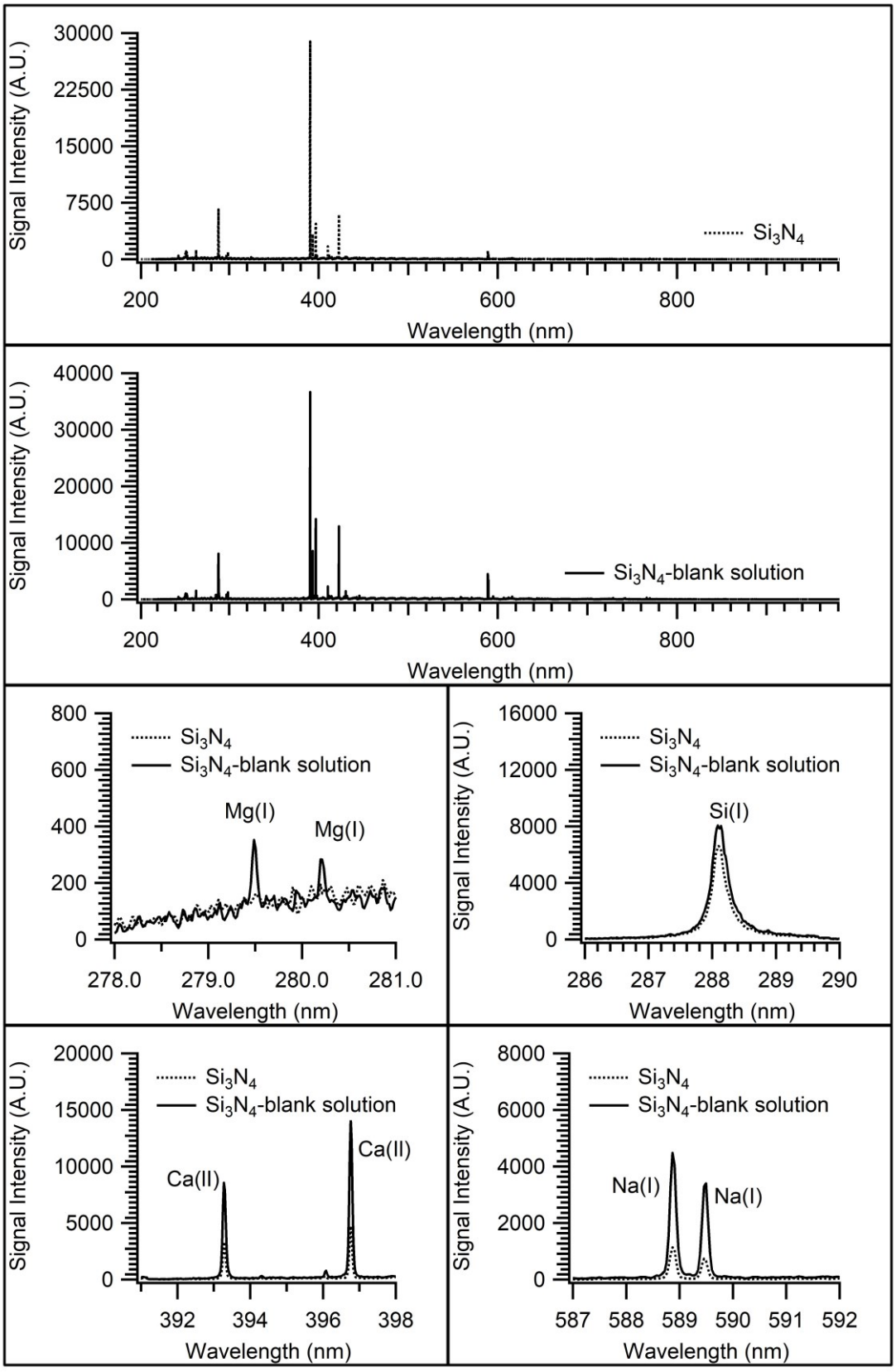

Figure 4.15. Full spectra of the Si_3N_4 wafer and Si_3N_4 wafer contained blank solution. Enlarged viewing of the spectral regions in which matrix emissions are observed.

To see the presence of analyte signals in the substrate and blank solution, spectra within the specific region of interest of each element were also examined. Overlay spectra of with and without a blank solution for cadmium, copper, chromium, manganese, and lead are shown in Figures 4.16, 4.17, and 4.18 for c-Si, SiO_2, and Si_3N_4 substrates, respectively. As shown in these figures no analyte signals were observed for all substrates in both cases. Possible spectral interferences that may occur in these regions are negligible for all substrates. Thus, all silicon-based substrates could be used for dried droplet analysis of the selected elements.

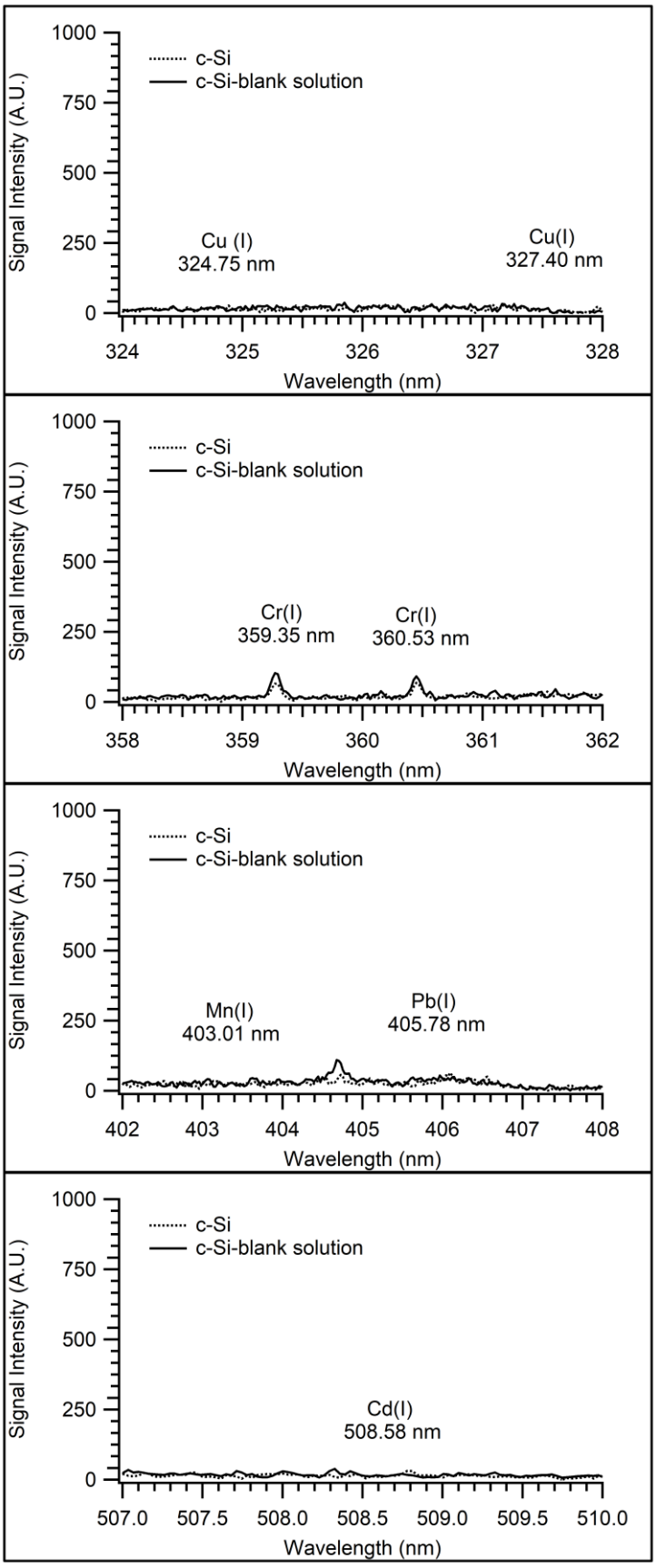

Figure 4.16. Enlarged viewing of the spectral regions of the c-Si substrate in which analyte emission signals are observed.

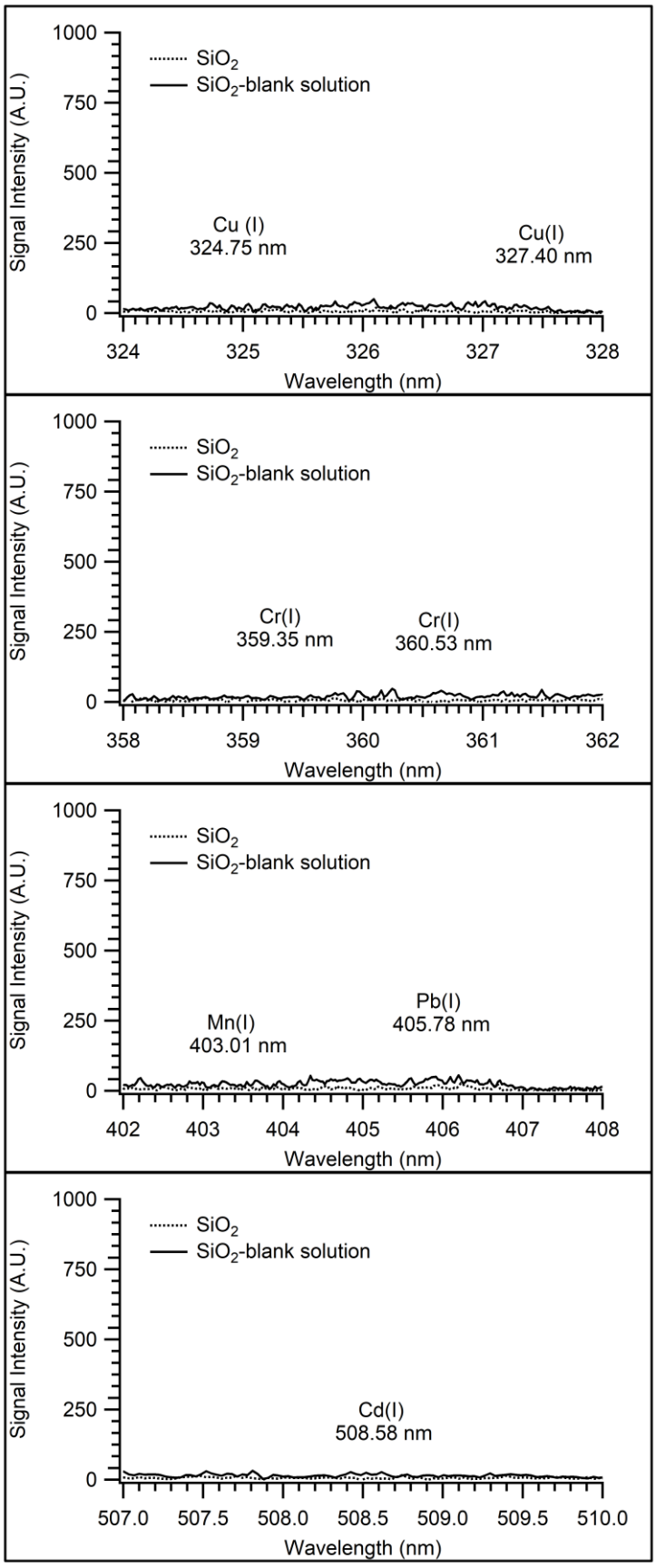

Figure 4.17. Enlarged viewing of the spectral regions of SiO_2 substrate in which analyte emission signals are observed.

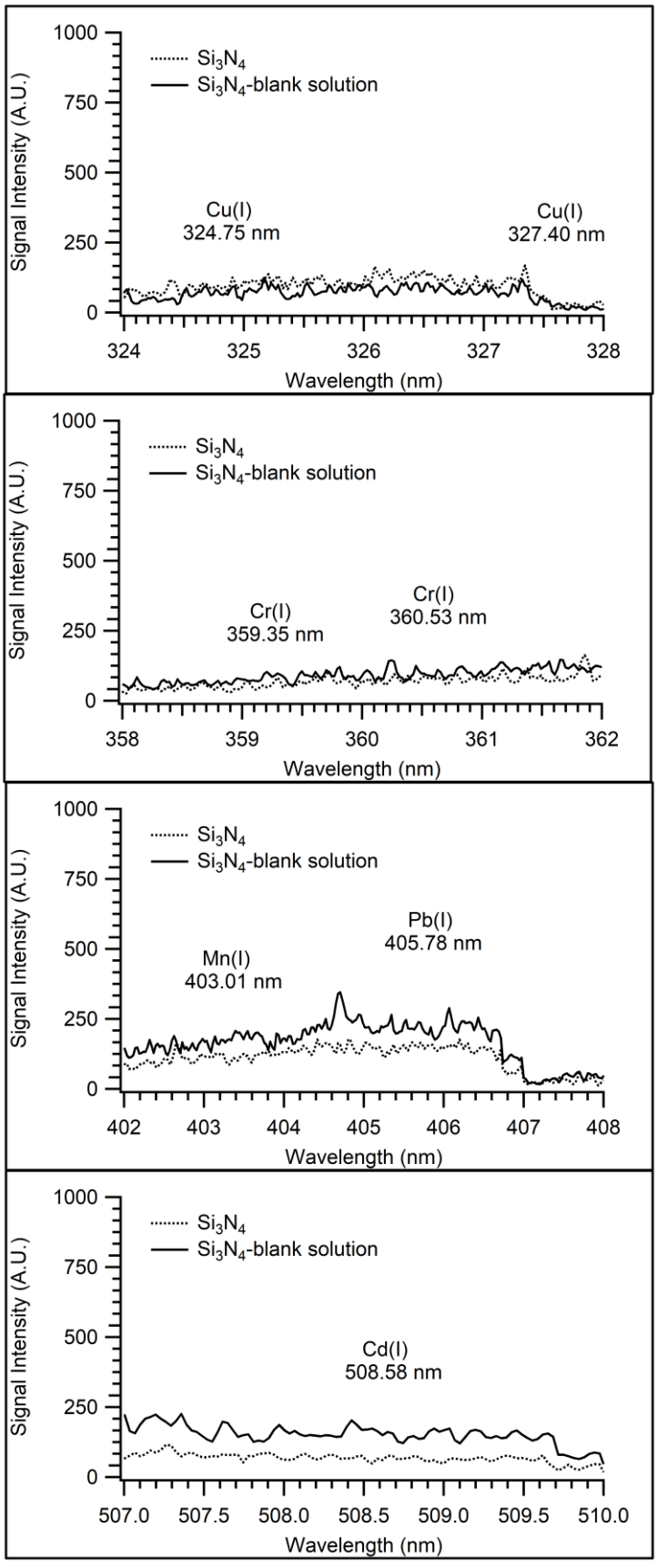

Figure 4.18. Enlarged viewing of the spectral regions of Si_3N_4 substrate in which analyte emission signals are observed.

4.3. Characterization of Substrates by SEM-EDX

Surface characteristics of the c-Si, SiO_2 and Si_3N_4 substrates were identified through SEM images and surface roughness measurements. Microscopic images of the three surfaces are given in figures 4.19, 4.20, and 4.21. The bright surface of the wafers resembles a mirror. The surface roughness is very low with an ultra-smooth surface. In order to obtain an elemental composition and quantitative compositional information about silicon wafers, EDX analyses were also performed. According to EDX results given in Tablo 3.4, no interfering elements are present on the bare/coated substrates. Weight percentages of 100 % silicon for c-Si wafer, 26.51 % oxygen and 73.49 % silicon for SiO_2 wafer, and 70.07 % silicon and 29.93 % nitrogen for Si_3N_4 wafer were obtained. EDX results support the results obtained by LIBS and each substrate contains just related elements. According to the chemical composition of the substrates, dried droplet analysis could perform without spectral interference by LIBS.

The results from EDX analyses are in agreement with LIBS analysis results and some of the elements like magnesium, sodium, calcium were also detected. This is due to the limitation of the detection limits by EDX with respect to the LIBS.

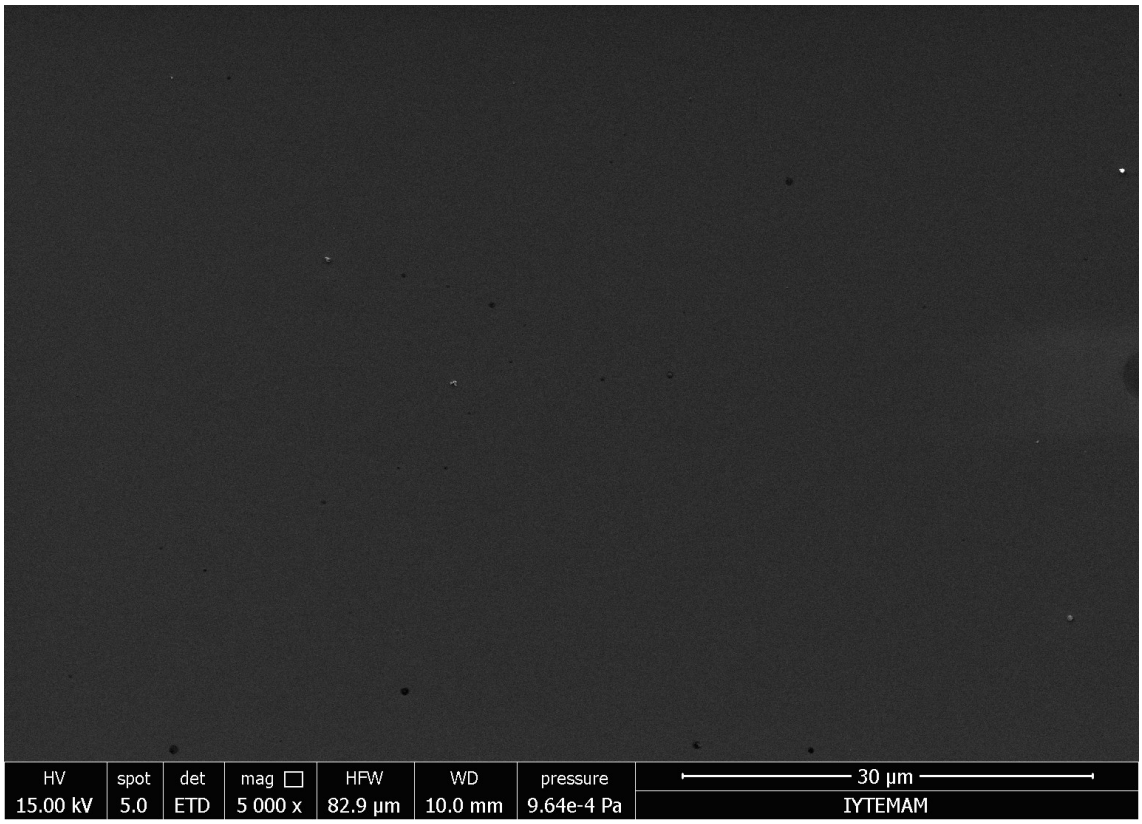

Figure 4.19. SEM image of a bare c-Si wafer.

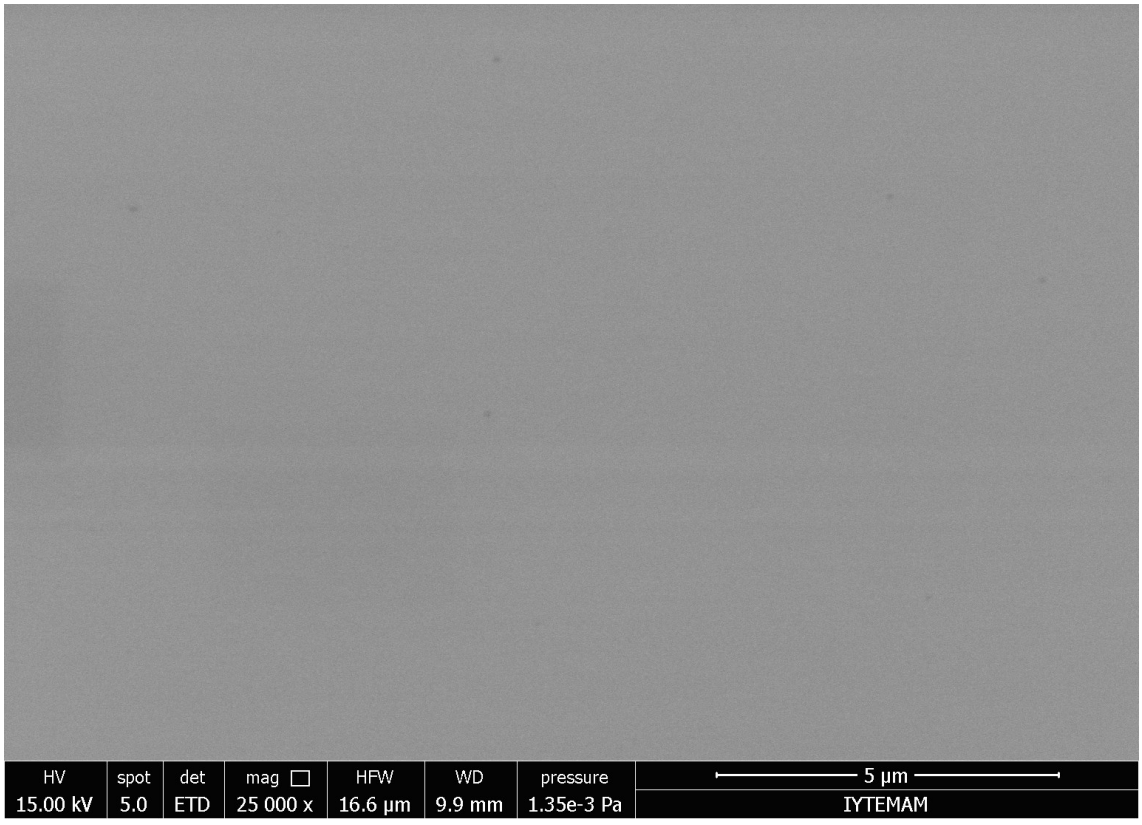

Figure 4.20. SEM image of SiO_2 wafer.

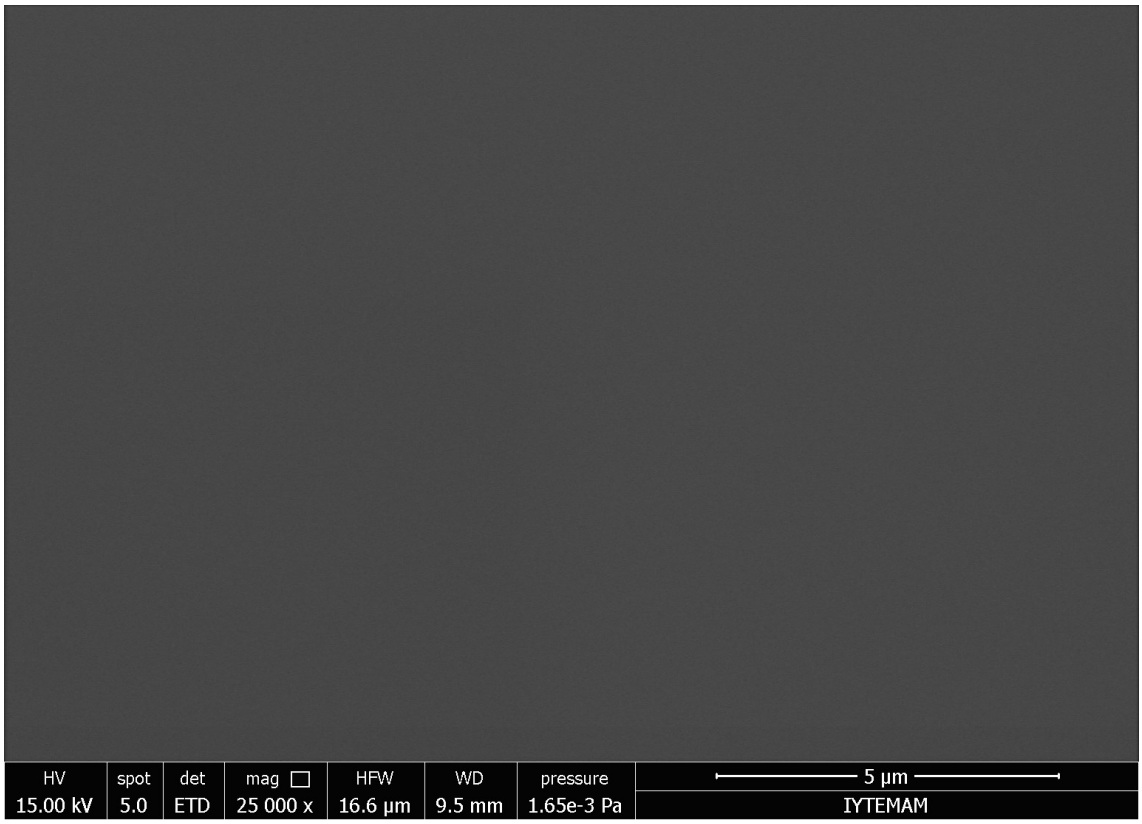

Figure 4.21. SEM image of Si_3N_4 wafer.

Table 4.3. EDX results of silicon wafer substrates.

c-Si			SiO_2			Si_3N_4		
Elements	Wt %	Atomic %	Elements	Wt %	Atomic %	Elements	Wt %	Atomic %
Si	100	100	Si	73.49	61.23	Si	70.07	53.87
-	-	-	O	26.51	38.77	N	29.93	46.13
Total	100	100	Total	100	100	Total	100	100

4.4. LIBS Analysis of Cd, Cr, Cu, Mn and Pb on Silicon Wafers

Laser-induced breakdown spectroscopic analysis of Cd, Cr, Cu, Mn and, Pb droplets on c-Si, SiO_2, and Si_3N_4 wafers was performed under the optimum instrumental conditions with laser pulses 1.3mm in diameter and around 150 mJ/pulse energy. Representative LIBS spectra obtained from these analyses for c-Si, SiO_2, and Si_3N_4 coated wafers under optimum experimental conditions are shown in Figures 4.22, 4.23, and 4.24, respectively. Signals from the prominent emission lines of each element are given, in each spectrum, enlarged.

For acquiring data, 0.5 µL aqueous analyte solutions of 1 µg mL^{-1} concentration were placed on each substrate, and these droplets were dried at room temperature in about 5 minutes. Then, solid residue with approximately 1.2 mm in diameter on substrates was ablated with a single laser shot of 1.3 mm spot size. In each spectrum, the regions in which the most prominent emission lines of each element are observed are also presented. As it can be seen in the figures 4.22, 4.23 and 4.24, the analyte emissions signals corresponding to 500 pg of each element (500nL* 1 mg/L) are clearly observed with high sensitivity in a single laser shot. Besides, strong emission lines of silicon (at 263.13 nm, 288.15 nm, and 390.55 nm), calcium (at 393.37 nm 396.85 nm, and 422.67 nm), sodium (at 589.0 nm and 589.6 nm) and, magnesium (at 279.55 nm and 280.27 nm) were also observed due to the content of substrates.

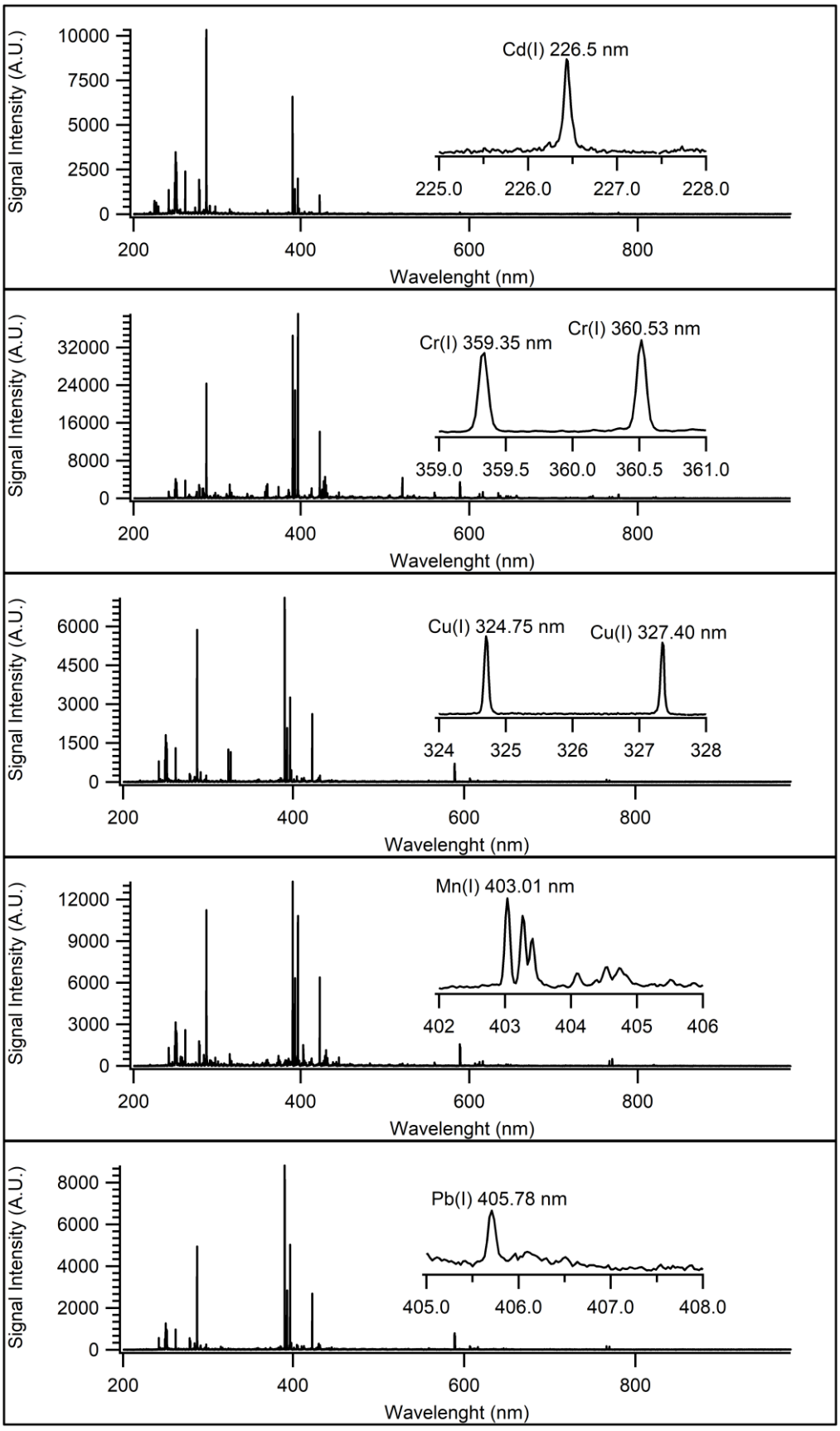

s

Figure 4.22. Full spectra of the c-Si substrate. Enlarged viewing of the regions where analyte emissions are observed.

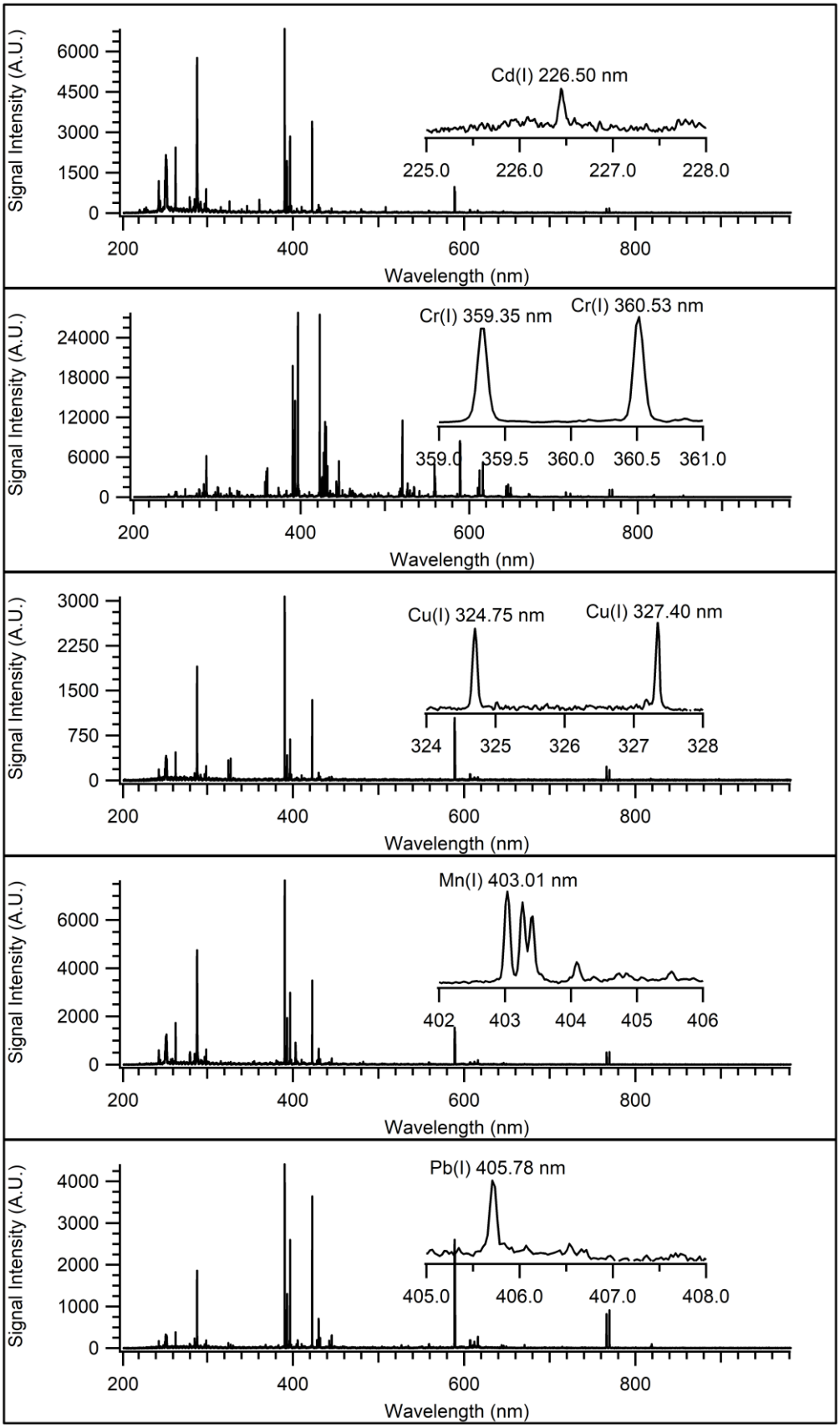

Figure 4.23. Full spectra of the SiO_2 substrate. Enlarged viewing of the regions where analyte emissions are observed.

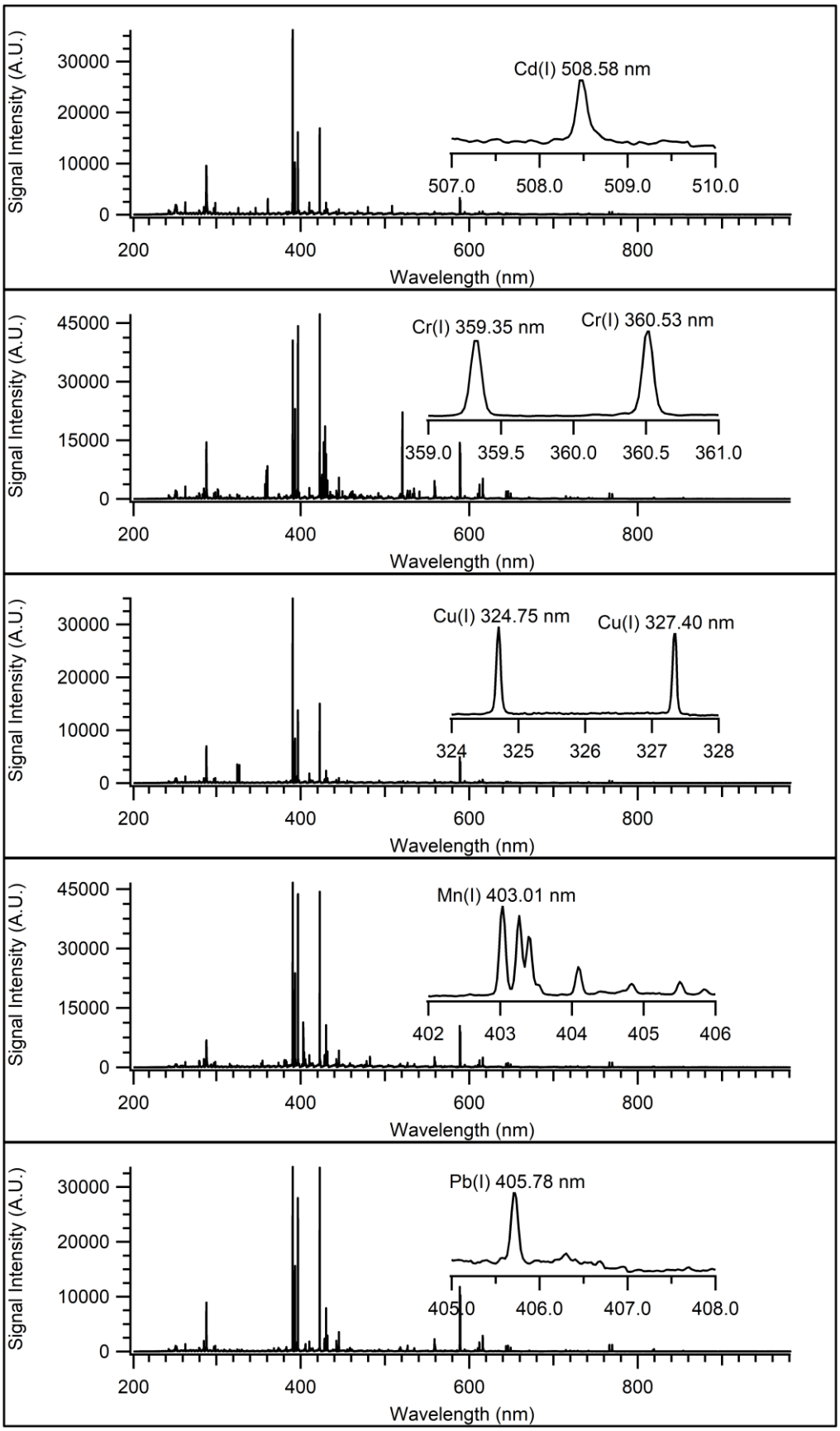

Figure 4.24. Full spectra of the Si_3N_4 substrate. Enlarged viewing of the regions where analyte emissions are observed.

4.5. Effect of Substrate Type on LIBS Analysis

Within the content of this thesis study, the type of substrate on analyte signal enhancement was studied. For this purpose, 0.5 µL, 1mg L^{-1} concentration analyte solutions dried on three different substrates, and LIBS analysis was performed under optimum experimental conditions. For each element studied, overlay spectra of the three substrates; c-Si, SiO_2, and Si_3N_4, for the elements of Cd, Cr, Cu, Mn, and Pb are shown in Figure 4.25. Data are obtained from the average signal of 5 droplets, each exposed to a single laser shot. Each analyte emission signal is background subtracted for data processing and quantification purposes.

As is clearly seen in the figure, the most intense analyte emission signal is always obtained from the Si_3N_4 coated substrate, for all the elements. The enhancement factors of Si_3N_4 coated substrate are calculated by rationing the signal strength of the analyte on nitride-coated substrate to that of c-Si and SiO_2 wafers and are listed in Table 4.4.

Maximum enhancement factors were observed for cadmium line emission at 508.58 nm in which 11 and 62 times enhancements with respect to SiO_2 and c-Si substrates were obtained. Signal enhancements varying from 3 to 12 were obtained for Cu, Mn, and Pb elements with the use of Si_3N_4 substrate with respect to the c-Si and SiO_2 ones. The minimum enhancement factors were obtained for the element of chromium in which Si_3N_4 substrate showed 2-3 times enhancement on LIBS results with respect to the c-Si and SiO_2 wafers.

These calculated enhancement factors are element dependent and vary from one element to another due to several factors however, emission signals observed on Si_3N_4 substrate were always more intense than others. Silicon nitride wafers are used in various fields due to their superior thermal and mechanical properties like high strength and fracture toughness at high temperatures. Also, the silicon nitride layer is used as an anti-reflection layer to reduce light reflection losses.

In order to further investigate the signal enhancements effect observed with silicon nitride wafers, compared to oxide coated and c-Si wafer, the reflectivity and surface characterization studies of the substrates were performed.

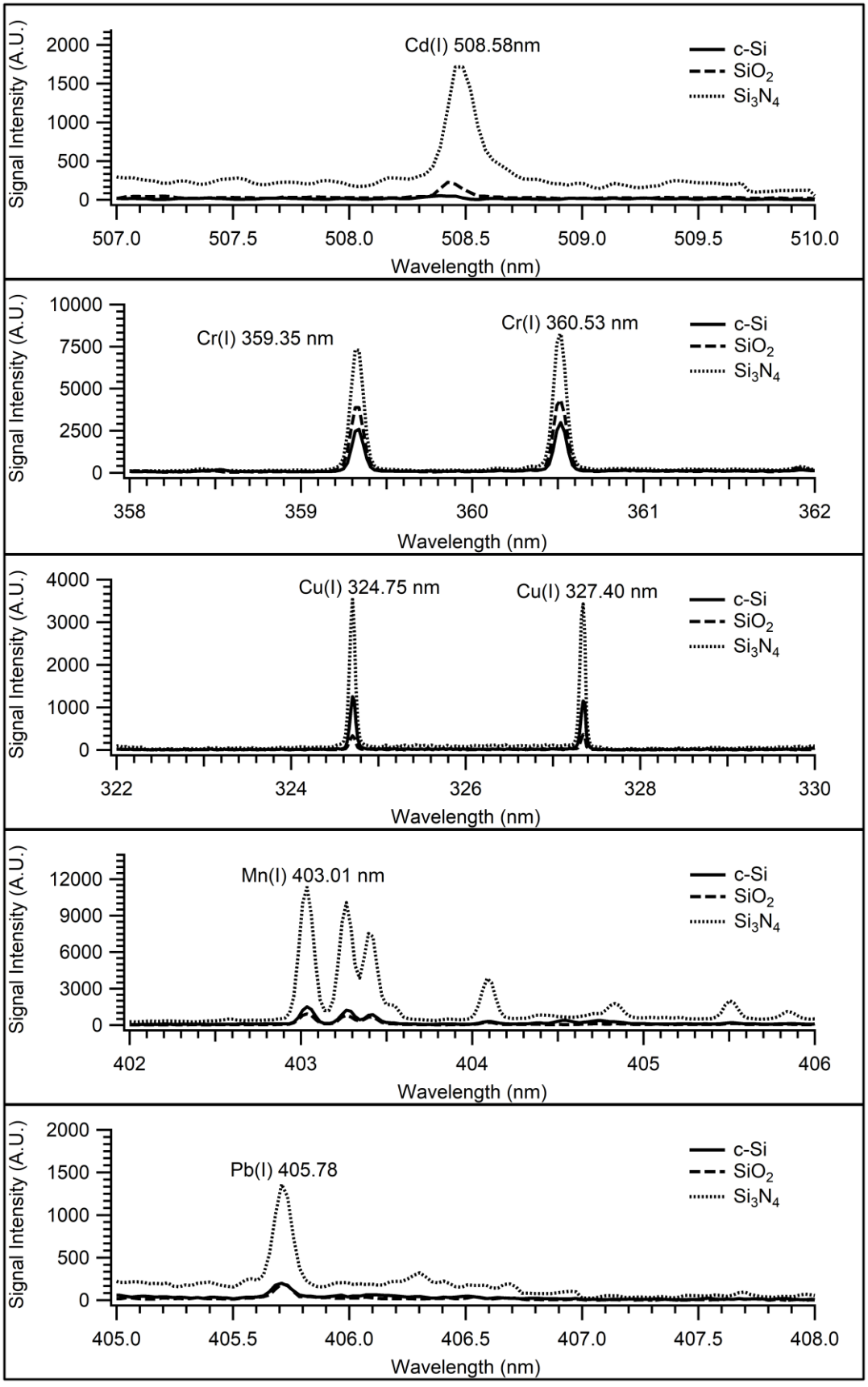

Figure 4.25. LIBS spectral regions representing the emission lines of Cd(I), Cr(I), Cu(I), Mn(I), and Pb(I) on the three silicon wafer-based substrates.

Table 4.4. Signal enhancement factors observed Si_3N_4 substrate over the c-Si and SiO_2 substrates.

Analyte	Enhancements factors	
	c-Si	**SiO_2**
Cd(I) 508.58 nm	62	11
Cr(I) 360.53 nm	3	2
Cu(I) 324.75 nm	3	11
Mn(I) 403.08 nm	8	12
Pb (I) 405.78 nm	7	6

4.5.1.Reflectivity Measurements of the Silicon Wafers

In the laser ablation process, some of the physical and chemical properties of the material like reflectivity, boiling point, heat of vaporization, and specific heat have a very important role. Reflectivity, a physical parameter that could affect the amount of ablated solid material from the surface, is by definition the ability of a surface to reflect radiation (Skoog, Holler et al. 2017). It has been shown by Benavides et. al that the total reflectivity of a surface is a function of laser fluence and at low fluences, the reflectivity is higher with no surface damage (Benavides, De la Cruz May et al. 2013). At higher fluences, where the plasma formation thresholds are approached, sharp reflectance drops are observed.

The relationship between the reflectivity and the maximum mass of the material, M, that could be evaporated from the solid surface is estimated by an equation given below

$$M = E\,(1 - R) / [C_P\,(T_b - T_0) + L_V] \qquad (4.1)$$

In this equation, E is the laser pulse energy, R is the reflectivity, C_P is the specific heat, T_b is the boiling point, T_0 is room temperature and L_V is the latent heat of vaporization. As shown in this equation, the amount of the evaporated mass increases with lower reflectivity values. Therefore, at high fluences where the ablation threshold of the materials is reached, the reflectivity of the materials decreases resulting in enhanced absorption maximizing the laser pulse energy on the target.

In order to evaluate the silicon wafer based substrates for their performance as a sample holder and sampling target material, the reflectance measurements were carried out via UV-Vis Spectrophotometer, as a function of wavelength. The variation of reflectance for each substrate is given in Figure 4.26.

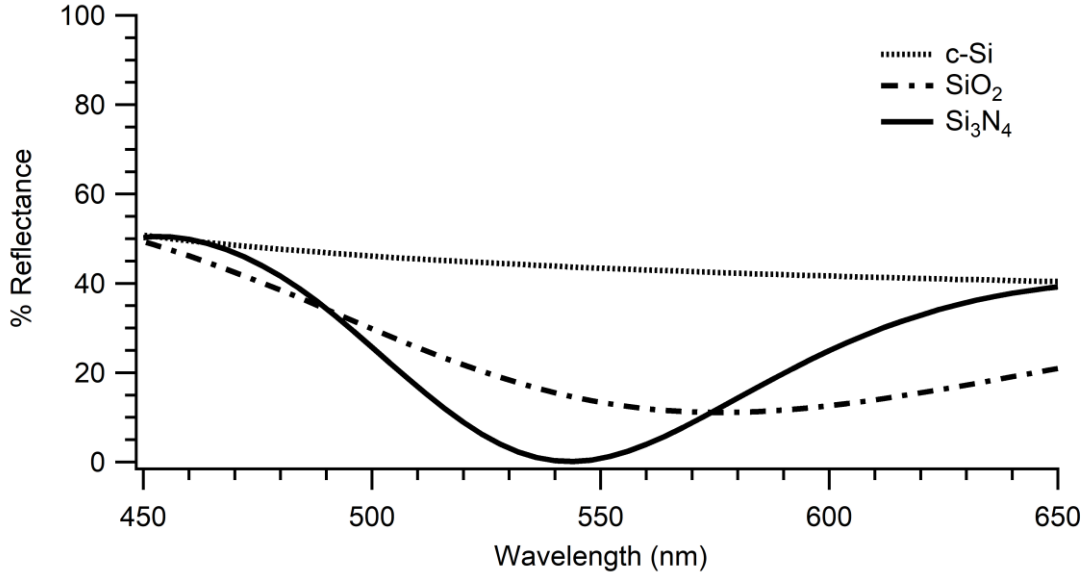

Figure 4.26. Reflectance spectra of the silicon wafer-based substrates as a function of wavelength.

Among all wafers, Si_3N_4 coated silicon wafer has the lowest reflectance value of 2% at the wavelength of 532 nm in which laser operates. Other reflectance values for the c-Si and SiO_2 wafers were 45% and 17%, respectively. Transferring the laser energy to the target is one of the important factors for efficient atomization and excitation of the species in the sample. Due to the nitride coated layer as an anti-reflective layer on the silicon wafer, this energy transfer to the analyte was carried out more efficiently. Thus, enhancement of LIBS signals on Si_3N_4 surfaces could be associated with the lower reflectivity values obtained in this wafer, compared to other types.

The thermal properties of the substrate also affect the signal enhancement. When the energy of the incident laser beam exceeds the substrate's evaporation temperature (1415K for c-Si, 1600 for SiO_2, 2150K for Si_3N_4), heat generated by the intense laser radiation's strong absorption causes rapid heating of the surface that could result in the phase transition from solid to vapor without melting. Due to the rapid heating of the substrate material, this phase transition mechanism could contribute to the rapid transfer of the analyte for more effective vaporization, atomization, and excitation.

Decomposition products of the surface material could affect signal intensity enhancement observed on different substrates. Si_3N_4 decomposes into gaseous nitrogen and liquid silicon, compared to SiO2 and c-Si surfaces and inert nitrogen atmosphere may contribute to signal enhancement in nitride coated surfaces.

4.5.2. Surface Characterization of the Substrates

The surface morphology of the substrates was also investigated if the observed enhancement effect is due to the nanoparticle formation during the LIBS measurements. Nanoparticle enhanced Laser-Induced Breakdown Spectroscopy (NELIBS) is one way to improve the capability of the LIBS technique for direct liquid analysis in which a small volume of the sample solution containing nanoparticles is deposited on the substrate surface. The SEM images of the dried residues on each substrate and laser-ablated craters on silicon wafer-based substrates are shown in Figures 4.27 and 4.29.

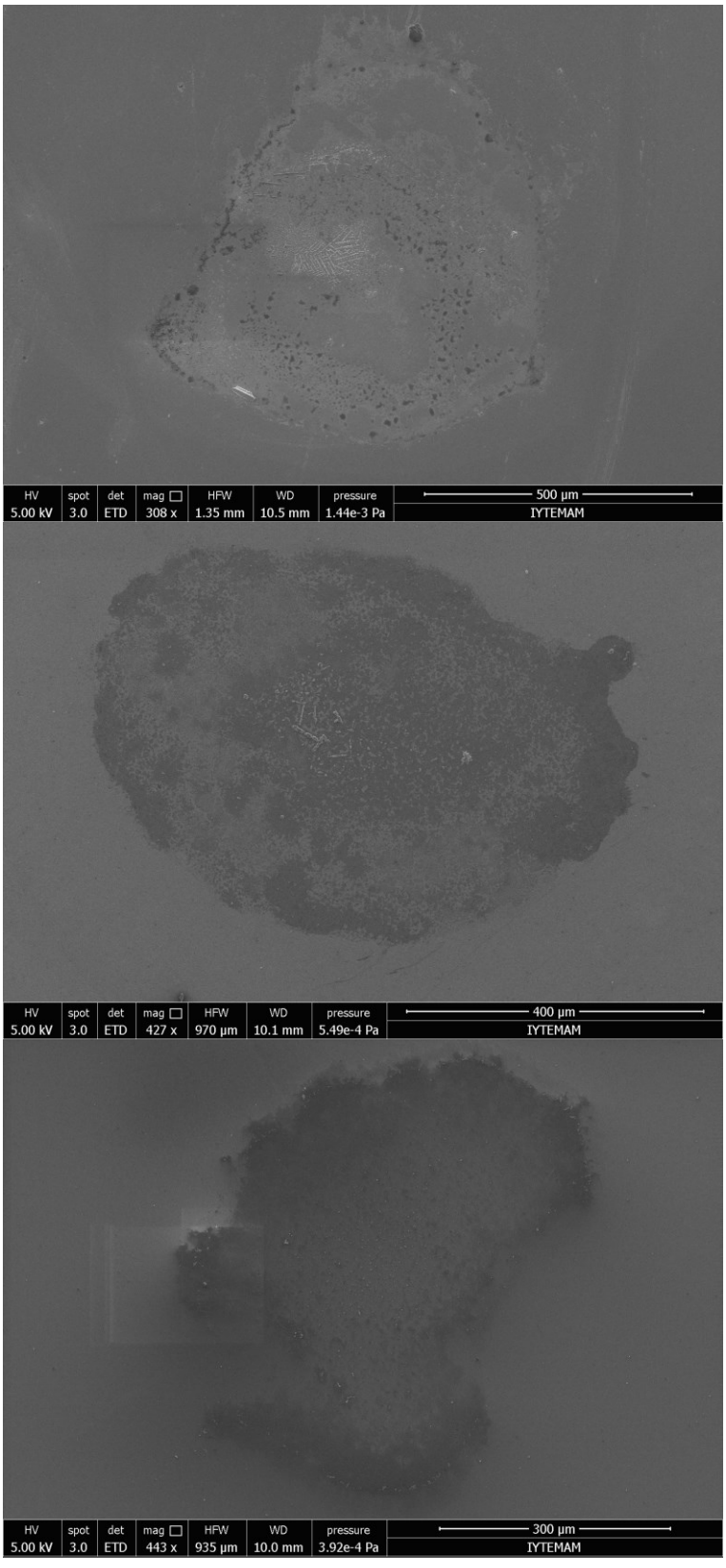

Figure 4.27. SEM images of dried droplets on c-Si, SiO_2, and Si_3N_4 wafers, respectively.

The dried droplets have irregular shapes on each substrate as shown in figure 4.27. Also, the enlarged image of the different parts of the solid residue in Figure 4.27 is

represented in Figure 4.28. Crystal formation at micron sizes is clearly shown in these figures due to the agglomeration of the metal species. As a result, the signal enhancements observed in this work could not be attributed to nanoparticle formation.

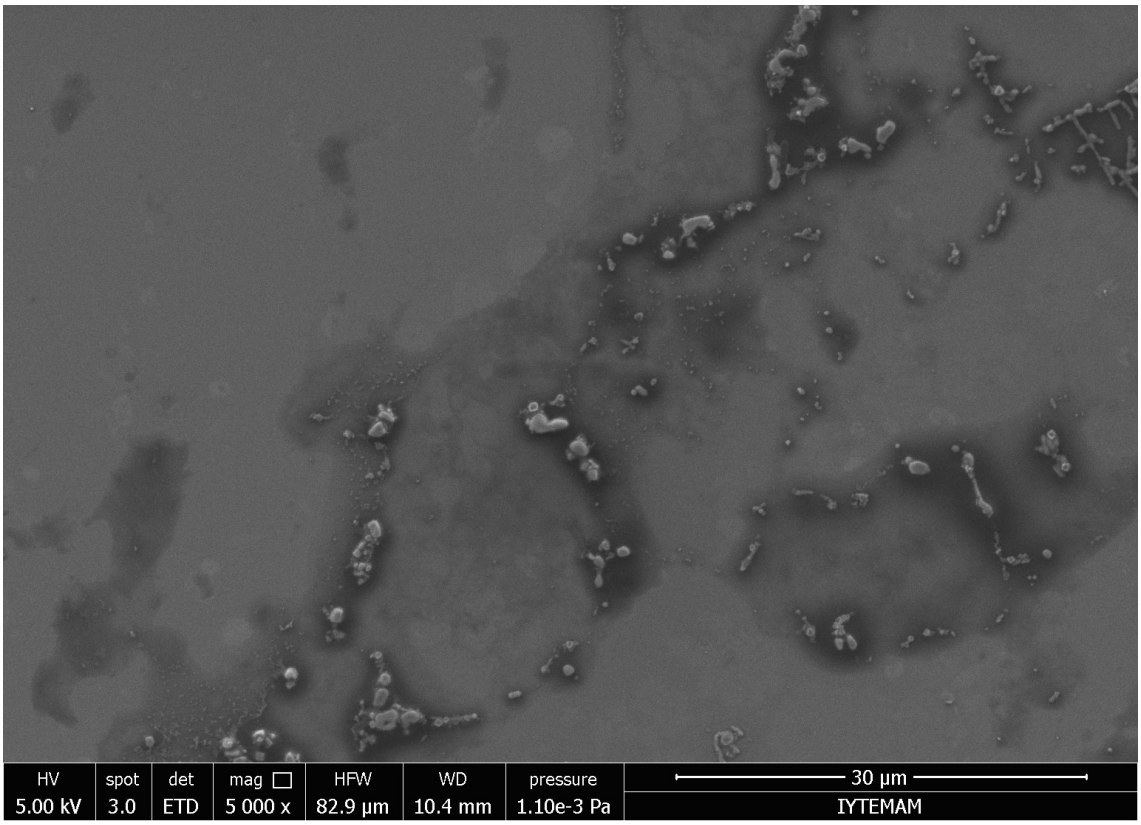

Figure 4.28. Crystal formation after drying process on the substrate.

Besides, SEM images of the laser-ablated craters on each substrate are shown in Figure 4.29 for c-Si, SiO_2, and Si_3N_4 substrates, respectively. These figures show different ablation characteristics of different types of silicon wafers. The craters have a smoother appearance and more uniform ablation characteristics on silicon oxide and silicon nitride coated substrates. However, in comparison to the oxide and nitride coated substrates, the c-Si substrate shows substrate melting, mechanical cracking, and material deposition around the crater. The more smooth appearance of the crater with oxide and nitride coated substrates could support the case for phase transition without melting. The rapid heating mechanism without phase transition contributes to the signal enhancement in which more effective vaporization, atomization, and excitation occurred.

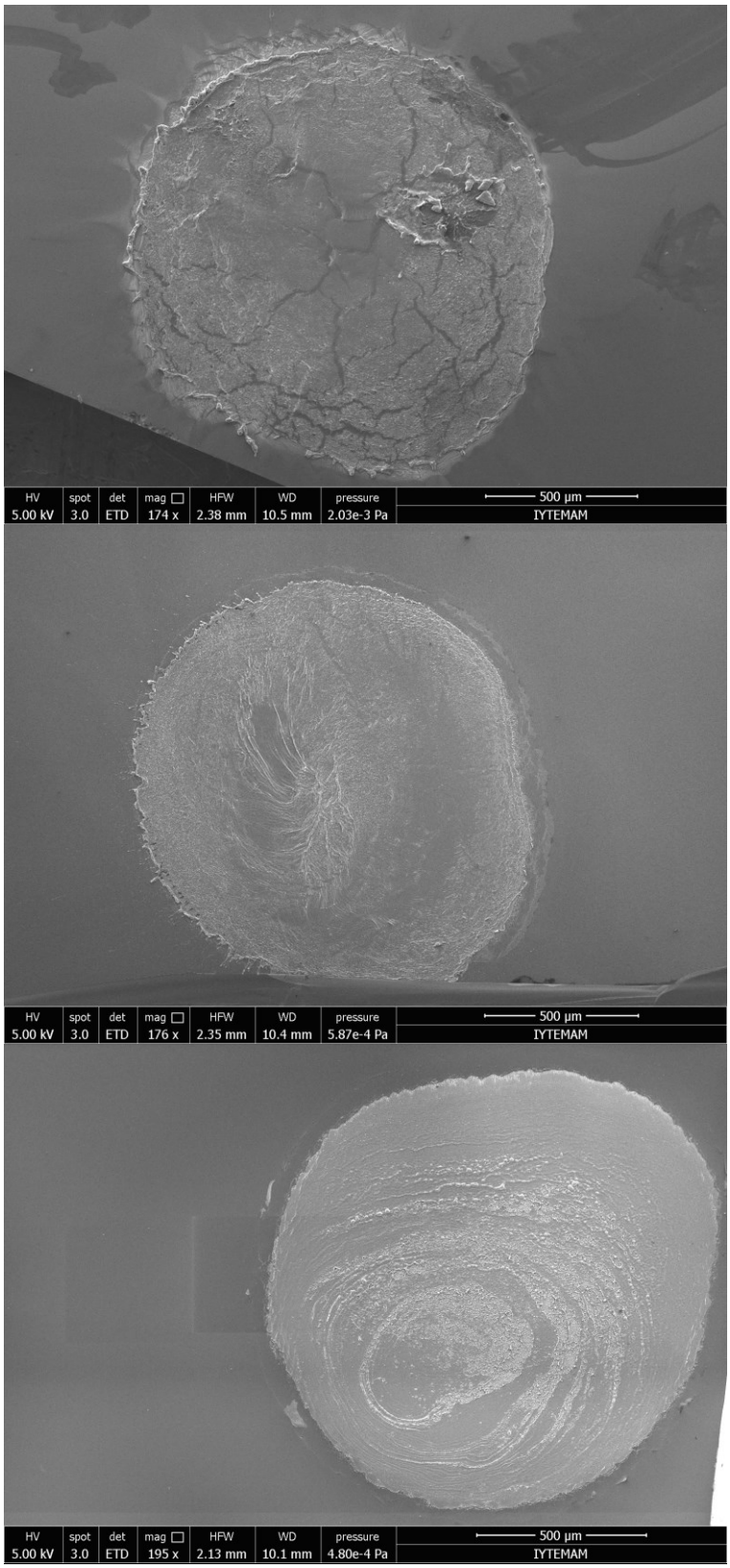

Figure 4.29. SEM images of laser-ablated craters on c-Si, SiO_2, and Si_3N_4 wafers, respectively.

4.5.3.Complete Removal of the Analyte from the Substrate Surface

Droplet analysis by LIBS is carried out by single or multiple laser pulses focused on the same position. Due to the shot-to-shot variations in laser pulse energy, it may negatively affect LIBS results with poor reproducibility. Also, ablation of solid analyte residue on the substrate or target by a single laser pulses offers rapid chemical analysis and less destructive measurements. In order to investigate complete the removal of the analyte residue from the substrate, subsequent laser pulses were sent to the substrates. The variation of the LIBS signal for lead, copper, manganese, and sodium on each substrate with respect to the sequential laser pulses is demonstrated in Figure 4.30. Almost more than 90 % of the analyte signal was observed within the first laser pulse for the Si_3N_4 wafer. However intense emission signals were observed from the subsequent laser pulses for c-Si and SiO_2 wafers. As shown in this figure, 99.9%, 86%, 94%, and 95% of the emission signal was extracted within the first laser pulse with Si_3N_4 wafer for Pb, Cu, Mn, and Na, respectively. These values obtained with the SiO_2 wafer was better whereas signal intensities with the c-Si wafer was lower for investigated all element. These results also support that the antireflective nitride layer on the silicon wafer surface makes the Si_3N_4 wafer highly absorptive. Thus, energy transfer from Si_3N_4 substrate to analyte residue was carried out efficiently compared to the other wafers.

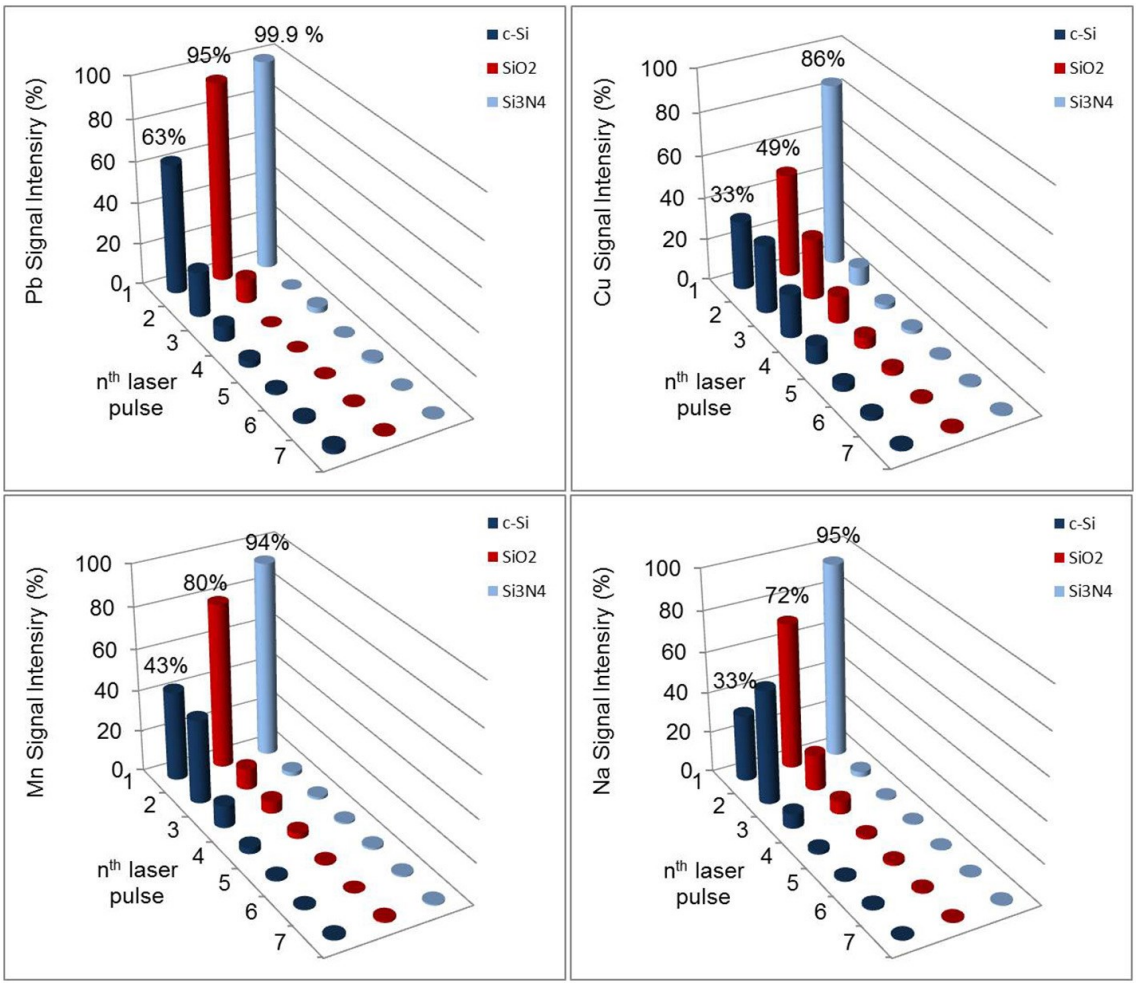

Figure 4.30. LIBS signal intensity variation of Pb, Cu, Mn, and Na signal with respect to the sequential laser pulses for c-Si, SiO_2, and Si_3N_4 wafers.

4.6. Quantitative Analysis of Dried Droplets by LIBS

Laser-Induced Breakdown Spectroscopy is considered as a semi-quantitative analysis technique due to high noise levels obtained as a result of shot-to-shot fluctuations in the laser pulse energy. However, recent studies especially the ones on liquids analysis, like nanoparticle enhanced LIBS or surface-enhanced LIBS approaches have brought drastic improvements in capability of the LIBS detection. It is now possible to make the analysis of samples with a few picograms amount if suitable analytical approaches are performed.

In this thesis study, in order to develop a methodology for quantitative analysis of metals in aqueous solutions, the dried-droplet method was utilized on various types of Si-

wafer substrates. Calibration curves were constructed for quantitative analysis of cadmium, chromium, copper, manganese, and lead droplets on different silicon wafer-based substrates, and limit of detection values were calculated for each element.

For this purpose, single standard solutions of Cd, Cr, Cu, Mn, and Pb were prepared from the 1000 μg mL^{-1} stock solution by several appropriate dilutions. 0.5 μL of analyte solutions with known concentrations were placed on the three silicon wafer-based substrates manually and then droplets were dried at room temperature. LIBS analyses were performed under optimum instrumental conditions. Data were obtained from the single-shot measurements of five separate droplets for each element. At the out-of-focus position, the laser beam was large enough to ablate all solid residue with a single laser shot. Signal intensity values were calculated from the peak area of the atomic emission lines of Cd, Cr, Cu, Mn, and Pb elements after background emissions were subtracted. Calibration curves were constructed from the prominent emission lines of Cd(I) 508.58 nm, Cr(I) 360.53nm, Cu(I) 324.75 nm, Mn(I) 403.01 nm, and Pb(I) 405.78 nm are given in Figure 4.31 – 4.35, for the three substrates. As shown in these figures, for all elements, linear responses were observed with minimum linear regression constant, R^2, of 0.96.

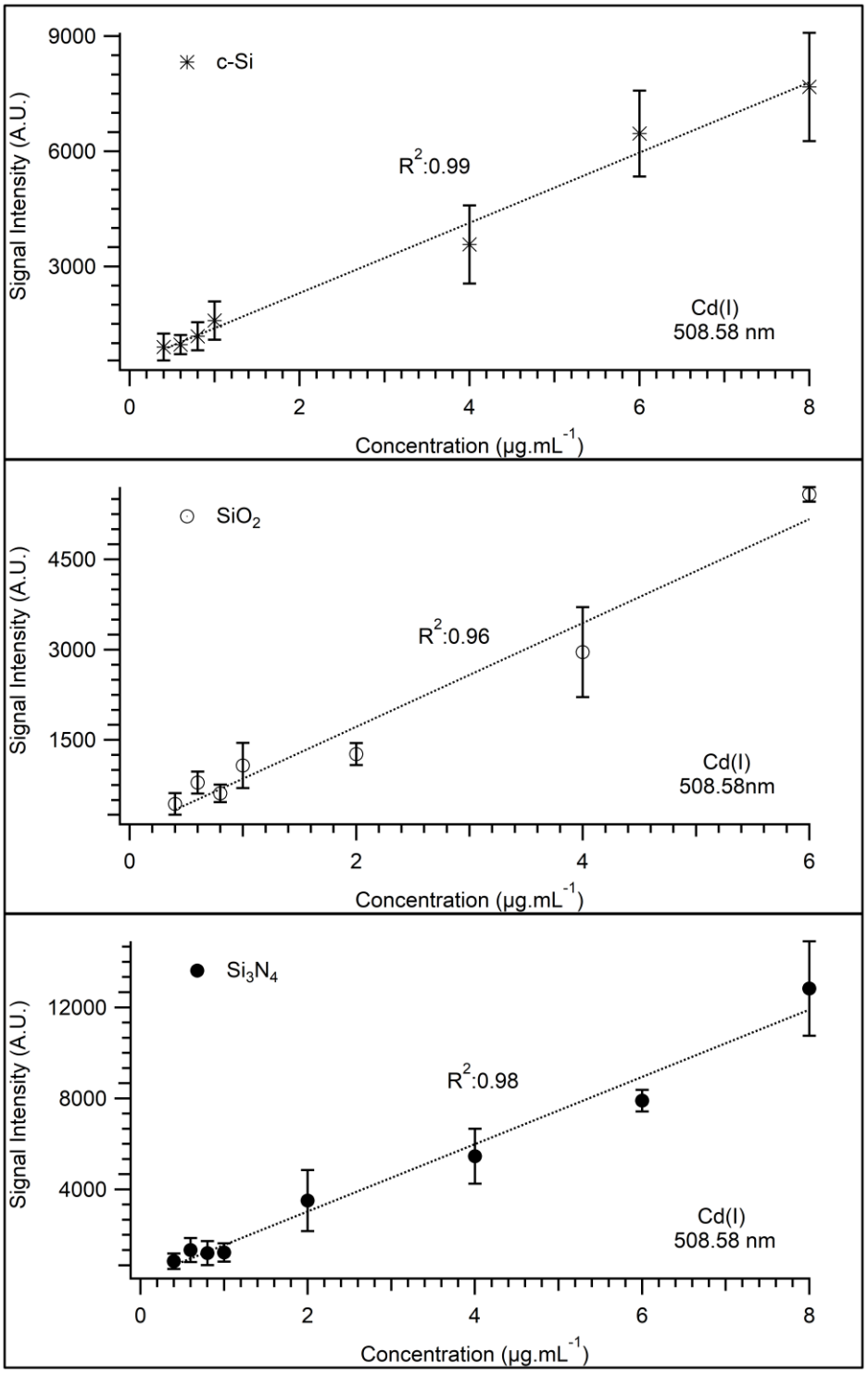

Figure 4.31. Calibration graphs of Cd(I) 508.58 nm with c-Si, SiO_2, and Si_3N_4 wafers.

The calibration curve of the cadmium constructed from the analysis of droplets on c-Si, SiO_2, and Si_3N_4 wafers was demonstrated in Figure 4.31. Calibration curves of cadmium demonstrate a linear behavior over a range of concentrations from 0.4 µg L^{-1} to 8 µg L^{-1} with R^2 0.99, 0.96, and 0.98 for c-Si, SiO_2, and Si_3N_4 wafers, respectively.

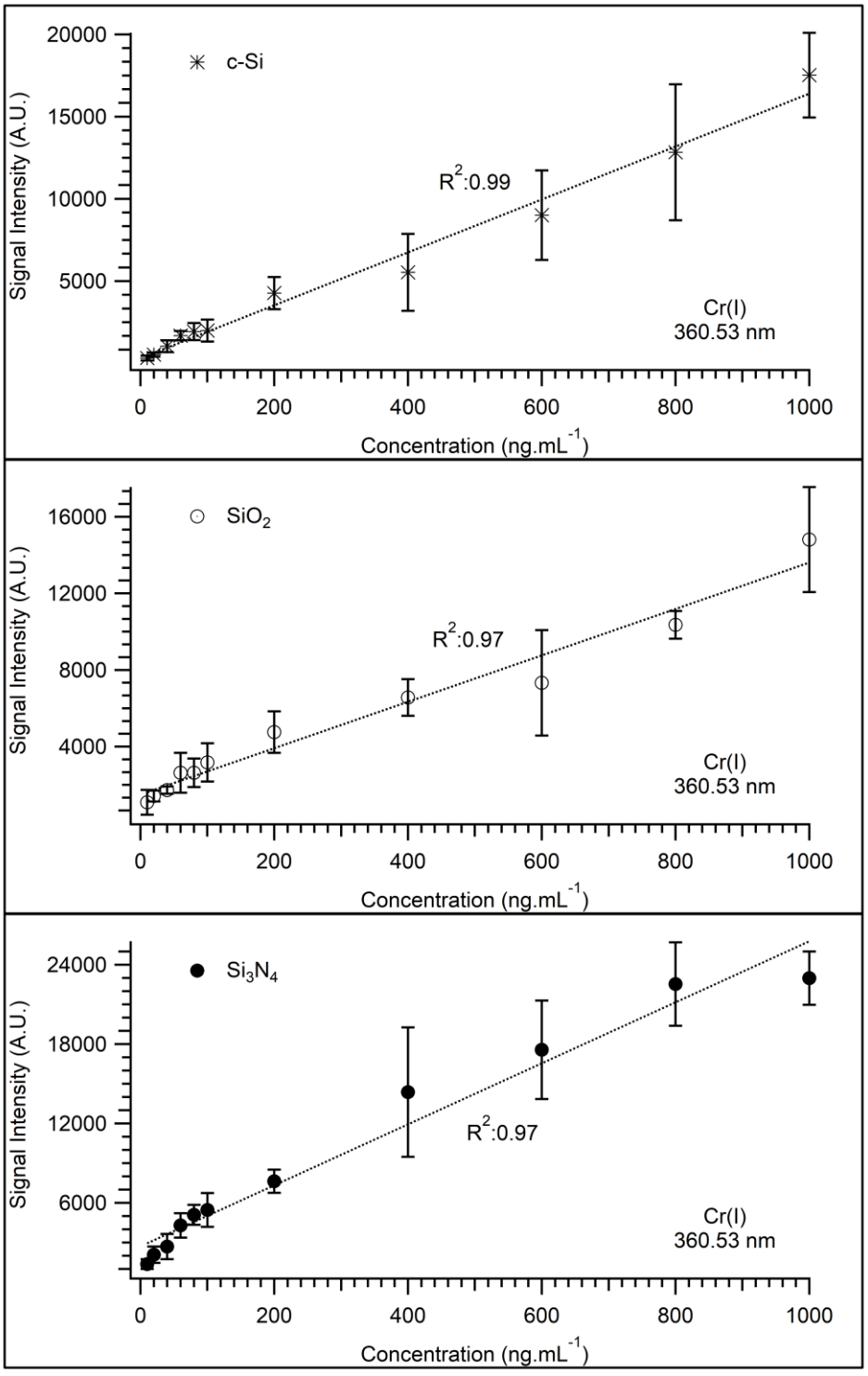

Figure 4.32. Calibration graphs of Cr(I) 360.53 nm with c-Si, SiO_2, and Si_3N_4 wafers.

Figure 4.32 shows the calibration curve of the chromium for all substrates. Emission signals of chromium at 360.53 nm show a linear increase at a concentration range from the 10 ng L^{-1} to 1000 ng L^{-1} with minimum regression constant of 0.97.

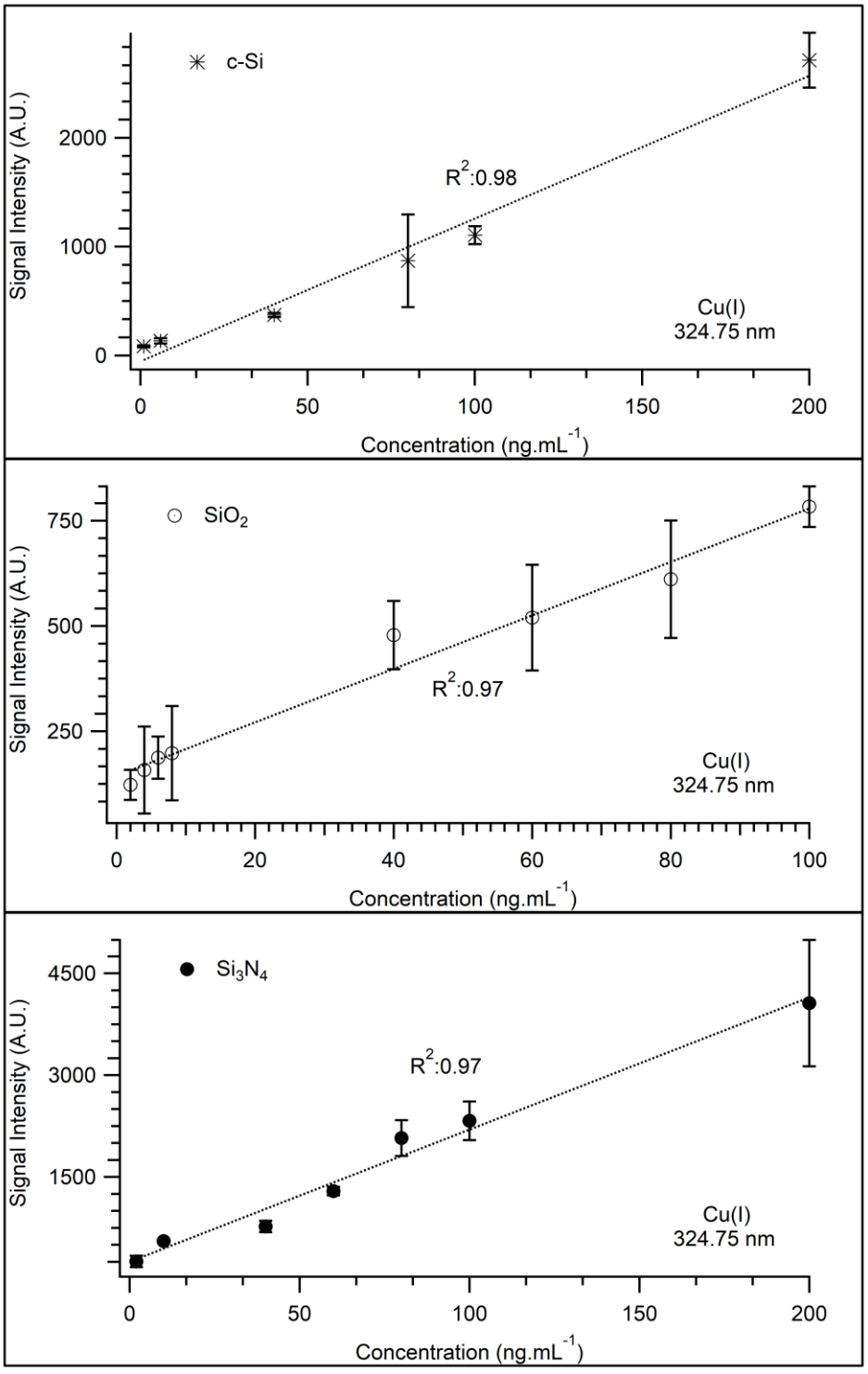

Figure 4.33. Calibration graphs of Cu(I) 324.75 nm with c-Si, SiO_2, and Si_3N_4 wafers

Figure 4.33 shows the growth curves of the emission line of neutral copper at 324.75 nm with copper content ranging from 1 ng L^{-1} to 200 ng L^{-1} for each substrate. Calibration curves obtained were linear with regression constants of 0.98, 0.97, and 0.97 for c-Si, SiO_2, and Si_3N_4 wafers, respectively.

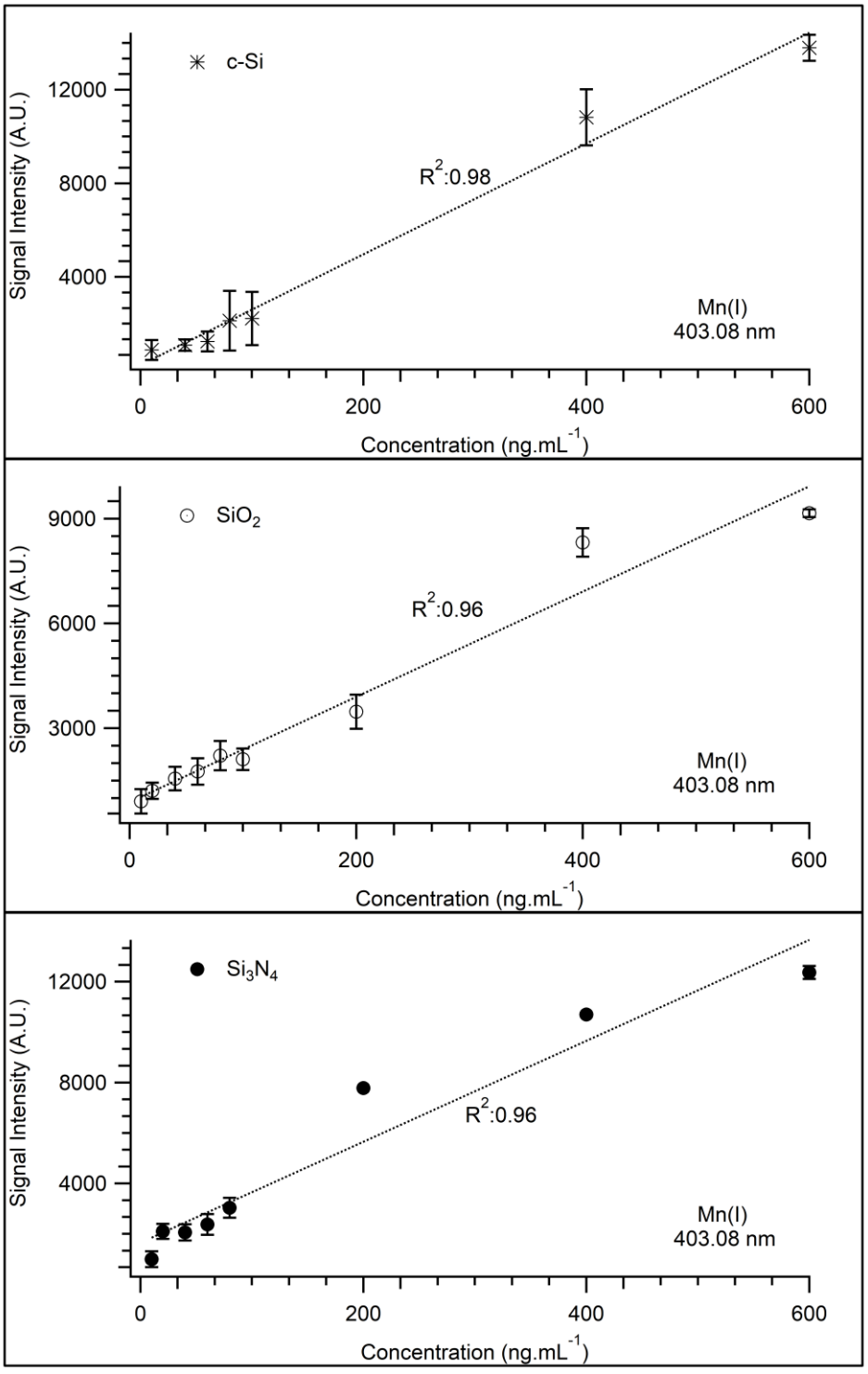

Figure 4.34. Calibration graphs of Mn(I)403.08 nm with c-Si, SiO_2, and Si_3N_4 wafers

The growth curves at three different substrates with manganese content ranging up to 600 ng mL^{-1} are presented in Figure 4.34 Calibration curves are almost linear whereas at higher concentration deviation starts due to the self-absorption of manganese emission at 403.08 nm.

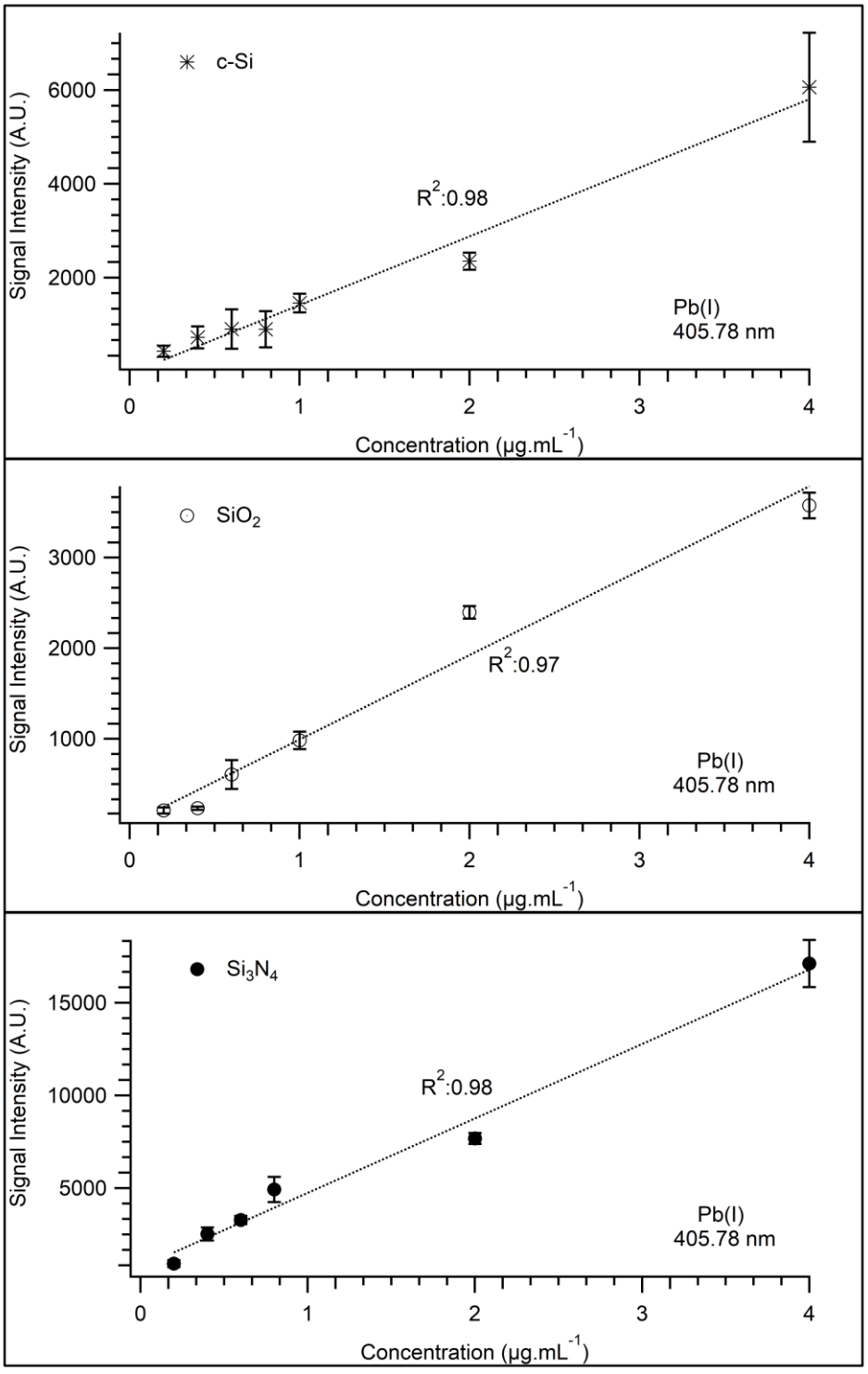

Figure 4.35. Calibration graphs of Pb(I) 405.78 nm with c-Si, SiO_2, and Si_3N_4 wafers

Calibration curves of lead were constructed from the analyte concentration range from 0.1 µg L^{-1} to 4 µg L^{-1}. As shown in this figure, linear responses are obtained with linear regression constants 0.98, 0.97, and 0.98 for each substrate, respectively.

4.6.1. Analytical Figures of Merit

Table 4.5 shows the analytical figures of merits including detection limits, dynamic range, and correlation coefficients for each element at different types of silicon-based wafers.

Limit of detection (LOD) was determined for each element according to the IUPAC definition with 95 % confidence level from the formula;

$$LOD = \frac{3\sigma}{\mathrm{m}} \tag{4.2}$$

In the equation, σ is the standard deviation of the background for the lowest concentration observed and m is the slope of the calibration curve. Relative standard deviation values were calculated from 5 replicate measurements to investigate the repeatability of the LIBS measurements and also RSD values were shown in each calibration graph as error bars. Also, the last column in this table indicates some LOD values from the literature studies performed with a similar methodology by LIBS.

Table 4.5. Analytical figures of merit for dried droplet analysis by LIBS

Elements	c-Si			SiO_2			Si_3N_4			Literature
	Linear range	R^2	LOD (ng mL^{-1})	Linear range	R^2	LOD (ng mL^{-1})	Linear range	R^2	LOD (ng mL^{-1})	(ng mL^{-1})
Cd(I) 508.58nm	0.4-8 µg mL^{-1}	0.99	201	0.4-6 µg mL^{-1}	0.96	151	0.4-8 µg mL^{-1}	0.98	124	184 (Niu, Zheng et al. 2018), 420 (Yang, Hao et al. 2016)
Cr(I) 360.53 nm	10-1000 ng mL^{-1}	0.99	4	10-1000 ng mL^{-1}	0.97	4	10-1000 ng mL^{-1}	0.97	3	19 (Papai, Sato et al. 2017), 25 (Yang, Hao et al. 2016)
Cu(I) 324.75 nm	1-200 ng mL^{-1}	0.98	5	1-100 ng mL^{-1}	0.97	4	1-200 ng mL^{-1}	0.97	1	250 (Yang, Hao et al. 2016)
Mn(I) 403.08 nm	10-600 ng mL^{-1}	0.98	18	10-600 ng mL^{-1}	0.96	7	10-600 ng mL^{-1}	0.96	4	6600 (Aguirre, Legnaioli et al. 2013)
Pb(I) 405.78 nm	0.1-4 µg mL^{-1}	0.98	80	0.1-4 µg mL^{-1}	0.97	37	0.1-4 µg mL^{-1}	0.98	22	118 (Yang, Hao et al. 2016)

LOD values for the c-Si wafer are given being as 201 ng mL^{-1} for Cd, 4 ng mL^{-1} for Cr, 5 ng mL^{-1} for Cu, 18 ng mL^{-1} for Mn, and 80 ng mL^{-1} for Pb, respectively. The detection limits of the SiO_2 wafer were calculated to be151 ng mL^{-1} for Cd, 4 ng mL^{-1} for Cr, 4 ng mL^{-1} for Cu, 7 ng mL^{-1} for Mn, and 37 ng mL^{-1} for Pb, respectively. The calculated best LOD values were obtained with Si_3N_4 wafer being as 124 ng mL^{-1} for Cd, 3 ng mL^{-1} for Cr, 1 ng mL^{-1} for Cu, 4 ng mL^{-1} for Mn, and 22 ng mL^{-1} for Pb, respectively.

Considering that 0.5 µL of droplet volume was utilized for the LIBS measurements, these LODs correspond to absolute detection of 100.5 pg, 75.5 pg, and 62 pg for cadmium, 2 pg, 2 pg, and 1.5 pg for chromium, 2.5 pg, 2 pg, and 0.5 pg for copper, 9 pg, 3.5 pg, and 2 pg for manganese, and 40 pg, 18.5 pg, and 11 pg for the lead at c-Si, SiO_2, and Si_3N_4 wafers, respectively. The calculated LOD values for copper, chromium, and manganese are also below the environmental minimum contaminant regulations and all three silicon-based wafer substrates could be used for droplet analysis of each element in drinking water. However, the proposed methodology is incapable of the analysis of lead and cadmium in drinking water but it may be useful for the analysis of these elements in wastewater. It may be possible that using more analyte solution or sequential loading of analyte solution to the substrate at the same position may allow the analysis of these elements with lower concentration values. According to these results among the three substrates, the lowest detection limits were obtained with Si_3N_4 substrate for all elements.

When we compare results with the studies in the literature, detection of trace-level heavy metal in solutions have been performed on a metallic aluminum target (Niu, Zheng et al. 2018). The LOD value of 184 µg L^{-1} cadmium was reported from the analysis of 1 mL analyte solution onto the target.

The same group also reported a LOD value of 19 µg L^{-1} chromium (Niu, Zheng et al. 2018), and the LOD value is almost six times higher than the one obtained in this work with Si_3N_4 wafer. Although some experimental parameters like irradiance and sample volume are relatively higher, the results are not any better than the results obtained in this work.

The recent study is based on the determination of Cu, Pb, Cd, and Cr elements using chemical replacement of metal ions on the magnesium alloy surface by SENLIBS (Yang, Hao et al. 2016). Detection limits were 250 µg L^{-1}, 118 µg L^{-1}, 420 µg L^{-1}, 25 µg L^{-1} for Cu, Pb, Cd, and Cr, respectively. LOD results obtained with Si_3N_4 wafer are nearly the order of magnitude better for chromium more than two orders of magnitude higher than for copper.

The LOD value of 301 μg L^{-1} Mn was reported by Aguirre et al. (Aguirre, Selva et al. 2015), and this study was based on the use of dispersive liquid-liquid microextraction for metal enrichments in water samples for LIBS measurements. Although they have observed about 4-5 times enhancement compared to the direct liquid analysis performed by LIBS, this result is almost two orders of magnitude higher than the ones presented in this study.

4.6.2. Applications on Reference Water Samples

The applicability of the dried droplet analysis by LIBS on three different types of silicon-based wafers for quantitative analysis of cadmium, chromium, copper, manganese, and lead was investigated on the certified reference water samples; Certified Reference Material-Trace Metals in Drinking Water, CRM-TMDW, and ICP multi-element standard sample, ICP-MES. For this purpose, the CRM-TMDW reference samples were directly placed on each substrate without any dilution, and ICP-MES reference samples were diluted 50 times due to the higher concentrations of Cadmium and Lead in this water standard. Samples of 0.5 μL reference water solutions were analyzed under optimum conditions and contents were calculated from the calibration graphs constructed for the standard solutions. Performance characteristics; like accuracy and precision, were evaluated after some statistical analysis of the data like percent error, and relative standard deviation are calculated. Calculations were based on the analysis of data from five separate samplings of dried droplet regions. Certifed values, Determined values, Percent error, and Precision values for the measurements of the CRM-TMDW and ICP-MES samples on three Si-wafer based substrates are tabulated in Table 4.6.

Table 4.6. Results of reference water samples in terms of accuracy and precision.

Elements	Certified value (ng mL^{-1})	Determined value (ng mL^{-1})			Error (%)			Precision (% RSD)		
		c-Si	SiO_2	Si_3N_4	c-Si	SiO_2	Si_3N_4	c-Si	SiO_2	Si_3N_4
Cd	500	433	378	487	-13	-24	-3	24	29	23
Cr	20±0.2	95	18	20	+373	-10	-1	23	23	6
Cu	20±0.2	37	21	20	+87	+4	-1	21	17	19
Mn	40±0.4	62	46	43	+56	+16	+7	12	12	12
Pb	500	456	586	537	-9	+17	+7	17	19	14

The accuracy of the technique is defined as the closeness of the determined values to the certified values. The Si_3N_4 coated silicon wafer substrate shows the best with percentage errors ranging between -3 to +7 %. Percent error values obtained with the SiO_2 wafer are relatively better compared to that of the c-Si wafer. These results suggest that Si_3N_4 coated silicon wafer favors over the c-Si and SiO_2 wafer for the droplet analysis by LIBS. Precision is also defined as the closeness of the analysis results to each other and it is described as the relative standard deviation of the measurements. % RSD shows the repeatability of the measurements performed under the same conditions. % RSD values ranging between 6% to %29 are in the range commonly observed in most LIBS measurements. Although the precision values are compatible with LIBS measurements, no significant difference is observed among the three substrates.

4.7. Enrichment Studies on the Pretreated Silicon Wafers

Until now, 0.5 µL of solution-loaded substrates have been used for LIBS measurements. The effect of analyte enrichment was evaluated by the sequential 10 loadings of the analyte solution at the same position on the substrate.

For this purpose, laser patterned silicon wafers were devised for the determination of the droplet area exactly and fiber laser was used for patterning. Each silicon-based substrate contains several sampling areas as shown in Figure 4.36. Each sampling area is a circular shape with 1.2 mm in diameter that is coherent with laser spot size at the out of focus position for ablation of solid residue from the substrate.

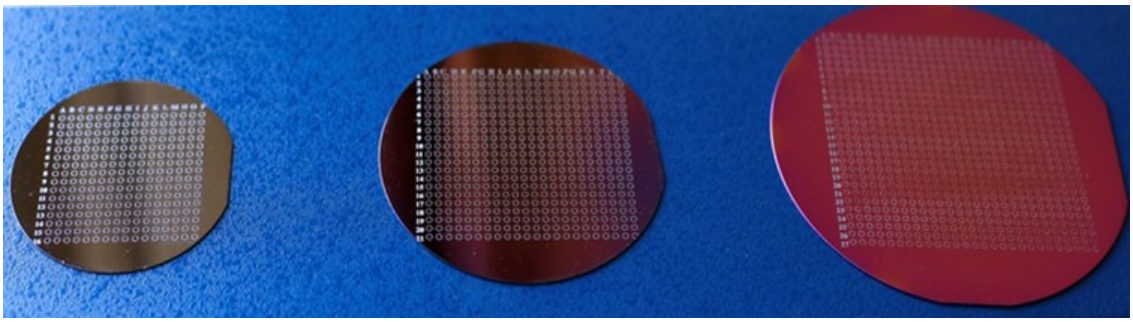

Figure 4.36. Laser-patterned silicon wafers for dried droplet analysis; c-Si, SiO_2, and Si_3N_4, respectively.

In order to evaluate the enhancement in LIBS signals, a single droplet residue, and 10 droplets residue placed at the same sampling area were analyzed under the same optimum experimental conditions. For that purpose, 0.5µL of 0.1 µg mL^{-1} standard lead solutions were loaded on the same spot 10 times after each loading has dried off. For comparison, a single droplet residue was also analyzed. Lead emission signal within the relevant spectral range from a single droplet and 10 times enriched droplet residue are given in Figure 4.37, for c-Si, SiO_2, and Si_3N_4 wafers, separately. Emission signals from a single droplet analysis are presented as a solid line while Pb(I) emission signals from the analysis of enriched droplet residue are represented as a dashed line in the figure. Data are the average of 5 single laser pulse samplings from the separate droplet regions.

As is clearly shown in the figure, for all three substrates, no signal related to the Pb(I) emission is observed from the analysis of single droplet loadings. However, Pb(I) emission at 405.78 nm appears clearly enriched in 10 times loading cases residue for all substrate types. Moreover, the Si_3N_4 substrate exhibited the highest sensitivity with respect to the c-Si and SiO_2 wafers. These enrichment studies appear to enhance the capability of the LIBS measurements for dried droplet analysis and have shown good performance in the use of non-metallic, Si-wafer based substrates for low concentrations of liquids analysis by LIBS.

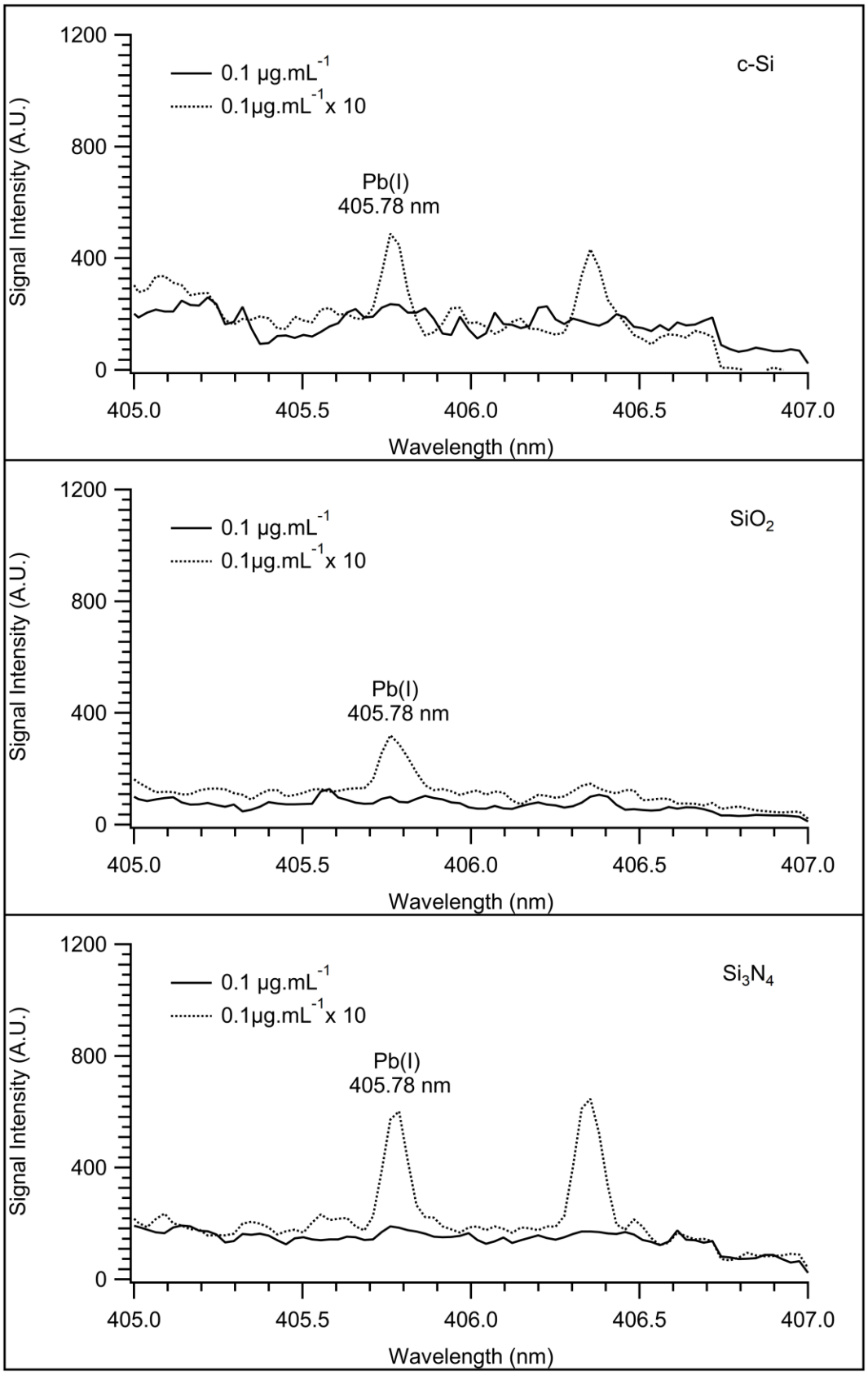

Figure 4.37. Lead signal intensities from 0.1 µg mL^{-1} of analyte solution. The dashed lines represent lead intensities for loaded sequential 10 droplets at the same position while solid lines represent single droplet residue.

4.8. Long Term Sample Storage on Si_3N_4 Wafer

To evaluate the long-term stability of the dried droplet residue on the substrate, analysis of dried droplets on Si_3N_4 wafer was carried out within eight weeks of the period. For this purpose, 0.5 µL of almost 100 droplets were placed on the Si_3N_4 wafer for LIBS measurements. The substrate was kept in a desiccator after the analysis was performed every week. A minimum of 10 droplet residues was analyzed every week. Temporal variation of Pb(I) signal intensity within the 8 weeks is given in Figure 4.38. As shown in this figure, Pb(I) emission intensity at 405.78 nm has remained nearly constant from the first week to the last week. Also, the RSD value of 15 % is within the typical range of most LIBS measurements and indicates the repeatability of the measurements. The long-term stability of the dried droplets on the nitride coated substrates provides an important advantage especially for samples that may decompose/oxidized in aqueous environments, for routine analysis.

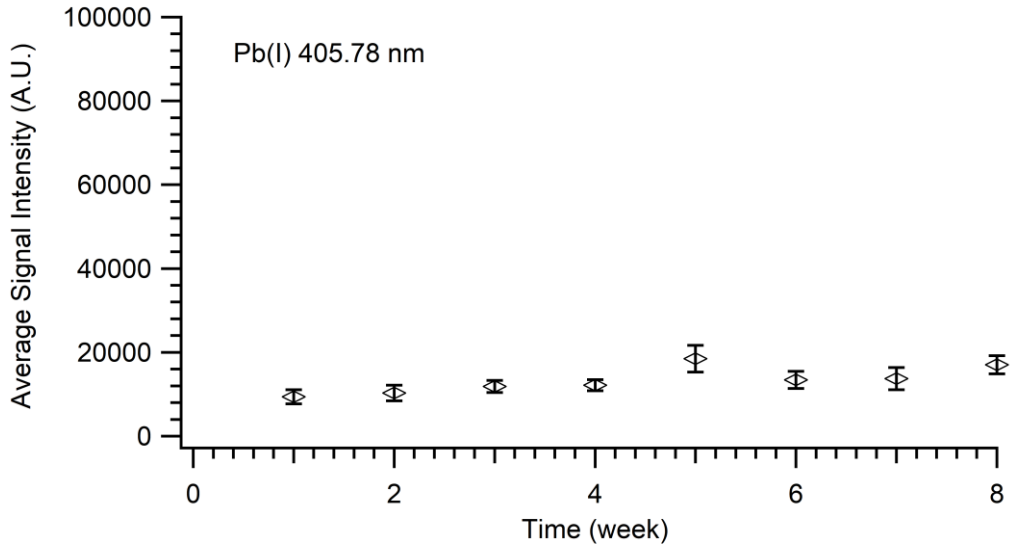

Figure 4.38. The signal intensity variation of dried droplets residue within the 8 weeks of the period.

CHAPTER 5

CONCLUSION

In this thesis study, in order to find a sample loading target for enhanced sensitivity in LIBS analysis of aqueous samples, three different types of non-metallic substrates; crystalline silicon wafer (c-Si), a thermally oxidized silicon wafer with 300 nm oxide layer (Si + SiO_2), and 300 nm silicon nitride coated wafer(Si + Si_3N_4) have been studied.

After drying, 0.5 µL of analyte solutions on the substrates have been exposed to the high-energy laser pulses with relatively large spot size. A plano-convex lens with a 17.5 cm focal length has been placed to the LIBS set-up from the 15 cm distance to the sample for the ablation of solid residue on the substrates in a single laser shot with a 1.3 mm beam size.

Instrumental parameters like laser pulse energy, detector delay time, and gate width have been optimized for the LIBS measurements. Also, the effect of the sample volume placed on the substrate has been investigated. Each substrate has been characterized by SEM and LIBS measurements for the determination of the elemental contents as substrates should be free from the investigated elements in the analyte solutions.

The growth curves under the optimum conditions have been constructed for Cd, Cr, Cu, Mn, and Pb for each substrate and then LOD values have been calculated for each element. A LOD value of 201 ng mL^{-1} for Cd, 4 ng mL^{-1} for Cr, 5 ng mL^{-1} for Cu, 18 ng mL^{-1} for Mn, and 80 ng mL^{-1} for Pb have been determined with the c-Si wafer. The detection limits obtained with as a substrate SiO_2 wafer have been calculated to be151 ng mL^{-1} for Cd, 4 ng mL^{-1} for Cr, 4 ng mL^{-1} for Cu, 7 ng mL^{-1} for Mn, and 37 ng mL^{-1} for Pb, respectively. Finally, the calculated LOD values have been obtained with Si_3N_4 wafer being as 124 ng mL^{-1} for Cd, 3 ng mL^{-1} for Cr, 1 ng mL^{-1} for Cu, 4 ng mL^{-1} for Mn, and 22 ng mL^{-1} for Pb, respectively. These values are also promising compared to similar studies in the literature.

The applicability of the dried droplet analysis by LIBS for quantitative analysis of Cd, Cr, Cu, Mn, and Pb have been evaluated by the analysis of the certified reference water sample, CRM-TMDW, and ICP multi-element standard sample, ICP-MES. Although percent error values have different values in each substrate, Si_3N_4 coated wafer ranging between -3 to +7 percent errors have shown the best values.

The effect of the silicon wafer-based substrates on measurements has been compared in terms of the enhancement of LIBS emission signals and detection limit for the Cd, Cu, Cr, Mn, and Pb elements. For all the studies, Si_3N_4 coated silicon wafer substrate achieves the best results compared to the obtained with c-Si and SiO_2 coated silicon wafers. It could be explained that the enhancement with Si_3N_4 coated silicon wafer is related to absorption of laser energy more efficiently that cause rapid heating of the substrate surface. The phase transition mechanism from solid to vapor without melting leads to the transferring of the species rapidly for more effective vaporization, atomization, and excitation. In addition, the inert nitrogen atmosphere due to the decomposition product of the Si_3N_4 coating layer on the substrate may contribute to the enhanced emission signals of the elements studied.

LODs corresponding to absolute amounts of 62 pg Cd, 1.5 pg Cr, 0.5 pg Cu, 2 pg Mn, and 11 pg Pb have been achieved from the analysis of 0.5 µL of droplet volume with Si_3N_4 coated silicon wafer substrate. Substantial enhancements have been observed at the detection limits for the direct liquid analysis by LIBS. It is also shown that sub-sequent sample loading on the substrate may improve the analytical capability of laser-induced breakdown spectroscopy for liquid analysis.

The results demonstrate the utility of the Si_3N_4 coated silicon wafer as a potential LIBS or SENLIBS target for the droplet analysis. Further studies on Si_3N_4 coated silicon wafer substrates including the thickness of the coating layer on the substrate, sampling area for larger sample volume could increase the performance and applicability of the proposed method.

REFERENCES

Aguirre, M., et al. (2013). "Elemental analysis by surface-enhanced Laser-Induced Breakdown Spectroscopy combined with liquid–liquid microextraction." Spectrochimica Acta Part B: Atomic Spectroscopy **79**: 88-93.

Aguirre, M., et al. (2015). "Hyphenation of single-drop microextraction with laser-induced breakdown spectrometry for trace analysis in liquid samples: a viability study." Analytical Methods **7**(3): 877-883.

Aguirre, M., et al. (2015). "Dispersive liquid–liquid microextraction for metals enrichment: A useful strategy for improving sensitivity of laser-induced breakdown spectroscopy in liquid samples analysis." Talanta **131**: 348-353.

Anzano, J. and R.-J. Lasheras (2009). "Strategies for the identification of urinary calculus by laser induced breakdown spectroscopy." Talanta **79**(2): 352-360.

Aras, N. and Ş. Yalçın (2016). "Development and validation of a laser-induced breakdown spectroscopic method for ultra-trace determination of Cu, Mn, Cd and Pb metals in aqueous droplets after drying." Talanta **149**: 53-61.

Aras, N. and Ş. Yalçın (2019). "Investigating silicon wafer based substrates for dried-droplet analysis by Laser-Induced Breakdown Spectroscopy." Spectrochimica Acta Part B: Atomic Spectroscopy **152**: 84-92.

Aras, N., et al. (2012). "Ultrasonic nebulization-sample introduction system for quantitative analysis of liquid samples by laser-induced breakdown spectroscopy." Spectrochimica Acta Part B: Atomic Spectroscopy **74**: 87-94.

Babushok, V., et al. (2006). "Double pulse laser ablation and plasma: Laser induced breakdown spectroscopy signal enhancement." Spectrochimica Acta Part B: Atomic Spectroscopy **61**(9): 999-1014.

Bae, D., et al. (2015). "Spreading a water droplet on the laser-patterned silicon wafer substrate for surface-enhanced laser-induced breakdown spectroscopy." Spectrochimica Acta Part B: Atomic Spectroscopy **113**: 70-78.

Baudelet, M., et al. (2006). "Femtosecond time-resolved laser-induced breakdown spectroscopy for detection and identification of bacteria: A comparison to the nanosecond regime." Journal of Applied Physics **99**(8): 084701.

Bukhari, M., et al. (2012). "Development of a method for the determination of chromium and cadmium in tannery wastewater using laser-induced breakdown spectroscopy." Journal of analytical methods in chemistry **2012**.

Chen, C., et al. (2016). "A novel method for metallic element analysis in particle samples using a laser-induced breakdown spectroscopy technique." Journal of analytical atomic spectrometry **31**(7): 1527-1533.

Chen, D., et al. (2010). "Heavy metal pollution in soil detected by laser induced breakdown spectroscopy." Zhongguo Jiguang(Chinese Journal of Lasers) **37**.

Chen, Z., et al. (2008). "Fast and sensitive trace metal analysis in aqueous solutions by laser-induced breakdown spectroscopy using wood slice substrates." Spectrochimica Acta Part B: Atomic Spectroscopy **63**(1): 64-68.

Colao, F., et al. (2002). "A comparison of single and double pulse laser-induced breakdown spectroscopy of aluminum samples." Spectrochimica Acta Part B: Atomic Spectroscopy **57**(7): 1167-1179.

Cremers, D. A. and L. J. Radziemski (1985). "Direct detection of beryllium on filters using the laser spark." Applied spectroscopy **39**(1): 57-63.

Cremers, D. A. and L. J. Radziemski (2006). "Handbook of Laser-Induced Breakdown Spectroscopy."

de Carvalho, G. G. A., et al. (2010). "Evaluation of laser induced breakdown spectrometry for the determination of macro and micronutrients in pharmaceutical tablets." Journal of analytical atomic spectrometry **25**(6): 803-809.

De Giacomo, A., et al. (2014). "Nanoparticle Enhanced Laser Induced Breakdown Spectroscopy: Effect of nanoparticles deposited on sample surface on laser ablation and plasma emission." Spectrochimica Acta Part B: Atomic Spectroscopy **98**: 19-27.

De Giacomo, A., et al. (2013). "Nanoparticle-enhanced laser-induced breakdown spectroscopy of metallic samples." Analytical Chemistry **85**(21): 10180-10187.

De Giacomo, A., et al. (2016). "Nanoparticle enhanced laser-induced breakdown spectroscopy for microdrop analysis at subppm level." Analytical Chemistry **88**(10): 5251-5257.

de Jesus, A. M., et al. (2014). "The determination of V and Mo by dispersive liquid–liquid microextraction (DLLME) combined with laser-induced breakdown spectroscopy (LIBS)." Journal of analytical atomic spectrometry **29**(10): 1813-1818.

Gallou, G., et al. (2011). "Aerosols analysis by LIBS for monitoring of air pollution by industrial sources." Aerosol Science and Technology **45**(8): 918-926.

Gaubeur, I., et al. (2015). "Dispersive liquid–liquid microextraction combined with laser-induced breakdown spectrometry and inductively coupled plasma optical emission spectrometry to elemental analysis." Microchemical Journal **121**: 219-226.

Gaudiuso, R., et al. (2010). "Laser induced breakdown spectroscopy for elemental analysis in environmental, cultural heritage and space applications: a review of methods and results." Sensors **10**(8): 7434-7468.

Hahn, D. W., et al. (2008). Laser-induced breakdown spectroscopy (LIBS) for aerosol analysis. Conference on Lasers and Electro-Optics, Optical Society of America.

Harmon, R. S., et al. (2009). "LIBS analysis of geomaterials: geochemical fingerprinting for the rapid analysis and discrimination of minerals." Applied Geochemistry **24**(6): 1125-1141.

Hiller, D., et al. (2010). "Low temperature silicon dioxide by thermal atomic layer deposition: Investigation of material properties." Journal of Applied Physics **107**(6): 064314.

Jantzi, S. C., et al. (2016). "Sample treatment and preparation for laser-induced breakdown spectroscopy." Spectrochimica Acta Part B: Atomic Spectroscopy **115**: 52-63.

Jiang, T.-J., et al. (2016). "Electrochemical laser induced breakdown spectroscopy for enhanced detection of Cd (II) without interference in rice on layer-by-layer assembly of graphene oxides." Electrochimica Acta **216**: 188-195.

Kumar, A., et al. (2004). "Characterization of malignant tissue cells by laser-induced breakdown spectroscopy." Applied optics **43**(28): 5399-5403.

Lawrence-Snyder, M., et al. (2007). "Sequential-pulse laser-induced breakdown spectroscopy of high-pressure bulk aqueous solutions." Applied spectroscopy **61**(2): 171-176.

Lin, Q., et al. (2016). "Ultra-trace metallic element detection in liquid samples using laser induced breakdown spectroscopy based on matrix conversion and crosslinked PVA polymer membrane." Journal of analytical atomic spectrometry **31**(8): 1622-1630.

Maji, S., et al. (2021). "Enhanced laser induced breakdown spectroscopy signal intensity in colloids: An application for estimation of Cu and Cr in aqueous solution." Spectrochimica Acta Part B: Atomic Spectroscopy **175**: 106010.

Miziolek, A., et al. (2008). Recent progress in LIBS-based technologies for security applications. Laser Applications to Chemical, Security and Environmental Analysis, Optical Society of America.

Miziolek, A. W., et al. (2006). Laser induced breakdown spectroscopy, Cambridge university press.

Nakamura, S., et al. (1996). "Determination of an iron suspension in water by laser-induced breakdown spectroscopy with two sequential laser pulses." Analytical Chemistry **68**(17): 2981-2986.

Niu, S., et al. (2018). "Laser-induced breakdown spectroscopic detection of trace level heavy metal in solutions on a laser-pretreated metallic target." Talanta **179**: 312-317.

Pace, D. D., et al. (2006). "Analysis of heavy metals in liquids using laser induced breakdown spectroscopy by liquid-to-solid matrix conversion." Spectrochimica Acta Part B: Atomic Spectroscopy **61**(8): 929-933.

Papai, R., et al. (2017). "Melted paraffin wax as an innovative liquid and solid extractant for elemental analysis by laser-induced breakdown spectroscopy." Analytical Chemistry **89**(5): 2807-2815.

Ravindra, N., et al. (2015). "Modeling of optical properties of black silicon/crystalline silicon." Silicon. J. Sci. Ind. Metrol. **1**(1): 100001.

Ruiz, F., et al. (2019). "Dispersive micro solid-phase extraction (DμSPE) with graphene oxide as adsorbent for sensitive elemental analysis of aqueous samples by laser induced breakdown spectroscopy (LIBS)." Talanta **191**: 162-170.

Samek, O., et al. (2000). "Clinical application of laser-induced breakdown spectroscopy to the analysis of teeth and dental materials." Journal of clinical laser medicine & surgery **18**(6): 281-289.

Sarkar, A., et al. (2010). "Determination of sub—ppm levels of boron in ground water samples by laser induced breakdown spectroscopy." Microchimica Acta **168**(1-2): 65-69.

Scaffidi, J., et al. (2003). "Dual-pulse laser-induced breakdown spectroscopy with combinations of femtosecond and nanosecond laser pulses." Applied optics **42**(30): 6099-6106.

Shi, Q., et al. (2014). "Exploration of a 3D nano-channel porous membrane material combined with laser-induced breakdown spectrometry for fast and sensitive heavy metal detection of solution samples." Journal of analytical atomic spectrometry **29**(12): 2302-2308.

Singh, J. P. and S. N. Thakur (2020). Laser-induced breakdown spectroscopy, Elsevier.

Sládková, L., et al. (2017). "Improvement of the Laser-Induced Breakdown Spectroscopy method sensitivity by the usage of combination of Ag-nanoparticles and vacuum conditions." Spectrochimica Acta Part B: Atomic Spectroscopy **127**: 48-55.

Sneddon, J., et al. (1996). Lasers in analytical atomic spectroscopy, John Wiley & Sons.

Sobral, H., et al. (2012). "Detection of trace elements in ice and water by laser-induced breakdown spectroscopy." Spectrochimica Acta Part B: Atomic Spectroscopy **78**: 62-66.

Wang, X., et al. (2014). "Simultaneous and sensitive analysis of Ag (I), Mn (II), and Cr (III) in aqueous solution by LIBS combined with dispersive solid phase micro-extraction using nano-graphite as an adsorbent." Journal of analytical atomic spectrometry **29**(6): 1098-1104.

Wang, X., et al. (2015). "Simple, fast matrix conversion and membrane separation method for ultrasensitive metal detection in aqueous samples by laser-induced breakdown spectroscopy." Analytical Chemistry **87**(11): 5577-5583.

Wilmart, Q., et al. (2019). "A versatile silicon-silicon nitride photonics platform for enhanced functionalities and applications." Applied Sciences **9**(2): 255.

Xue, B., et al. (2019). "Characteristics of the secondary breakdown of DP-LIBS in bulk water with different axial focusing arrangements and laser energies." Spectrochimica Acta Part B: Atomic Spectroscopy **151**: 20-25.

Yang, X., et al. (2016). "Sensitive determinations of Cu, Pb, Cd, and Cr elements in aqueous solutions using chemical replacement combined with surface-enhanced laser-induced breakdown spectroscopy." Optics express **24**(12): 13410-13417.

Yang, X., et al. (2017). "Simultaneous determination of La, Ce, Pr, and Nd elements in aqueous solution using surface-enhanced laser-induced breakdown spectroscopy." Talanta **163**: 127-131.

Yang, X., et al. (2020). "Improving the sensitivity of surface-enhanced laser-induced breakdown spectroscopy by repeating sample preparation." Frontiers in Physics **8**: 194.

Zhang, D., et al. (2021). "Influence of substrate temperature on detection sensitivity of surface-enhanced LIBS for analysis of heavy metallic elements in water." Journal of analytical atomic spectrometry.

Zhang, L., et al. (2013). "Comparative Studies on the Excitation Mechanism of Fe II Lines in Low-Pressure Laser-Induced Plasma of Argon and Neon." Spectroscopy Letters **46**(1): 1-12.

Zheng, L., et al. (2016). "Comparative study of the matrix effect in Cl analysis with laser-induced breakdown spectroscopy in a pellet or in a dried solution layer on a metallic target." Spectrochimica Acta Part B: Atomic Spectroscopy **118**: 66-71.

Zhu, D., et al. (2012). "Laser-induced breakdown spectroscopy for determination of trace metals in aqueous solution using bamboo charcoal as a solid-phase extraction adsorbent." Analytical Methods **4**(3): 819-823.

VITA

PERSONAL INFORMATION

Name Surname Nadir ARAS

EDUCATION

[2012-2021]	**Ph.D.** (Faculty of Science, Dept. of Chemistry) Izmir Institute of Technology
[2009-2012]	**M.Sc.** (Faculty of Science, Dept. of Chemistry) Izmir Institute of Technology
[2003-2008]	**B.Sc.** (Faculty of Education,Chemistry Education) Dokuz Eylül University
[2010-2014]	**B.Sc.** (Faculty of Business Administration, Business Administration), Anadolu University
[2015-2017]	**A.S.** (The faculty of Open Education, Electric Power Generation, Transmission and Distribution) Anadolu University

WORK EXPERIENCE

[2018- present]	**Instructor** (Environmental Development Application and Research Center) Izmir Institute of Technology
[2010-2018]	**Teaching and Research Assistant** (Faculty of Science, Dept. of Chemistry) İzmir Institute of Technology

PUBLICATIONS

Aras, N. and Ş. Yalçın (2019). "Investigating silicon wafer based substrates for dried-droplet analysis by Laser-Induced Breakdown Spectroscopy." Spectrochimica Acta Part B: Atomic Spectroscopy **152**: 84-92.

Aras, N. and Ş. Yalçın (2016). "Development and validation of a laser-induced breakdown spectroscopic method for ultra-trace determination of Cu, Mn, Cd and Pb metals in aqueous droplets after drying." Talanta **149**: 53-61.

Aras, N. and Ş. Yalçın (2014). "Rapid identification of phosphorus containing proteins in electrophoresis gel spots by Laser-Induced Breakdown Spectroscopy, LIBS." Journal of Analytical Atomic Spectrometry **29**(3): 545-552.

Aras, N., S. Ü. Yeşiller, D. A. Ateş and Ş. Yalçın (2012). "Ultrasonic nebulization-sample introduction system for quantitative analysis of liquid samples by laser-induced breakdown spectroscopy." Spectrochimica Acta Part B: Atomic Spectroscopy **74**: 87-94.

Sağın, E. U., H. Böke, N. Aras and Ş. Yalçın (2012). "Determination of CaCO 3 and SiO 2 content in the binders of historic lime mortars." Materials and Structures **45**(6): 841-849.